

WM-296

27
07/23/80 AM.
24
TIS

SAND80-1464
Unlimited Release
UC-70

Evaluation of Tuff as a Medium for a Nuclear Waste Repository: Interim Status Report on the Properties of Tuff

MASTER

J. Keith Johnstone, Kurt Wolfsberg, Editors



Sandia National Laboratories

HYDROLOGY DOCUMENT NUMBER 200

DISTRIBUTION OF THIS DOCUMENT IS U

SAND80-1464
Unlimited Release
Printed July 1980

Distribution
Category UC-70

EVALUATION OF TUFF AS A MEDIUM FOR A NUCLEAR
WASTE REPOSITORY: INTERIM STATUS REPORT ON THE
PROPERTIES OF TUFF

Edited by

J. Keith Johnstone
Geological Projects Division 4537
Sandia National Laboratories
Albuquerque, NM 87185

Kurt Wolfsberg
Chemistry and Nuclear Chemistry Division
Los Alamos Scientific Laboratory
Los Alamos, NM 87545

Contributors

B. P. Bayhurst, LASL
J. D. Blacic, LASL
B. R. Erdal, LASL
K. L. Erickson, SNL
G. R. Hadley, SNL
P. M. Halleck, LASL,
J. K. Johnstone, SNL
B. S. Langkopf, SNL
A. R. Lappin, SNL
W. A. Olsson, SNL
J. R. Smyth, LASL
M. L. Sykes, LASL
L. W. Teufel, SNL
L. D. Tyler, SNL
E. N. Vine, LASL
K. Wolfsberg, LASL

DISCLAIMER

This work was prepared as an account of work sponsored by or for the United States Government
under the United States Government contract number... For the United States Government, neither the
United States Government nor the Sandia Corporation, nor any of their employees, makes any
warranty, expressed or implied, or assumes any legal liability or responsibility for the accuracy
or completeness of any information, technical data, or any process disclosed, or for the results
obtained from the use of the information, technical data, or any process disclosed, or for the
injury to persons or property resulting from its use. The United States Government and the Sandia
Corporation are authorized to reproduce and distribute reprints for government purposes not
withstanding any copyright notation that may appear hereon.

ACKNOWLEDGEMENTS

We wish to acknowledge R. D. Aguilar (LASL), E. S. Ames (SNL), R. Andersen (LASL), A. C. Arthur (SNL), M. L. Bevier (LASL), S. P. Breeze (SNL), W. T. Brown (SNL), B. M. Bulmer (SNL), F. Caporuscio (LASL), W. R. Daniels (LASL), S. J. DeVilliers (LASL), C. O. Duimstra (SNL), G. H. Heiken (LASL), P. Johnson (LASL), A. K. Jones (SNL), C. B. Finabrew (SNL), D. Krier (UNM), R. T. Laws (SNL), R. Z. Lawson (SNL), J. T. Lindman (SNL), S. Maestas (LASL), D. A. Mann (LASL), D. F. McVey (SNL), K. D. Murphy (SNL), P. Q. Oliver (LASL), S. Orell (EG&G), J. W. Schwarz (SNL), G. Smith (UNM), T. J. Stetz (SNL), J. L. Thompson (LASL), J. E. R. Turner (SNL), and D. R. Waymire (SNL) for their technical support of the work reported here.

ABSTRACT

This report is the second in a series of summary briefings to the National Academy of Science's (NAS) Committee on Radioactive Waste Management dealing with the feasibility of disposal of heat-producing radioactive waste in silicic tuff. We discuss the interim status of studies of tuff properties determined on samples obtained from Yucca Mountain and Rainier Mesa (G-tunnel) located on the Nevada Test Site (NTS). In particular, we describe progress on resolving issues identified during the first briefing to the NAS which include behavior of water in tuff when heated, the effect of the presence or absence of water and joints on the thermal/physical properties of tuff and the detailed/complex sorptive properties of highly altered and unaltered tuff. Initial correlations of thermal/physical and sorptive properties with the highly variable porosity and mineralogy are described. Three in-situ, at-depth field experiments, one nearly completed and two just getting underway are described. In particular, the current status of mineralogy and petrology, geochemistry, thermal and mechanical, radiation effects and water behavior studies are described. The goals and initial results of a Mine Design Working Group are discussed. Regional factors such as seismicity, volcanism and hydrology are not discussed.

CONTENTS

	<u>Page</u>
1. EXECUTIVE SUMMARY	13
2. INTRODUCTION	23
3. TUFF PROPERTIES	25
3.1 Mineralogy and Petrology	25
3.1.1 General Description	25
3.1.2 Location-Specific Studies	27
3.1.2.1 Yucca Mountain	27
3.1.2.2 G-Tunnel	36
3.1.3 Zeolite Stability Studies	37
3.1.4 The Soaking Experiments	38
3.2 Geochemistry	39
3.2.1 Sorptive Properties of Tuff and Nuclide Transport and Retardation	39
3.2.2 Joint Flow Experiments and Modeling	48
3.3 Thermal Properties	51
3.3.1 Thermal Conductivity	51
3.3.2 Thermal Expansion	58
3.3.3 Heat Capacity and Thermal Diffusivity	63
3.4 Mechanical Properties of Tuffs	64
3.5 Radiation Effects on Tuff	75
3.6 Behavior of Water in Tuff	76
3.6.1 Water Loss by Drying from Welded Tuff	76
3.6.2 In-Situ Tuff Water-Migration/Heater Experiment	79
4. MINE DESIGN WORKING GROUP	85
4.1 Thermal Scoping Studies	87
4.1.1 Spent-Fuel Results	88
4.1.2 High-Level Waste Results	91
4.2 Thermomechanical and Hydrothermal Scoping Studies	92
4.3 Future Studies	96

CONTENTS (cont)

	<u>Page</u>
5. IN-SITU (FIELD) EXPERIMENTS	97
5.1 Underground Rock-Mechanics Laboratory	97
5.2 Nuclide-Migration Field Experiments	97
6. CONCLUSIONS	101
7. UNRESOLVED ISSUES	103
7.1 Water and Joint Effects on Tuff Properties and Models	103
7.2 Sorptive Properties and Transport or Retardation	103
7.3 Creep	104
7.4 Mineralogy and Petrology	104
References	106
APPENDIX A -- Correlation of Sorptive Properties of Tuff with Mineralogy	111
APPENDIX B -- Crushed Rock Columns: A Comparison with Batch Measurements	119
APPENDIX C -- Mine Design	129

ILLUSTRATIONS

Figure

1	Schematic Cross Section Through an Ash-Flow Tuff Cooling Unit with Typical Bulk and Grain Densities	27
2	Generalized Geologic Map of the Yucca Mountain Area, NTS, Showing Positions of Drill Sites UE25a-1 and J-13	28
3	Stratigraphic Section of Test Well J-13 Showing Major Authigenic Phases	29
4	Stratigraphic Section of Drillhole UE25a-1 Showing Major Authigenic Phases	30
5	Cross Section of Units Between Drill Sites UE25a-1 and J-13	31
6	Chemical Variations in Zeolites as a Function of Depth in Drillhole UE25a-1	34

ILLUSTRATIONS (cont)

		<u>Page</u>
7	Thermal Conductivity Versus Grain Density for Phases Occurring in Silicic Tuffs	53
8	Theoretical Variations in Tuff Zero-Porosity Matrix Conductivity as a Function of Postemplacement Mineralogical Reactions	54
9	Extrapolated Zero-Porosity Thermal Conductivity of Measured Tuffs Versus Grain Density	57
10	Average Linear Expansion Coefficient on Tuffs Between Ambient Temperature and 200°C as a Function of Porosity	59
11	Linear Expansion to 500°C to Two Welded Tuffs	60
12	Representative Compressive Stress-Strain Curves for Unconfined Samples with Different Porosities (P)	66
13	Representative Compressive Stress-Strain Curves Showing the Effect of Confining Pressure (20 MPa) on Samples with Different Porosities (P)	66
14	Anisotropy of the Elastic Moduli as a Function of Porosity	67
15	Compressive Strength as a Function of Porosity and Confining Pressure for Air-Dried Samples and a Strain Rate of 10^{-3} s^{-1}	69
16	Brazil Tensile Strength Versus Porosity for Samples of Calico Hills and Tonopah Springs Tuff	70
17	The Effect of Strain Rate and Water Content on the Maximum Compressive Stress of Welded Tuffs	71
18	Coefficient of Friction (35° Saw cut) Versus Displacement Rate for Dry Samples and a Confining Pressure of 10 MPa	74
19	The Effect of Water on Increasing the Coefficient of Friction (35° Saw cut) as the Displacement Rate Decreases	75
20	Results of Drying Welded Tuff at Room Temperature	77
21	Schematic of Models Used to Explain Drying Behavior	78
22	Experimental Hole Array	80

ILLUSTRATIONS (cont)

		<u>Page</u>
23	Schematic of Symmetrical Orientation of the Experimental Holes Around the Heater Midplane	81
24	Vertical Orientation of the Experimental Holes in Relation to the Alcove and G-Tunnel	82
25	Water-Collection Rates for the Heater Hole (HH-1) and Two of the Water-Migration Holes (WM-1, WM-2) as a Function of Julian (J) Days	83
26	Temperature History at Selected Points Through Midplane of Spent-Fuel Canister for ER of 20%, GTL of 75 kW/Acre, and Boiling of Porewater (Ambient Rock Temperature of 55°C)	89
27	Spatial Temperature Distribution Through Midplane of Spent-Fuel Waste Canister (Ambient Rock Temperature of 55°C)	90
28	Time-Temperature History for Three Room Locations for ER = 0.2, GTL = 75 kW/Acre, 100° Boiling, and Saturated Backfill (Ambient Rock Temperature of 55°C)	90
29	Far Field Temperature Profile Along the Vertical Centerline for GTL of 75 kW/Acre	91
30	Effect of Tuff Conductivity on Maximum Canister Temperature (Time = 2 yr, 75 kW/acre, ER = 20%, Ambient Rock Temperature = 55°C)	93
31	Effect of Tuff Conductivity on Maximum Tuff Temperature (Time = 2 yr, 75 kW/acre, ER = 20%, Ambient Rock Temperature = 55°C)	93
32	Peak Floor Temperature vs GTL (Ambient Rock Temperature = 55°C)	94
33	Peak Pillar Centerline Temperature vs GTL (Ambient Rock Temperature = 55°C)	94
34	Temperature Profile Along the Vertical Centerline for HLW and 75 kW/Acre GTL	95

TABLES

<u>Table</u>		<u>Page</u>
1	Ranges of Sorption Ratios	42
2	Values for the Various Argillite Modeling Parameters Determined from the Batch Experiments and Physical Characterizations	51
3	Thermal, Thermogravimetric, and Structural Data for the Most Common Zeolites in Silicic Tuffs	63
4	Mechanical Properties of Tuff from Hole UE25a-1	65

1. EXECUTIVE SUMMARY

This report is the second in a series of briefings to the National Academy of Science's Committee on Radioactive Waste Management dealing with the feasibility of disposal of heat-producing nuclear waste in silicic tuff. This document is an interim status report of ongoing studies of the properties of tuff determined within the framework of the Nevada Nuclear Waste Storage Investigations Project (NNWSI). We discuss properties of tuffs from two locations on the Nevada Test Site; Yucca Mountain and G-tunnel (Rainier Mesa). In particular, the report discusses progress in resolving issues raised during the first briefing to the NAS and, in some cases, raises new issues for future consideration. Regional issues such as seismicity, volcanism and hydrology are not discussed.

Mineralogy and Petrology of Tuffs of Yucca Mountain

Mineralogy and petrology of the Tertiary age Paintbrush and Crater Flat Tuffs of the Nevada Test Site have been described with samples from drill hole UE25a-1 (Yucca Mountain) and test well J-13 (Jackass Flats). Results indicate these units have largely been altered by post-depositional processes which resulted in replacement of original glassy material with crystalline phases.

1. Devitrification, which involves crystallization of glass to feldspar plus cristobalite or quartz during post-emplacement cooling, is the dominant alteration process in densely welded horizons throughout the section.
2. Zeolitization, which results in the formation of hydrous (up to 20% H₂O), low-density silicate minerals

by the interaction of glass with groundwater, occurs at UE25a-1 and J-13 in stratigraphically equivalent horizons: (1) the nonwelded base of the Topopah Springs Member through the nonwelded Bedded Tuffs of Calico Hills (upper horizon), and (2) the nonwelded portion of the Prow Pass Member (lower horizon). High-silica clinoptilolite with $Ca > K > Na$ comprises up to 90% of samples from the upper horizons of both sections, and is also dominant in the lower zeolitized horizon at UE25a-1. At J-13 analcime is dominant in the lower horizon, and forms by replacement of some precursor zeolite, probably heulandite or clinoptilolite. The lower part of the Bullfrog Member in J-13 (not reached in drill hole UE25a-1) also contains minor analcime.

3. Stratigraphic units are thinner at J-13 than at UE25a-1; this is most likely due to the greater distance of J-13 from source areas rather than paleotopography. Differences in authigenic phases in the two sites are probably due to the greater depth of the J-13 hole, different hydrologic settings, or some combination of these factors.

Geochemistry - Sorptive Properties of Tuffs

Sorption varies with the lithology of tuff and, in some cases, with the atmosphere (oxidizing or nonoxidizing-nitrogen). Tuff samples being studied range from those containing significant percentages of zeolites to others which are devitrified and contain mainly feldspars and silica minerals with little or no zeolites, as well as those containing clays. The most significant results to date indicate that:

1. Cesium, strontium and barium generally sorb better on zeolitized tuff (2000 to 130,000 mL/g) than on

devitrified tuff (50 to 1500 mL/g). No atmospheric effects were observed.

2. Plutonium sorbs moderately well (50 to 150 mL/g) in air on both zeolitized, devitrified, clayey tuffs. Sorption ratios in a nitrogen atmosphere are high (>600 mL/g) for zeolitized tuff and moderate to high (100 to 600 mL/g) for devitrified tuff.
3. Sorption ratios for americium and the lanthanides cover a rather large range and do not correlate with mineralogy except that sorption appears highest for a tuff containing clay. The chemistry of the actinides and lanthanides in groundwaters is complex and poorly understood and a significant effort will be necessary to achieve proper understanding and adequate prediction of transport behavior.
4. Sorption of anionic species - iodine, technetium, and uranium which is complexed by the carbonate in the groundwater - is quite low (<25 mL/g) for all tuffs studied. Sorption of technetium and uranium was somewhat higher in a nitrogen atmosphere.
5. Simple equilibrium cannot adequately explain the observations. Sorption ratios are generally lower for batch determinations than desorption ratios. The values tend to agree within a factor of two for ions of strontium, cesium, and barium which are thought to sorb and desorb predominantly by an ion exchange mechanism. For the lanthanides, actinides, technetium, and uranium the values may differ by more than an order of magnitude. The "irreversible" sorption or much slower desorption may be due to speciation changes, diffusion into minerals, crystallization reactions on solids, or

non-ionic sorption of colloids or precipitates. These possibilities require further investigation.

6. Migration rates determined from flow experiments in columns containing crushed tuff are sometimes faster than values predicted from batch experiments with the same material.

Joint Flow Experiments and Modeling

We are modeling nuclide transport through jointed media. The experiments use rock columns containing a single, artificial (saw cut) fracture. Presently, the analyses indicate that the important parameters controlling radionuclide transport along fractures are intergranular porosity and penetration depth, fracture aperture, fracture length, fluid velocity and sorption distribution coefficient (including those factors that control sorption).

Thermal Conductivity/Expansion

Because of the mineralogical variability of tuff and the need for near- and far-field thermal and thermomechanical modeling, considerable effort has been aimed at understanding the thermal properties of tuff. We have developed a means of predicting the minimum theoretical matrix thermal conductivity of tuff based on the grain density (which incorporates the mineralogical variations). By including the porosity (either saturated or dry), the conductivity of a broad range of tuffs can be routinely predicted to 15% or better.

The thermal expansion measurements have been limited to ambient pressure studies. Results to date indicate that:

1. The thermal expansion of devitrified welded tuffs is generally linear with temperature and independent of

both porosity and heating rate. The only mineralogic factors affecting expansion behavior were the presence or absence of cristobalite and altered biotite. The presence of cristobalite causes markedly nonlinear expansion above 200°C. The altered biotite causes contraction at the boiling point of water followed by expansion at higher temperature.

2. The behavior of the nonwelded tuff is complex, but in general is characterized by thermal contraction. The contraction appears to be a function of complex dehydration reactions, probably of zeolite (clinoptilolite, heulandite), hydrated glass, and/or clay.

Mechanical Properties

To date, the mechanical property studies have concentrated on ambient temperature properties. Particular emphasis has been placed on the effects of confining pressure, water content, joints, and, recently, strain (displacement) rate. Results indicate that:

1. A clear relation between strength (compressive and tensile) and porosity (degree of welding) has been demonstrated. Welded tuff (low porosity) is as much as 3 times stronger than the nonwelded tuff (high porosity).
2. Water content plays a significant role in the strength of tuff. The compressive strength of dry welded tuff is about 25% greater than for saturated samples tested under the same conditions.
3. We have observed anisotropy in the elastic moduli of tuffs. The welded tuff is stiffest perpendicular to bedding while the nonwelded tuff is stiffest parallel

to bedding. This may have an impact on the mechanical modeling of tuffs.

4. Preliminary compression tests at 200°C on welded and partially welded tuff show a 30% decrease in strength compared to room temperature data.
5. Both saturated and dry samples of welded tuff show an approximate 6% decrease in compressive strength per decade of decrease in strain rate (for rates from 10^{-2} to 10^{-6} s⁻¹).
6. The coefficient of friction of artificial fractures in welded tuff is dependent on water content and displacement rate. It is about 9% higher for saturated samples than for dry samples (at a displacement rate of 10^{-6} cm/s). The coefficient increases as the displacement rate decreases. The effect is greater for saturated samples than for dry samples.

As just described, we have demonstrated a very strong strain (displacement) rate effect but we have not performed any creep tests. Such tests are in this year's (FY80) program plan and should be underway shortly.

Water Loss by Drying from Welded Tuff

Initial studies of water loss from welded tuff have been performed in an attempt to understand such phenomena in canister holes, mine shafts, and pillars when exposed to a drying atmosphere. The effect is important because of the difference in properties between saturated and dry rock and in the potential migration of water into the waste canister holes. The studies have shown that significant drying of small samples can occur within a period of days (90% of the water lost within 72 hours). A model developed for these experiments is consistent with water loss via vapor diffusion (not Darcy flow) through the pores of the rock.

In-Situ Tuff Water-Migration/Heater Experiment

The behavior of water in the welded tuff around a heat-producing waste canister was one of the issues raised before the NAS during the initial briefing. An in-situ experiment designed to assess the water response to a thermal source in a deep underground environment is in progress. In addition, the experiment provides support for computer code and instrumentation development, and attempted to measure in-situ rock thermal properties. Developmental instruments in this experiment included remote stress gauges, relative humidity gauges and a laser interferometer for measuring rock displacement.

Water was collected continuously during the heating phase (63 days) of the experiment in the heater hole (~60 liters) and in two (1.5 and 3.6 liters) of the three satellite water collection holes. Water generation ceased abruptly when the heater power was shut off. Preliminary analysis suggests that, in the immediate vicinity of the heater hole, water movement is by vapor diffusion into the hole. Water migration into the satellite holes appears to be by Darcy flow driven by the high partial pressure of water at the vaporization front. Posttest activities are in progress.

Mine Design Working Group

A Mine Design Working Group was established as a focus for the tuff properties studies. The objectives of the working group are to identify model needs and critical data needs, to develop conceptual test plans for in-situ experiments, to define the environment for a repository in welded tuff above and below the water table, and to integrate the results into a data base for a conceptual repository design. The Mine Design Working Group is composed of representatives from Sandia National Laboratories, Los Alamos Scientific Laboratory, RE/SPEC, Inc., and Texas A&M University.

To date, a series of thermal scoping studies has been completed for spent fuel and reprocessed high-level waste. Input parameters include boiling conditions and the property changes due to boiling, gross thermal loading, canister pitch and extraction ratio. Near- and far-field calculations were performed. Examples are presented in this report. The results of the thermal studies are used as input for the thermomechanical calculations currently underway.

Rock-Mechanics Laboratory in G-Tunnel

An underground rock mechanics laboratory is currently in planning to support the Mine Design Working Group activities. The working group will formalize the plans for in-situ experiments to study rock mass properties, test analytical models, and evaluate the application of laboratory data to a field experiment.

Nuclide-Migration Experiment in G-Tunnel

We (with Argonne National Laboratory) have begun a 3.5 - 4 year experiment to study nuclide migration in a single fracture in an underground environment. The experiment will be carried out in the Tunnel Beds formations in G-tunnel. These units are composed of high porosity, low permeability bedded tuffs.

The fundamental question being addressed is: If the physical and chemical properties of a rock and a solution are measured in the laboratory, can accurate predictions of nuclide migration through that rock in the field be formulated? The major features of the experiment include a laboratory program to characterize the rock and the groundwater in order to predict the nuclide migration behavior, detailed characterization of the field site (matrix permeability, fracture permeability, fracture aperture, mineralogy, etc), two fracture flow experiments - one "cold" (non-radioactive or short-lived nuclides) and one "hot" (radioactive nuclides), and detailed post flow analyses of the rock involving removal of the

entire fracture flow path. Two flow experiments are required because we intend to use actinides in the "hot" experiment. The cold experiment is to demonstrate the safe handling procedures and mineback and fracture recovery techniques as well as the experimental method itself.

Other Studies

Two other studies are in progress but have not produced any results yet.

- Soaking Tests. A series of long-term, exploratory, hydrothermal experiments are underway to identify possible mineral alteration and to determine what changes result in the thermal/physical and chemical properties due to these alterations.
- Radiation Effects Studies. A series of total dose gamma radiation exposure tests are in progress to determine the effects of radiation on the properties of dry and saturated welded tuff.

2. INTRODUCTION

This report is the second in a series of status reports to the National Academy of Science's Committee on Radioactive Waste Management dealing with feasibility of long-term isolation of heat-producing nuclear waste in silicic tuff as part of the Nevada Nuclear Waste Storage Investigations (NNWSI) Project. The first report, late in 1978, summarized the relatively young program established to evaluate tuffs on the Nevada Test Site (NTS). During that meeting and in the letter following from Chairman E. F. Gloyna,¹ several issues were identified regarding the suitability of tuff as a repository medium. These issues are:

- a. The behavior of the potentially large quantities of water (up to 40 vol%) in tuffs
- b. Radionuclide sorption properties of tuff--zeolitized and nonzeolitized
- c. Stability of tuff in the presence of hot electrolyte solutions
- d. Interactions between tuff, water, and waste (including canister, overpack, and engineered barriers)*
- e. Seismic and volcanic factors
- f. Hydrology
- g. Ability to characterize and model complex bodies and media
- h. Resource conflict potential

This document is an interim status report of ongoing studies on the properties of tuff. It is supported by several published reports and unpublished memoranda that are attached for the Committee's use. In it we will discuss, however briefly, the effects of water on the properties of tuff (Items a, c, and d); the sorptive properties of tuff (Item b); and

*Our parentheses

property variation and initial modeling attempts (Item g). In addition, although not specifically mentioned previously, the effects of joints caused by cooling or tectonic activity on the properties of tuff are included where applicable. The report will not discuss area seismicity, volcanism, hydrology, or resource potential (Items e, f, and h).

At first glance, this report presents a series of independent studies on tuff. In fact, a Mine Design Working Group has recently been established as a focus for the properties studies. The group is composed of representatives from Sandia National Laboratories, Los Alamos Scientific Laboratory, Re/Spec, Inc., and Texas A&M University. The Mine Design Study uses the data and existing (or developing) state-of-the-art models to predict the response of tuff to individual mine openings and waste loadings representative of a repository. As a consequence, deficiencies in laboratory data, in-situ experiment needs, and model limitations are identified for each of the individual activities. The ultimate goal is assembly of an information base which will allow confident conceptual design of a repository in welded tuff. Characteristics of that design could lead to a decision whether or not tuff is a suitable repository medium.

Tuff from two locations--Yucca Mountain in the southwest quadrant of the NTS and G-tunnel in the north-central region of the NTS--are being used in the current studies. Only Yucca Mountain is presently considered a potential repository location. The value of G-tunnel is that it offers a supply of tuff not limited by core availability (limited range of lithologies) and it is a deep (~400 m), underground facility suitable for generic in-situ experiments.

In this report, we discuss mineralogy and petrology, sorption transport behavior, thermal properties, mechanical properties, radiation studies, and water behavior in tuff. In addition, initial results of the Mine Design Study are presented and three in-situ experiments are discussed. Each section includes a brief description of the study, examples of the significant results, and a description of future work. Because of the wide variability in mineralogy and porosity of tuffs, the studies constantly attempt to correlate these variables with the properties measured.

3. TUFF PROPERTIES

3.1 Mineralogy and Petrology

3.1.1 General Description (J. R. Smyth and M. L. Sykes, LASL)

Tuff is a geological term for rocks composed principally of indurated volcanoclastic material. Such rocks may be deposited either directly by explosive volcanic events, or they may be reworked and redeposited by surface processes. Because silicic volcanism (e.g., rhyolitic) tends to be more explosive than the eruption of more mafic magmas, silicic tuff tends to be much more voluminous and widespread than basaltic tuff despite the much greater volumes of basaltic volcanic rocks on a global scale. In the western United States, particularly in the Basin-and-Range physiographic province, accumulations of tuff locally exceed 3000 m in thickness, and individual units may be tens of kilometres in lateral extent. Our understanding of these rocks has increased greatly over the past 20 years due in large part to the work of Smith^{2,3} and Smith and Bailey.⁴

Eruptions of silicic magmas vary in volume from a few cubic kilometres to massive, catastrophic events depositing hundreds of cubic kilometres of ash and lava in a single eruptive event. On eruption, silicic magmas most commonly contain <10% primary crystals (phenocrysts), and incorporate <10% lithic fragments, so that generally >80% of the material deposited is glass. Eruption may occur as a relatively small, quiescent flow of very viscous lava that commonly quenches to form an obsidian. However, in large eruptions, the great majority of material is ejected explosively as fine ash, shards, and pumice because of the high viscosity and high volatile content of silicic magmas.

Large explosive eruptions commonly begin with ejection of pumice, shards, and ash that are deposited downwind of the vent as a cool, unsorted layer of low-density material termed an air-fall or ash-fall deposit.

As eruption proceeds and increases in intensity, clouds of incandescent ash propelled by evolving gases are formed over the vent and collapse down-slope, depositing heated material in thick blankets. It is this latter type of deposit that is volumetrically most significant. As eruption then proceeds, the rocks overlying the magma chamber collapse to form a caldera, which may then also fill with thick sequences of volcanoclastic deposits. Materials deposited above $\sim 500^{\circ}\text{C}$ will compact and weld by viscous deformation of the glass. Compacted material that cools rapidly (i.e., weeks to months) may remain glassy, while that which cools more slowly will crystallize to cristobalite, quartz, and a mixture of feldspars.

The net result is a complex deposit up to several hundred metres thick, which has cooled as a single unit, and is commonly referred to as a cooling unit. A schematic cross section through this type of deposit is given in Figure 1. Such a deposit commonly has a core of welded material, most of which may have devitrified (i.e., crystallized) to quartz and feldspar plus or minus cristobalite. At the base of the welded zone there is commonly a layer of densely welded material that has not crystallized, but that remains a dense glass called a vitrophyre. Welding decreases outward from the core so that the welded zone is surrounded by zones of material decreasing in density, thermal conductivity, coherence, and strength. Commonly at the base of the ash-flow deposit is an unsorted, nonwelded, horizon of loosely aggregated pumice and ash called the air-fall unit. Because the surface material is also loosely aggregated, it is readily reworked by surface processes and may be redeposited by streams and ponds or by volcanoclastic mudflows (lahars). Such processes give rise to sorted, bedded deposits called bedded tuff.

Because glass is thermodynamically unstable, it commonly alters to various crystalline phases. At elevated temperatures quartz, cristobalite, and feldspars crystallize, as found in welded zones. If porosity is high and water of suitable composition is present, glass may alter completely to zeolites in as little as 10,000 years⁵ even at temperatures below 100°C . If such water is not present, or if the porosity is low as in vitrophyres, alteration will not occur and the material may remain glassy for millions of years. There is no evidence that material once

crystallized to quartz and feldspar will later alter to zeolites under conditions common in these rocks, although feldspars may alter slowly to clays particularly in the presence of acid groundwaters.

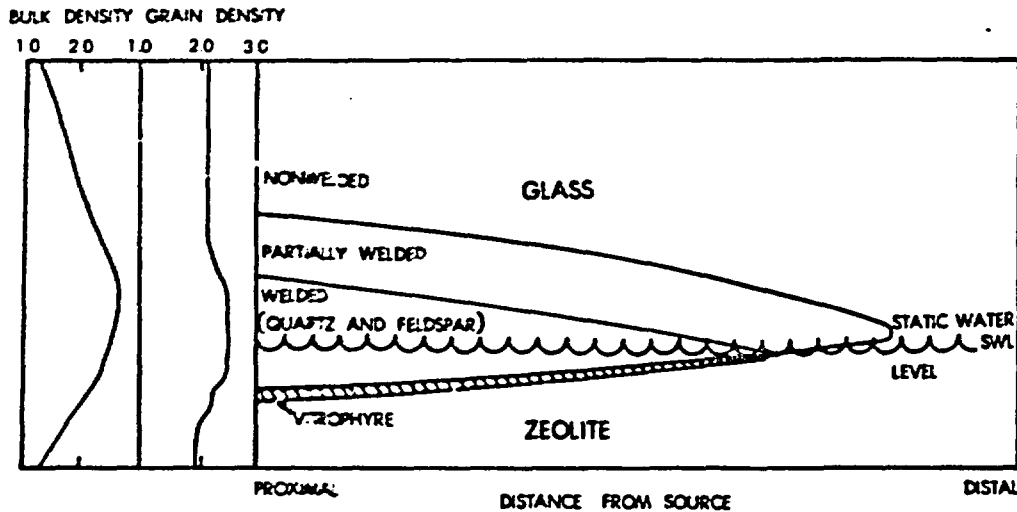


Figure 1. Schematic Cross Section Through an Ash-Flow Tuff Cooling Unit with Typical Bulk and Grain Densities

3.1.2 Location-Specific Studies

3.1.2.1 Yucca Mountain (M. L. Sykes and J. R. Smyth, LASL)

a. General — Characterization of tuff units (at NTS) under investigation as potential repository media began in 1977 with studies of core recovered from water-well Drillhole J-13 (Test-well 6) near Forty-Mile Wash in western Jackass Flat (Figure 2). This drillhole extends to a depth of 780 m and penetrates the Tiva Canyon and Topopah Spring Members of the Paintbrush Tuff, the Bedded Tuff of Calico Hills, and the Bullfrog and Prow Pass Members of the Crater Flat Tuff. Detailed petrographic descriptions of the units are given by Heiken and Bevier.⁶ The mineralogy and some physical properties of the units are outlined in Figure 3. The units under investigation represent an extreme range of lithologies, and physical properties and data should be relevant to most sites in silicic tuff.

In the summer of 1978, Drillhole UE25a-1 was drilled to a depth of 700 m in the western margin of NTS on the eastern flank of Yucca Mountain. The locations of the two holes are shown in Figure 2. This drillhole penetrated essentially the same units as J-13. Detailed petrographic descriptions of the units are given by Sykes et al,⁷ and the mineralogy and properties of the various units are outlined in Figure 4. A schematic cross section through the two holes is given in Figure 5. A drillhole to a planned depth of 1829 m (6000 ft) ~1 mi west of UE25a-1 is currently under way.

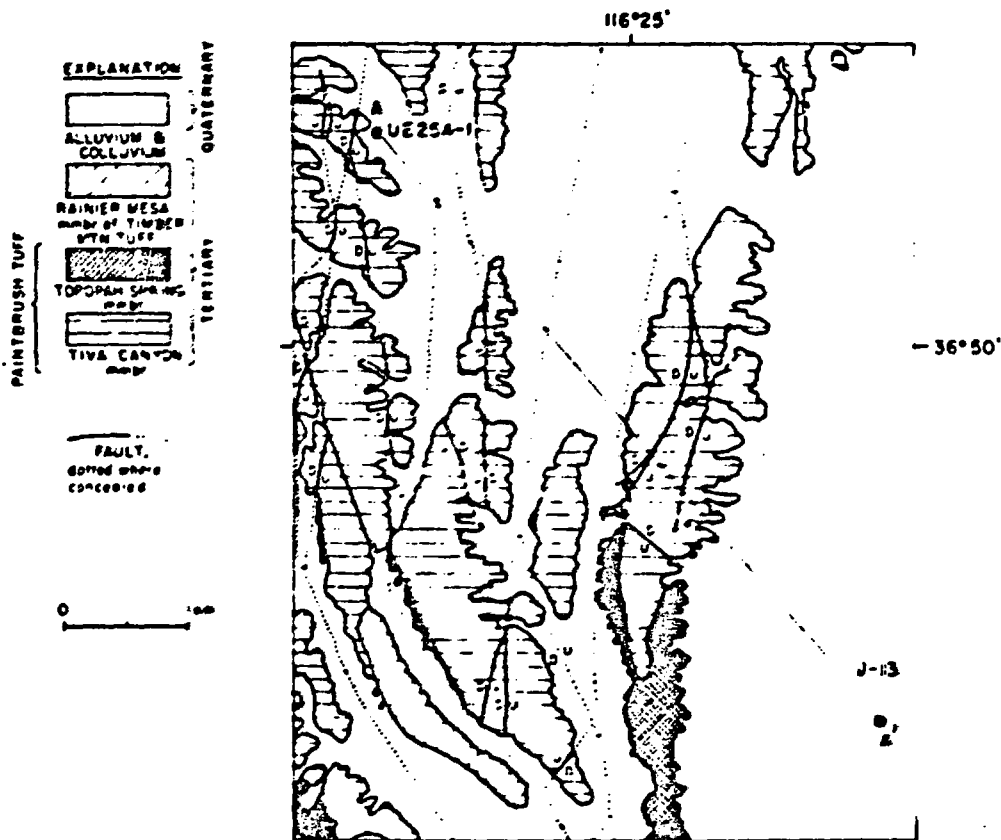


Figure 2. Generalized Geologic Map of the Yucca Mountain Area, NTS, Showing Positions of Drill Sites UE25a-1 and J-13 (after Lipman and McKay⁸)

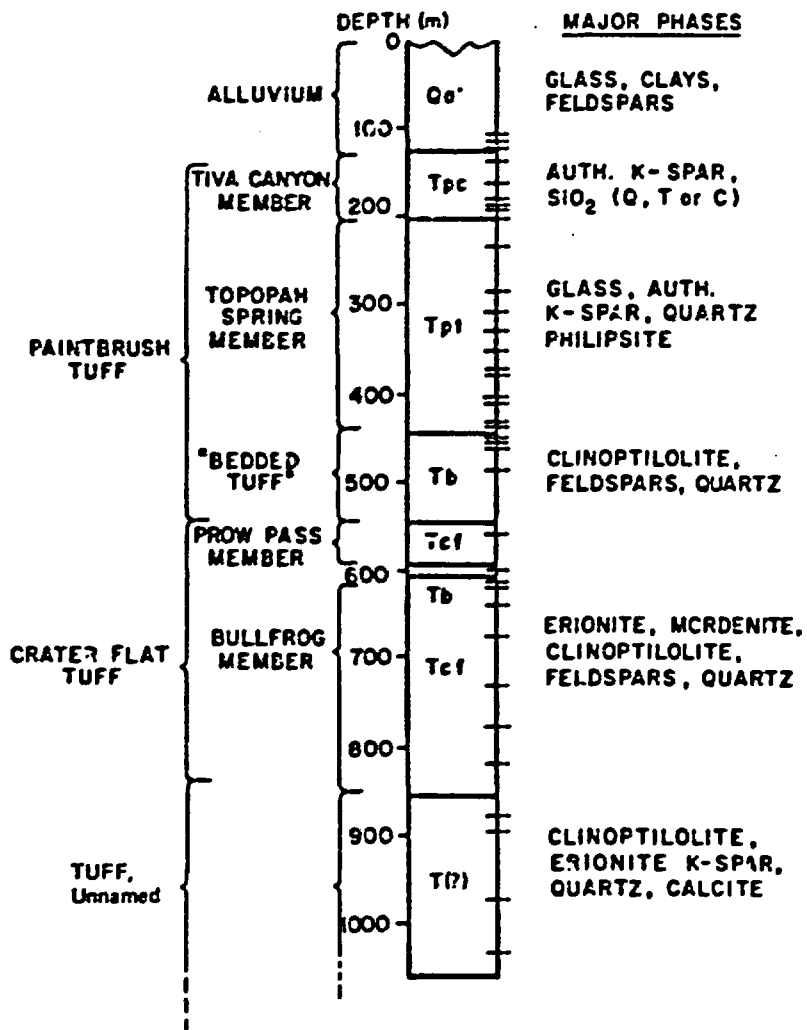


Figure 3. Stratigraphic Section of Test Well J-13 Showing Major Authigenic Phases

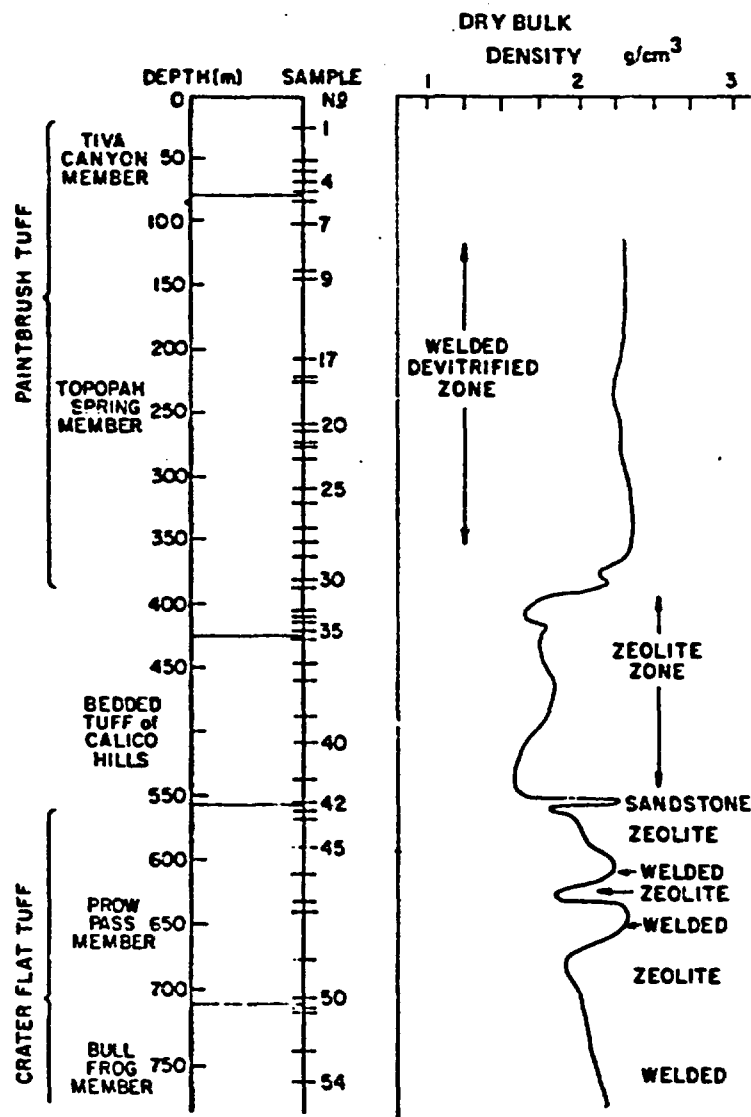


Figure 4. Stratigraphic Section of Drillhole UE25a-1 Showing Major Authigenic Phases

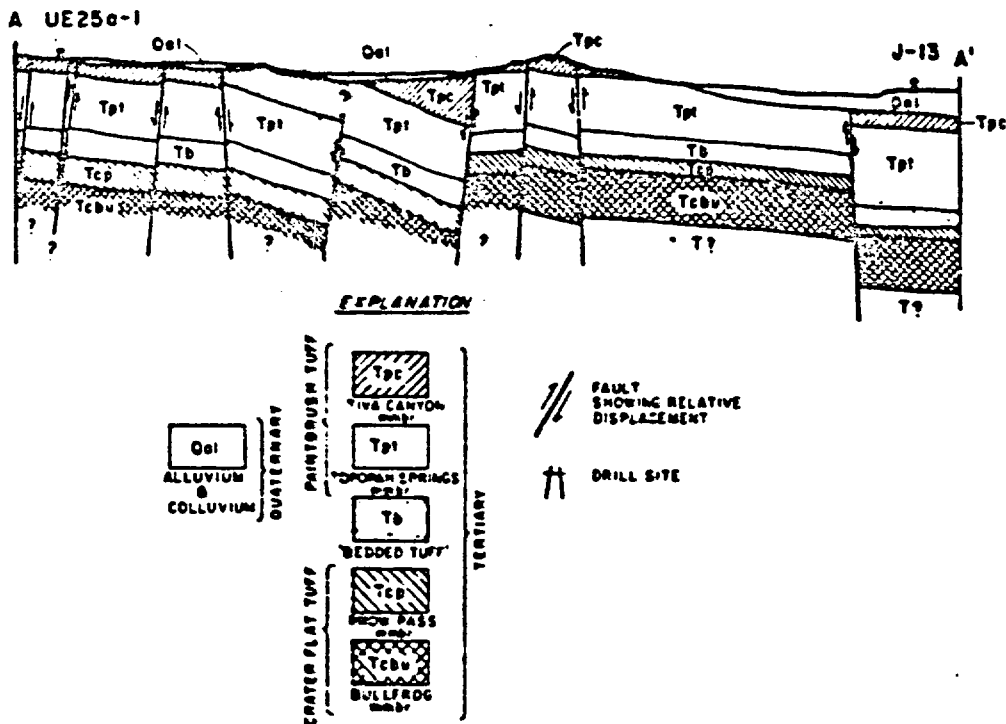


Figure 5. Cross Section of Units Between Drill Sites UE25a-1 and J-13⁷ (See Figure 2 for location of A and A'.)

b. Stratigraphy — Distinct changes in thickness and authigenic phase mineralogy occur between Drillholes UE25a-1 and J-13 (see Figures 3, 4, and 5), although these sites are only about 6.1 km (3.8 mi) apart (Figure 2). Thickness variations may be caused either by thinning away from source areas or paleotopography. Differences in authigenic phase mineralogy are more difficult to interpret, but hydrologic setting is probably an important factor.

(1) Unnamed Tuff Unit Below the Crater Flat Tuff -- This gray-green, nonwelded, ash-flow tuff is the oldest unit encountered and is penetrated only at J-13. Total thickness is unknown but exceeds 205 m. The 10 to 14% phenocrysts consist mostly of sanidine, plagioclase, and resorb-ed quartz, with minor biotite, hornblende, and opaques. Lithic fragments of rhyolitic glass and altered andesite and welded tuff increase from 5 to 12% with depth. Authigenic feldspar and quartz with minor

clinoptilolite and analcime (both zeolites) replace glass in abundant pumice pyroclasts. Clinoptilolite also occurs as vug filling as does calcite; the latter is also pseudomorphous of some plagioclase crystals.

Correlation of this unit with known, mapped tuff units has not been possible due to limited data. Petrographically it is somewhat similar to the Redrock Valley Tuff.^{9,10} Alternatively, it may correspond to the Fraction Tuff,¹¹ or may be a previously unrecognized unit of the Crater Flat Tuff.¹²

(2) Crater Flat Tuff

(a) Bullfrog Member -- This gray, biotite-rich, largely welded ash-flow tuff is the oldest unit encountered at UE25a-1. Fifty one metres of the Bullfrog Member were penetrated at UE25a-1 without going through the unit, compared to a total thickness of 250 m at J-13. The 10 to 20% phenocrysts include sanidine, plagioclase, quartz, biotite, and magnetite. Occasional xenocrysts of mafic phases, now altered to phlogopite plus hematite, also occur. Lithic fragments of welded tuff and rhyolitic glass are concentrated near the base of this member at J-13, but otherwise are rare.

At J-13, authigenic phases replacing pyroclasts in the lower part of the Bullfrog Member consist primarily of fibrous to spherulitic quartz and K-feldspar with minor erionite (zeolite). Analcime occurs in addition to the above in the upper part of the member. At UE25a-1 the primary mode of alteration is granophyric devitrification to K-feldspar plus quartz, which obscures relict textures. No zeolitization is observed.

An immature coarse sandstone interbedded with thin air-fall layers occurs between the Bullfrog and Prow Pass Members of the Crater Flat Tuff at J-13.

(b) Prow Pass Member -- This vitric-crystal tuff consists of a lower nonwelded sequence of thinly bedded air-fall and ash-flow

deposits and an upper welded ash-flow deposit. Thickness varies from 152 m at UE25a-1 to 50 to 60 m at J-13. Phenocrysts of sanidine, resorbed quartz, and plagioclase, with minor anorthoclase, biotite, pyroxene, and magnetite make up 18 to 20% of J-13 samples. At UE25a-1 crystal content varies from 5 to 8% in nonwelded samples, to 10 to 14% in welded samples. Lithic clasts of altered welded tuff and mudstone vary from <1% to 5% in abundance.

At J-13, nonwelded tuffs are altered to analcime + quartz + K-feldspar with minor clinoptilolite. The upper welded zone consists predominantly of finely crystalline authigenic quartz and K-feldspar with minor analcime and clinoptilolite. Calcite is pseudomorphous of some plagioclase phenocrysts. At UE25a-1 the nonwelded zone is also zeolitized, but the dominant phase is high silica Ca, Na-clinoptilolite as defined by Boles.¹³ Variations in zeolite composition and mineralogy with depth for UE25a-1 are shown in Figure 6. Welded samples are devitrified to feldspar and quartz; vapor-phase crystallization occurs as coarse vug lining or fillings.

(3) Bedded Tuff of Calico Hills

This complex unit consists of a sequence of bedded, air-fall and ash-flow tuffs, and volcanoclastic sediments. Thickness varies from 141 m at UE25a-1 to 95 m at J-13. At J-13 this unit has been called the Indian Trail Formation¹⁴ but is now correlated with the Bedded Tuff of Calico Hills.¹⁵

A very immature feldspathic sandstone (litharenite) occurs at the base of the Calico Hills. Clasts consist predominantly of lithic fragments of devitrified or zeolitized tuff, perlite, and flow rocks and crystals (andesine, biotite, and magnetite). Calcite fills fractures and is pseudomorphous of some plagioclase crystals.

In the nonwelded bedded tuffs the 2 to 16% phenocrysts include oligoclase, sanidine, quartz, and occasional biotite. Lithic clasts of altered welded tuff and flow rocks comprise 3 to 9% of samples.

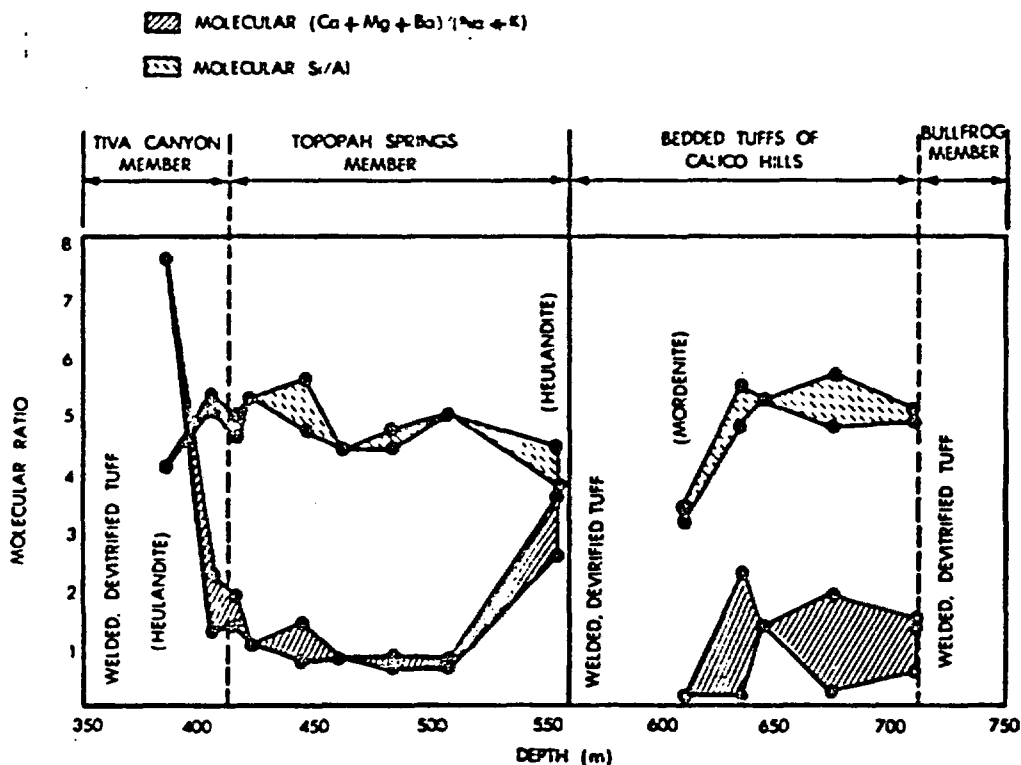


Figure 6. Chemical Variations in Zeolites as a Function of Depth in Drillhole UE25a-1. (All zeolites are classified as clinoptilolite except where noted.)

At UE25a-1 the upper 50 m of tuff is zeolitized to clinoptilolite. Below 50 m minor silicification of the matrix accompanies zeolitization, and K-feldspar and quartz occur as vug linings and fillings. Authigenic phases in the limited Calico Hills samples from J-13 are similar to those at UE25a-1, with the exception of the presence of minor analcime.

(4) Paintbrush Tuff

(a) Topopah Springs Member -- The geology and petrology of this compositionally zoned ash-flow tuff has been described by Lipman, et al.¹⁶ Welding variations are typical of thick, compound cooling units: the nonwelded base grades upward into a densely welded vitrophyre overlain by a thick sequence of devitrified welded tuff. Thickness varies

from 333 m at UE25a-1 to 240 m at J-13. Crystal content varies from <1% at the base to 17% near the top; phenocrysts include sanidine, plagioclase, and lesser amounts of quartz, biotite, and opaques. Lithic fragments of welded tuff, perlite, and chert comprise up to 12% of the non-welded base but are generally scarce in the upper welded zone.

The uppermost densely welded zone and basal vitrophyre are nearly unaltered; glass is of dacitic to rhyolitic composition, respectively. The rest of the upper welded zone is extensively devitrified to fibrous/spherulitic or granular intergrowths of feldspar and cristobalite. Vapor-phase crystallization and lithophysal cavities are developed variably.

The shallowest occurrence of zeolite in the drillholes is at ~385 m depth in UE25a-1 and ~400 m depth in J-13. Heulandite here occurs as fracture filling and minor vug lining in the basal vitrophyre of the Topopah Springs. The lower nonwelded tuffs are extensively zeolitized to clinoptilolite. Very minor amounts of phillipsite and erionite occur in J-13 samples at depths of 340 and 360 m, respectively.

An epiclastic, immature sandstone occurs between the Topopah Springs and Tiva Canyon Members at J-13. Volcanic lithic fragments and mineral grains rest in a matrix of dark-brown clay; authigenic K-feldspar, silica, and calcite fill voids.

(b) Tiva Canyon Member -- This youngest unit encountered consists of a lower bedded, air-fall tuff and an upper ash-flow tuff. This member is only 64 m thick at UE25a-1 and 80 m at J-13, corresponding to the lowermost crystal-poor sanidine and hornblende-bearing zone of Byers et al.⁹ Presumably erosion has removed the upper parts of this member; 9 m of alluvium cover it at UE25a-1 and ~125 m at J-13.

The bedded tuff and basal nonwelded ash-flow tuff contain ~11% and 14%, respectively, phenocrysts of plagioclase, sanidine, biotite, magnetite, and orthopyroxene. The upper welded ash-flow tuff contains <5% sanidine, magnetite, plagioclase, hornblende, and sphene.

Lithic fragments, usually of altered welded tuff, make up 2 to 6% of nonwelded samples and are virtually absent in welded zones.

Authigenic phases in the nonwelded portion of the Tiva Canyon Member are predominantly montmorillonite plus opal/cristobalite that outline still-glassy pyroclasts. Welded samples are devitrified to very fine fibrous/spherulitic or granular intergrowths of alkali feldspar and cristobalite. Vapor-phase crystallization occurs as coarse vug linings or fillings.

3.1.2.2 G-Tunnel (A. R. Lappin, SNL)

a. General -- The U12g tunnel (G-tunnel) complex is at a depth of ~400 m below Rainier Mesa in the north-central region of the NTS. The welded portion of the Grouse Canyon Member of the Belted Range Tuff lies above G-tunnel with only the basal portion partly exposed in the ceiling. The unit strikes approximately N30E and dips 7° northwest. Several fully cored holes have been drilled in the welded tuff in order to characterize the formation.

Characterization studies have included determination of formation thickness (12.5 m), mineralogy, and joint properties for comparison with the wall-mapping result. Joint properties such as frequency, orientation, width, morphology, mineralogy, and predictability have been studied. Downhole TV scans were correlated with core observations.

Four major joint sets were identified. In general, the formation is highly fractured. The joint frequency depends upon the measurement method and increases with method in the following order: tunnel wall mapping, downhole TV scan, and core determination. Core indices (a measure of core integrity) ranged from 30 to 100. Many of the joint surfaces are mineralized, and intense argillization was observed in several of the fracture zones. These zones are apparently water-transmissive.

b. Stratigraphy -- The tuff is composed almost entirely of feldspars and silica polymorphs (quartz + cristobalite). Vitric material is

noted only occasionally in the basal vitrophyre. Phenocryst phases reported from within the Grouse Canyon include sodic sanidine, anorthoclase, and quartz, with the sanidine dominant. Widespread accessories include fayalite, apatite, zircon, and sodic Fe-pyroxene.¹⁷ The tuff is rarely zeolitized. Devitrification textures are common, but not masked by growth of authigenic phases. The welded tuff, which lies at least 200 m above the water table,¹⁸ contains 13 to 25 vol% porosity and is >85% saturated with perched water.

3.1.3 Zeolite Stability Studies (J. R. Smyth and M. L. Sykes, LASL)

The thermal stability of tuff plays an important role in affecting bulk physical properties through such processes as dehydration and mineral breakdown reactions.

Devitrified welded tuff and zeolitized nonwelded tuff may be considered as end members with respect to thermal stability. Devitrified welded tuff may contain as little as 1 to 2 wt% adsorbed (loosely bound) water; constituent phases are mostly anhydrous and stable to high temperature. Nonwelded tuff may contain >80% zeolite, which can have up to 18% structural water plus several percent adsorbed water and are thermodynamically unstable at relatively low temperatures. Thus, zeolitized nonwelded tuffs are of particular interest, due to their potential high water content and potential mineralogical instability.

The most abundant zeolite in samples studied is clinoptilolite, which is isostructural with t-ulanite but with sodium and potassium as the dominant cations rather than calcium. Heating of cored samples containing 30 to 80% clinoptilolite to 200°C under ambient pressure, produced 7 to 10 wt% water loss, respectively, and volume decreases of up to 1.3%. Heating these same samples to 400°C produced further losses of 2 wt% water and 1% in volume. (Note that both of these temperatures are well above those expected in nonwelded units surrounding a repository.) These weight and volume changes are reversible. X-ray diffraction analyses indicate retention of structural integrity at 400°C despite reversible decreases in unit cell volume of up to ~10%. These results are compatible with those

of Boles,¹³ who determined that thermally induced contraction is reversible below 700°C for clinoptilolite and 350°C for heulandite. Supplementary data on type (i.e., adsorbed or structural), amount, and temperature of water loss through dehydration will be obtained from experiments planned to measure hydrogen and oxygen isotopic contents of zeolitized tuffs.

The second most-abundant zeolite present in studied samples is analcime, which forms by reaction of groundwater with less stable zeolites such as clinoptilolite at low temperatures. Analcime may itself break down to form feldspar + quartz at temperatures and pressures as low as 200°C and 1000 bar.¹⁹

These breakdown reactions, as well as dehydration of zeolites, result in the formation of denser, less hydrous phases. Thermal effects in zeolitized tuff could potentially cause volume loss leading to shrinkage fractures, and evolution of water vapor. Further work is under way to quantify the thermal stability of zeolites such as clinoptilolite and analcime at both atmospheric and higher pressures.

3.1.4 The Soaking Experiments (P. M. Halleck and J. D. Blacic, LASL)

The hydrous nature of zeolites and their relatively low-temperature stability indicate that the breakdown reactions and dehydration effects should be greatly dependent on water pressure. Further, the kinetics of reactions between silicates at temperatures <500°C cause reactions to be very sluggish and difficult to observe and characterize. The water-pressure dependence of these reactions is currently being investigated in a series of long-duration heating experiments under separately controlled conditions of confining (lithostatic) and pore (hydrostatic) pressures. These experiments are exploratory in nature, and the results will be used to plan any necessary subsequent experiments.

Two tuff types representing limiting lithologies have been selected for these studies: densely welded, devitrified Topopah Springs and non-welded zeolitized Bedded Tuff of Calico Hills. The former consists almost

entirely of quartz, cristobalite, and alkali feldspar and has a porosity of <5%, while the latter consists of >80% clinoptilolite with minor amounts of quartz and feldspar and has a porosity >20% (by volume). The samples are being exposed to three temperatures, 50°, 150°, 250°C, for 6 mo under two pressure regimens. The first pressure regime simulates a burial depth of 500 m, and above the static water level with a confining pressure of 100 bars (10 MPa) and a pore pressure of 5 bars (0.5 MPa). The second simulates a burial depth of 1000 m, 500 m below the water table, with a confining pressure of 200 bars (20 MPa) and a pore pressure of 50 bars (5 MPa). Before and after heating, the following measurements will be made on each sample: mineralogy and petrology (X-ray and thin section), thermal expansion, thermal conductivity, permeability, compressive strength, tensile strength, density, and porosity.

3.2 Geochemistry

3.2.1 Sorptive Properties of Tuff and Nuclide Transport and Retardation (K. Wolfsberg, LASL)

The most likely processes for release of nuclides from a deeply buried repository to the biosphere involve breaching of the repository by groundwater, attack of the container and the waste form by the water with consequent dissolution or dispersion, and nuclide transport by the water through engineered barriers and geologic formations. An important reason for the consideration of tuff as a geologic medium for isolation of radioactive wastes is the presence of highly sorptive minerals in many lithologic types of tuff, which together with long hydrologic flow paths typical of the NTS region,²⁰ should provide an excellent natural barrier to radionuclide migration to the biosphere. This section summarizes completed work, work in progress, and planned work to understand mechanisms of sorption on tuff and of transport and retardation of nuclides in tuff. Details of this work can be found in Reference 21 and 22. Sorptive properties of tuff are compared to those of granite and argillite from NTS in References 23, 24, and 25.

Sorptive properties of tuff are being investigated both by batch techniques, in which crushed rock is shaken with groundwater under

appropriate and controlled conditions, and by dynamic techniques, in which water flows through crushed or solid rocks, the latter of which may or may not contain natural or artificial fractures. Although the dynamic methods of study more closely approximate the flow of water and transport of nuclides in geologic formations, the number of such studies is limited by equipment requirements and the time necessary for each study. Batch measurements are relatively easy and fast. They allow for intercomparison of many experiments and reveal the effects of numerous variables. Variables investigated thus far with batch techniques include lithologic type of tuff, nuclide or element studied, rock particle size, temperature, time, atmosphere, and composition of groundwater.

The distribution coefficient K_d is conventionally used to define the distribution of activity between a solid and liquid phase at equilibrium. We use a similar quantity, the sorption ratio R_d , to express the distribution of activity between phases. It is identical to K_d , but does not imply equilibrium. It is defined as

$$R_d = \frac{\text{activity in solid phase per unit mass of solid}}{\text{activity in solution per unit volume of solution}}$$

Ideally a K_d value should be the same whether equilibrium is approached from a condition with the activity initially all in solution (sorption) or with the activity initially on the solid (desorption). This is not usually the case for R_d values, as will be discussed below.

As might be expected, there is a large variation of sorptive properties with variation in lithologic type and abundance of phases in tuff. In correlating sorption ratios with abundances of minerals in tuff samples from various depths of two drillholes at NTS, Hole J-13 at Jackass Flats and Hole UE25a-1 on Yucca Mountain (designated JA and YM, respectively), we identify a rough relationship between sorption ratios and two categories of tuff. In one category are tuffs that contain significant percentages (>20%) of zeolites, principally clinoptilolite or heulandite, with the rest of the rock composed of one or more of the following phases: quartz, cristobalite, alkali feldspars, and glass. In the other category

of tuffs are the devitrified tuffs that are high in silica minerals (quartz and cristobalite) and feldspars and that contain <5% clays or zeolites. Table 1 summarizes the ranges of sorption ratios obtained for these categories. It is noted in this report that many tuff samples fit into one of these categories (Appendix A). Highest sorption ratios are generally found for tuff containing zeolite minerals, particularly for ions of strontium, cesium, and barium for which sorption seems to be predominantly due to cation exchange. Sorption of the lanthanides (cerium and europium have been studied) is generally high and independent of zeolite content. Sorption on devitrified but nonzeolitized tuff is somewhat lower but still high in most cases. A formation of this last type of tuff may be best suited for an actual repository because of favorable thermal and mechanical properties; however, any water intruding into the repository would later have to pass through tuff with high zeolite content before reaching the biosphere. Fractures in the tuff aquifer zones are often also lined with zeolites or other secondary minerals.⁷

Study of the sorption of plutonium and americium (and perhaps other actinides and the lanthanides) on tuff as well as on other geologic media is complicated by the complex, largely unknown, and poorly understood chemistry of these elements in neutral-to-slightly basic groundwater typical of NTS. These elements, which in macro amounts are insoluble, form polymeric and colloidal species at the trace level in these waters. Problems encountered in the sorption experiments involve methods of preparing the traced solutions and of separating solutions from colloids. Although sorption ratios for americium and plutonium are generally high, with the highest values for zeolitized tuff, a problem that must be addressed involves the possible transport of colloids, perhaps even of fine particulates, through tuff. A more general problem that should be given a high priority is to gain a fundamental understanding of the chemistry of these elements in near-neutral solutions.

Sorption of strontium, cesium, barium, cerium, europium, and plutonium does not differ greatly for experiments done in air or in a nitrogen

atmosphere. Except for plutonium these elements exist in only one oxidation state in air or in slightly reducing conditions. Small differences

Table 1
Ranges of Sorption Ratios (mL/g)*

<u>Element</u>	<u>Devitrified Tuff</u>	<u>Zeolitized Tuff</u>
Cs, Sorption	150 to 870	8600 to 29 000
Cs, Desorption	310 to 630	13 000 to 33 000
Sr, Sorption	53 to 190	1800 to 20 000
Sr, Desorption	56 to 200	2700 to 20 000
Ba, Sorption	430 to 1500	15 000 to 130 000
Ba, Desorption	440 to 1300	34 000 to 190 000
Ce, Sorption	80 to 15 000	550 to 2000
Ce, Desorption	400 to 15 000	1200 to 13 000
Eu, Sorption	90 to 7500	1200 to 2500
Eu, Desorption	800 to 7300	2100 to 8700
Am, Sorption	130	180
Am, Desorption	2200	1100
Pu, Sorption	110	120
Pu, Desorption	1100	340
Tc (air), Sorption	0.3	0.2
Tc (air), Desorption	1.2	2.0
Tc (N ₂), Sorption	8 to 26	13
Tc, (N ₂) Desorption	18 to 79	118
U (air), Sorption	1.6 to 2.2	2.3 to 5.1
U (air), Desorption	6 to 13	15
U (N ₂), Sorption	0.5 to 1.5	15
U (N ₂), Desorption	2 to 14	57
I, Sorption	0	0

*Summarized from Appendix A. These values are average values for times ranging from 1 to 12 wk. Determinations were made under ambient atmosphere and room temperature conditions except where anoxic conditions (N₂) are noted.

in sorption may be due to a lower carbonate concentration in the water under the nitrogen atmosphere.

Sorption of uranium(VI) and technetium(VII) on tuff is generally low in both air and a nonoxidizing nitrogen atmosphere (<0.2 ppm oxygen and <20 ppm carbon dioxide) with higher sorption (10 to 100 times in the case of technetium) in the nitrogen atmosphere. Values for both atmospheres are listed in Table 1. The increased sorption in the nonoxidizing atmosphere may be due to some reduction of pertechnetate by reducing minerals and to a decrease in carbonate complexing of uranium since there is very little carbon dioxide in the nitrogen atmosphere.

There is no iodide sorption on tuff samples. It appears that since anion exchange on tuff is quite low in general, suitable engineered barriers or overpacks may be desirable to ensure containment of some anionic species from nuclear waste. However, the nuclide ^{129}I may or may not be a component of high-level wastes.

We are planning a detailed correlation of sorption ratios with mineralogy of tuff. It may be necessary to do some work on fairly pure minerals or mineral fractions. We plan to obtain such samples by performing mineral separations on selected tuffs.

Sorption ratios of nuclides, cation exchange capacities, and surface areas are found not to be very dependent on the particle size of a particular tuff. Sorption ratios tend to increase with time with some increase still being observed after 60 days.

Sorption ratios are generally lower for determinations in which "equilibrium" is approached with the radionuclide initially in solution (sorption) than when it is approached with the radionuclide already sorbed on the solid (desorption). Results from the two types of experiments are listed in Table 1. For strontium, cesium, and barium, which are thought to sorb and desorb predominantly by ion exchange, the average sorption ratios by the two routes agree in many instances to within 20%; however, there are other cases where the values differ by as much as a factor of 3.

Ratios determined by desorption differ from those determined by sorption for the lanthanides, americium, and plutonium, often by factors between 5 and 10, and for technetium by as much as 70. The "irreversible" sorption or slower desorption may be due to speciation changes, surface alteration, diffusion into minerals, or nonionic sorption of colloids or precipitates; the result of such phenomena may be greater retardation along an actual flow path in comparison with that expected, assuming equilibrium, from bulk sorption data alone.

In general, sorption is greater at 70°C than at 22°C, with differences varying from very little to factors of 5. Decreases in sorption have been noted for some lanthanides or actinides with increasing temperature; these may be caused by increased solubility of the sorbed (or precipitated) species.

The effects of groundwater composition and changes in groundwater composition are important in the understanding of sorption mechanisms and in predicting migration if water intruding into a repository is of a different composition from the local groundwater. Concentrations of major constituents of the waters have been shown to be a significant factor in sorption. The effect of concentration of minor constituents will be investigated. Work so far has been performed mostly with elemental concentrations of tracers $<10^{-6}$ M. Sorption of technetium does not vary between 10^{-3} and 10^{-12} M; nor does that of Pu vary significantly between 10^{-6} and 10^{-13} M. Further experimentation on concentration effects is in progress.

It is not known whether systems of tuff, porewaters in tuff, and waters flowing through tuff aquifers involve reducing or oxidizing conditions. The redox conditions will influence the solubility of the waste and also the species of some nuclides present. In-situ measurements of Eh are difficult and expensive, and it will probably be some time before they are made as part of the hydrology program. In the interim we are planning to make iron(II)/iron(III) ratio measurements on rocks and groundwaters studied, as well as Eh measurements in the laboratory to gain some knowledge of the redox conditions. Nuclides of plutonium, neptunium, uranium, and technetium are among those whose oxidation state can be affected by

redox conditions. We are designing a system for control of the redox potential in laboratory experiments.

Column experiments are being performed using some of the same crushed tuff samples used in the batch studies. Elution of activity with groundwater from a number of columns of a variety of types of tuff gives elution curves similar to those from ion-exchange columns with well-defined peaks; however, some columns, particularly those with high sorption ratios or with sorption ratios quite different than desorption ratios, do not behave in this manner and their elutions exhibit "leaking" behavior. Sorption ratios determined from peak positions by the column method are generally less than those from the batch method; however, they usually agree within a factor of 2 to 3. Elution positions are fairly independent of flow rates. For most experiments flow rates are $\sim 10^{-4}$ cm/s (~ 30 m/yr) compared to geologic flow rates of 10^{-7} to 10^{-3} cm/s. With flow rates of ~ 30 m/yr it is practical to measure only those sorption ratios less than ~ 1000 mL/g in the laboratory. We are running one column (zeolitized tuff) at a much faster rate, ~ 0.012 cm/s, corresponding to ~ 32 column volumes/h. A sorption ratio of ~ 9000 mL/g had been determined for cesium on this tuff by the batch method; no activity was eluted from this column during the first 25 days, which corresponds to a sorption ratio > 5700 mL/g. After 25 days a slowly increasing peakless elution began. After ~ 80 days, 50% of the activity had been eluted (a peak would correspond to a K_d of 22,000 mL/g). Work with crushed columns is summarized in Appendix B.

Equipment on the centimeter scale has been constructed for study of transport and retardation of nuclides in solid-rock cores or cores containing natural or artificial fractures, techniques are being developed, and initial experiments are under way. Strontium activity is being eluted from one solid tuff (devitrified) core, and a "leaking" behavior is being observed. Uranium (essentially nonsorbing) was partially eluted from other rock cores, which were then sectioned and examined by autoradiography to determine flow paths and sorption sites. Americium was infiltrated into rock cores, and autoradiography was used to determine distribution in the core and sorption sites. Elution experiments on other cores and with

a number of nuclides are planned. Such experiments will be given high priority.

Microautoradiography has been shown to be useful in determining sorption sites. The method and early results are presented in References 26 and 27. The method confirms the high sorptive power of zeolites, clays, and alteration bands around some minerals relative to other minerals such as quartz and feldspars. It also indicates the presence and nonspecific sorption of colloids. With filtration methods the technique can be used to gain insight into the state of aggregation of actinide species in solutions. It may be possible to use the method for studying the transport of colloids in tuff.

Some of the research still in progress and some future plans and needs were discussed above. In support of the exploration program of the NNWSI we will continue to examine selected samples from new drill holes by batch techniques, thus gaining possible site-specific information while extending the generic data base on sorptive properties. In addition, tuffs from the G-tunnel at NTS and the Bandelier Tuff from Los Alamos will be investigated to expand the basic understanding of sorptive properties of tuff.

The following list of parameters and properties should be investigated to achieve an adequate understanding of the migration rate of radionuclides in tuff: (1) rate constants of the reactions involved in a rock-fluid system, (2) solubility products for the precipitated compounds, (3) long-term stable oxidation states of the radionuclides in a tuff environment, and (4) the effect of the redox potentials of the tuff media on tuff retardation properties and groundwater chemistry. There is also a possibility that volume diffusion into dead-end pores along the pathway may be an important retardation mechanism. Studies designed to address these areas are being planned or are currently under way.

Several other investigations are planned. Some experiments must be performed under anoxic conditions with more carbon dioxide present than was used in the controlled-atmosphere studies. Nuclides of other elements

that are components of nuclear wastes and their behavior will be studied. Column studies will be continued with emphasis on porous flow through permeable tuffs and fracture flow through nonpermeable tuffs. The small-core experiments must be scaled up to larger cores and blocks at the laboratory "bench" scale as an intermediate size to "field" experiments. Sorption and transport must be investigated for other rock types along potential pathways from tuff formations to the biosphere, e.g., the Paleozoic rocks in the carbonate aquifer underlying tuffs in Nevada.

Given the diversity of chemical species that may be present in groundwaters and of the interactions that may take place with minerals, a radionuclide transport model must be devised that includes a description of the geochemical system. This model must include knowledge of the physical chemistry of the elements in solution, the factors that can influence change in the chemical species, and the kinetics of such changes. Ideally it would also include a detailed description of the abundances and occurrences of the minerals along the flow path as well as of the mechanisms, equilibria, and kinetics of the interactions of the radionuclides with these minerals and the factors influencing these interactions. Of necessity, the chemical part of this model will be specific for each element considered. One must also superimpose the hydrologic regime on the local chemistry. This includes effects such as hydrodynamic dispersion, distance, pore/fluid velocity, and saturated or unsaturated flow. For fracture tuff one has the additional complication of flow dominated by the hydrology and mineralogy of the fracture system. We are in the initial stages of development of such models; one aspect of the problem is described in the following section.

Effects of those "near-field" phenomena in tuff formations that are expected to result from the presence of a repository must be addressed. Heat and radiation, along with the presence of porewater, may cause mineralogic alteration and fracturing. We are altering tuffs hydrothermally in the laboratory to investigate the effects of such a change. These near-field phenomena may cause changes in chemical and mineralogic properties, such as expansion and phase changes, which affect transport and retardation. Some nuclides may be ejected or excluded from the changed minerals,

and diffusion characteristics may change. Migration under the influence of temperature gradients should be studied. Buffer materials should be studied in relation to waste forms, tuff, groundwater, heat, and radiation. Lastly, the interaction of the waste form itself in this setting is very important and must be considered.

3.2.2 Joint Flow Experiments and Modeling (K. L. Erickson, SNL)

Initial work has been conducted to develop a theoretical approach that will provide a basis for analyzing radionuclide transport in jointed geologic media. The modeling effort was initially applied to argillite and is currently being applied to tuff. A transport model for relatively simple joint systems was developed and limited transport analyses were performed that identified some of the important parameters controlling radionuclide transport in jointed media and some possible deficiencies in current methods of parameter evaluation.^{28,29}

The theoretical approach is based on the differential continuity equations for radionuclides in the mobile and immobile phases and on the assumption that sorption equilibrium exists at the interface between mobile and immobile phases.

Based on the literature concerning ion-exchange kinetics and boundary layer thicknesses,³⁰ we expected diffusion into the relatively long, narrow intergranular regions would dominate the rate of mass transfer across the interface between mobile and immobile phases. The flux expression describing mass transfer across the interface and the material balance for the bulk of the intergranular regions were developed by assuming local sorption equilibrium between the bulk stagnant solution and impermeable surface, constant-valued parameters, continuous physical and chemical properties, by assuming that solution-phase nuclide concentrations were sufficiently dilute so that Fick's law was valid, that diffusion was essentially one-dimensional, and that any surface diffusion effects could be neglected.

A fundamental radionuclide transport model for cesium solutions in laminar, one-dimensional flow through linear fractures was obtained by combining the material balance for the immobile phase and the interfacial flux expression with the general continuity equation for the mobile phase and by then assuming constant, uniform dimensions and constant, continuous properties for the fractures. Furthermore, the parabolic velocity profile was replaced by an appropriate average velocity; the fracture wall spacing was assumed sufficiently small so that diffusion perpendicular to the fracture walls, in the mobile phase, can be approximated as a quasi-steady-state process; terms due to nuclear decay were neglected, and constant-valued parameters were assumed. The result was a set of equations analogous to those developed by Rosen.^{31,32}

Initial batch equilibration and rate experiments have been conducted using tuff samples contacted with simulant groundwater solutions containing cesium, barium, strontium, and promethium. The experiments involving strontium and promethium were apparently complicated by competing chemical reactions in the solution phase, and further experiments will be required.

Scanning-electron micrographs of samples of welded tuff indicated an average microporosity of ~10%. Reasonably characteristic dimensions of the micropores are on the order of 5 μm equivalent diameter and ~50 μm equivalent length. The surfaces of the bulk rock and of the micropores appear to be extremely "rough," with a high density of intergranular cavities on the order of microns in depth and tenths of microns in equivalent diameter. For 30 to 60 mesh particles, surface areas determined by the BET method were ~7 m^2/g . The cesium sorption equilibrium isotherm at room temperature, determined from batch equilibration experiments, was found to be represented by the expression

$$\bar{C} = \left[0.0014 \text{ cm} + \left(\frac{0.10 \text{ cm}}{1 + 10^9 \frac{\text{L}}{\text{mole C}}} \right) \right] C \quad (1)$$

where \bar{C} is the immobile-phase concentration, C is the molar mobile-phase concentration, and $10^{-3}M < C < 10^{-10}M$.

Sorption rate data were obtained from independent batch experiments using tuff tablets that were ~0.6 cm thick by 6 cm diameter. Based on autoradiographs, it appeared that most sorption occurred in intergranular regions having effective lengths of 0.01 cm or less, which was consistent with the surface area measurements and estimated intergranular porosities.

The batch-rate experiments were described mathematically by simultaneously solving the material balance for the intergranular regions and the material balance for the batch reactor. Analysis of the rate data from the tuff experiments involving cesium was complicated by the nonlinear nature of the sorption isotherm for the concentration range obtained in the experiments, and it has not been possible to rigorously analyze the data. However, experiments using argillite were amenable to analysis, and the agreement between calculated and experimental data appeared sufficiently good to support the validity of the equations and parameter values used.

Initial experiments were conducted in which stable cesium solutions ($C_0 \approx 10^{-3}M$) were pumped through artificial (saw cut) fractures in argillite samples. Quantitative analysis of the data was complicated by the nonlinear nature of the sorption isotherm.

Values for the various modeling parameters determined from the batch experiments and physical characterizations for argillite are given in Table 2. Based on qualitative comparisons, it appears that the parameter values for welded tuff would be reasonably similar, with the possible exception of the parameters K and \bar{K} . The transport analyses indicated that important parameters controlling radionuclide transport include the intergranular porosity and penetration depth, the fracture plate spacing and length, the fluid velocity, and the sorption distribution coefficient. Also as a result of the transport analyses, criteria were developed for determining when the assumption of local equilibrium between bulk phases can be applied to radionuclide transport in jointed geologic media.^{28,29}

These criteria were developed in terms of the system parameters discussed above. Furthermore, many of these parameters represent physical quantities or processes that can be characterized in the laboratory. However, parameters such as joint widths and fluid velocities must be obtained from the field, and methods must be developed to establish reliable bounds on the uncertainties in the values of such field-determined parameters.

Table 2

Values for Various Argillite Modeling Parameters Determined from the Batch Experiments and Physical Characterizations

<u>Parameter</u>	<u>Value</u>	
a	Surface roughness	1
a_t^2	Intergranular tortuosity	2
D	Solution-phase diffusion coefficient	$2 \times 10^{-5} \text{ cm}^2/\text{s}$
h	Perimeter/surface area for intergranular region	$6 \times 10^6 \text{ cm}^{-1}$
a_c	Intergranular roughness	$\sqrt{2}$
K	Distribution coefficient	0.05 cm
\bar{K}	$1 + a_c h K$	4×10^5
\bar{D}_e	$D/\bar{K} a_t$	$2.5 \times 10^{-11} \text{ cm}^2/\text{s}$
\bar{H}	Intergranular penetration depth	0.005 cm
p	Intergranular surface porosity	0.03

3.3 Thermal Properties (A. R. Lappin, SNL)

3.3.1 Thermal Conductivity

As shown in 3.1.2.1.b and 3.1.2.2.b, one of the fundamental characteristics of silicic tuffs is their mineralogical and textural variability. Because of this variability, and the need to perform both near-field and far-field thermomechanical modeling, it is important that a predictive formalism be developed for tuff thermal conductivity, and that this formalism be used conservatively. The brief discussion given below is taken

from Reference 33, which represents the present status of this development effort.

The available data on the thermal conductivity of many of the phases occurring in silicic tuffs are summarized in Figure 7. As shown, limited data exist for silicic glasses and zeolites, and are also available for feldspars, quartz, and cristobalite, but not for mixed-layer clays or montmorillonites. In Figure 8, numerous trends of varying "zero-porosity" matrix conductivity are indicated as a result of mineralogical reactions. Primary silicic glass should have a conductivity of near 1.35 W/m°C. Hydration of this glass will almost certainly decrease this value by an unknown amount. Devitrification, in which the original glass is replaced by a very fine-grained intergrowth of feldspars and cristobalite, occasionally with some quartz, should cause increasing conductivity and grain density, within the region labeled "A" in Figure 8. Curve II, at the end of Trend A, reflects the uncertainty in conductivity resulting from compositionally controlled variations in the cristobalite/feldspar ratio in the devitrified tuff. If a given tuff devitrifies slowly enough for partial inversion of cristobalite to quartz to occur, then the matrix conductivity of the devitrified tuff should lie somewhere between Curves II and III, within the field covered by Trend B. If complete inversion of the cristobalite takes place, the matrix conductivity of the resulting tuff should lie along Curve III, reflecting the sensitivity of conductivity to quartz content. The processes leading to Curves II and III are isochemical, or nearly so.

Zeolitization is a common alteration process in silicic tuffs. In Figure 8, zeolitization of an initially glassy tuff is represented by Trend C, and of a devitrified tuff, by Trend D. As shown, zeolitization of a glassy tuff should have little effect on the matrix conductivity. Although zeolitization of a fully devitrified tuff has not been observed, such a process should decrease the conductivity markedly. Silicification of tuffs, by reaction with groundwater either below or above the water table, is represented by Trend E in Figure 8, and should always increase conductivity.

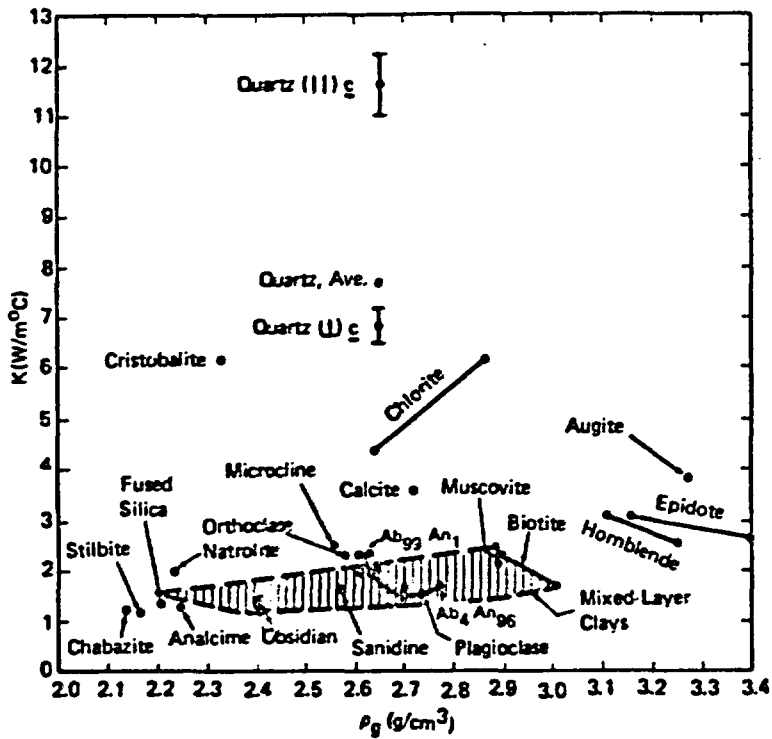
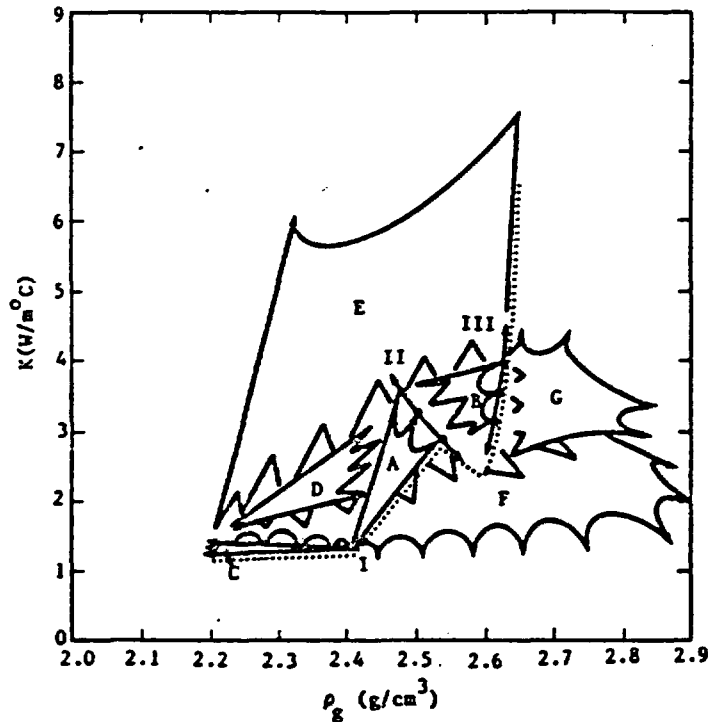


Figure 7. Thermal Conductivity Versus Grain Density for Phases Occurring in Silicic Tuffs (Conductivity field for mixed-layer clays is calculated; all other values are from references contained in Reference 33.)



Point I: Assumed conductivity and grain density of primary silicic glass

Trend A: Devitrification to cristobalite plus feldspars

Curve II: Uncertainties in conductivity of simply devitrified tuff as function of variable cristobalite/feldspar. Specific points shown (with increasing conductivity are 25/75, 35/65, 45/55)

Trend B: Partial to complete inversion of cristobalite to quartz in devitrified tuffs

Curve III: Uncertainties in conductivity of quartz-bearing tuffs as function of variable quartz/feldspars. Specific points shown (with increasing conductivity) are 25/75, 35/65, and 45/55

Trend C: Zeolitization of initially vitric tuff

Trend D: Zeolitization of devitrified tuff

Trend E: Silicification of zeolitized to quartz-rich tuffs. End points are cristobalite (low-density) and quartz

Trend F: Argillic alteration

Trend G: Propylitic alteration

Dotted line: Minimum bounding curve for tuffs that are either still vitric or have undergone alteration processes A to E

Figure 8. Theoretical Variations in Tuff Zero-Porosity Matrix Conductivity as a Function of Postemplacement Mineralogical Reactions (See text for definition of individual trends and curves.)

In Figure 8, a bounding curve (dotted line) has been drawn on the lower conductivity side of the trends described thus far, and would appear to predict minimum zero-porosity conductivity values for tuffs that have undergone reactions represented by Trends A through E. This curve, and the predictive curves related to it, do not apply to tuffs that have undergone either argillization (Trend F), by which clay minerals are formed in altered tuffs, or propylitic alteration (Trend G), as a result of which one or more of the minerals epidote, calcite, or chlorite are formed. The zero-porosity matrix conductivity of tuffs that are partially devitrified, fully devitrified (in which cristobalite has fully inverted to quartz), or which have undergone simple zeolitization, should fall near the bounding curve in Figure 8. The conductivity of partially zeolitized devitrified tuffs and of silicified tuffs should fall above the given curve.

As part of this study, the thermal conductivities of 12 tuffs varying widely in mineralogy and porosity have been analyzed. Extrapolated conductivities at 0% porosity are shown as a function of grain density in Figure 9 and compared with the theoretical curves and bounding envelopes in Figure 8. Although the data extrapolated from experiment are sparse, they do fall in zones parallel to the theoretical bounding curve, but consistently below it. This is similar to results of other studies, in which the measured conductivity of silicate rocks falls below theoretical values.^{34,35} There is, however, good general agreement between the mineralogical composition of the analyzed samples and the general portion of the theoretical curves near which they lie. Samples 1949, 1966, 2365, 2432, and 2443 are all from the Crater Flat Tuff at Tucca Mountain, NTS, and consist almost entirely of quartz and feldspars. Calculated zero-porosity conductivities for these samples fall on a well-defined curve that is parallel to the theoretical curve showing variations in conductivity of quartz-bearing tuffs as a function of quartz content. Sample 1253, from the devitrified lower portion of the Topopah Springs Member of the Paintbrush Tuff, has a calculated matrix conductivity falling along a curve parallel to the theoretical curve representing uncertainties in conductivity of completely devitrified tuffs. Sample 1555, from the Bedded Tuff of Calico Hills, has a matrix conductivity reflecting, and consistent

with, the mix of glass, feldspars, and silica polymorphs (typical devitrification products), and zeolites found in this sample. Sample 82 is partially devitrified welded tuff, and Samples 22 and 25 are both very glass-rich, though partially devitrified. In the case of Samples 63 and 64, it would appear that the inversion of cristobalite to quartz is incomplete or that the conductivity reflects the presence of partially vitric pumice clots.

For purposes of application to feasibility studies in tuff, the predictive curves shown in Figure 9 appear capable of predicting the natural-state conductivity of analyzed samples to within better than 15%, when combined with porosity and saturation data in a geometric-means formulation. Except for Samples 1555, 63, and 64, the agreement is to within ~10%.

Since waste emplacement might result in rock temperatures $>100^{\circ}\text{C}$, it is also necessary to be able to predict the thermal conductivities of fully dehydrated tuffs. Comparison of measured and predicted dehydrated conductivities of the analyzed tuffs indicates that this is possible to within ~15%, but requires use of an average thermal conductivity of air of $0.12 \text{ W/m}^{\circ}\text{C}$, as opposed to the literature value of $0.026 \text{ W/m}^{\circ}\text{C}$. This conclusion is similar to that reached in other studies of silicate rocks.^{34,35} It is not clear at present whether this discrepancy is because there is radiant-heat transfer across pore spaces in these rocks, even at low temperatures, or is a result of some inadequacy in the thermal formalism.

It is obviously risky to base a four-segment bounding curve on only 12 data points. It has been necessary to do so in this case, however, due to the relative sophistication of modeling and material properties data-collection efforts. In order for much confidence to be placed in the curves developed here, many more thermal conductivity measurements will be made on varied tuffs, especially those from the Crater Flat, Topopah Springs, and G-Tunnel tuffs. In these cases, more detailed petrography does not appear to be essential. Since the Bedded Tuff of Calico Hills forms an extensive layer in the Yucca Mountain area, and appears to have a

low thermal conductivity (but higher than predicted by the curves developed here); several more measurements of conductivity on tuffs from this interval must be made. These measurements must be coupled with petrography that is detailed enough to determine the relative proportions of glass, devitrification products, and zeolites in these samples.

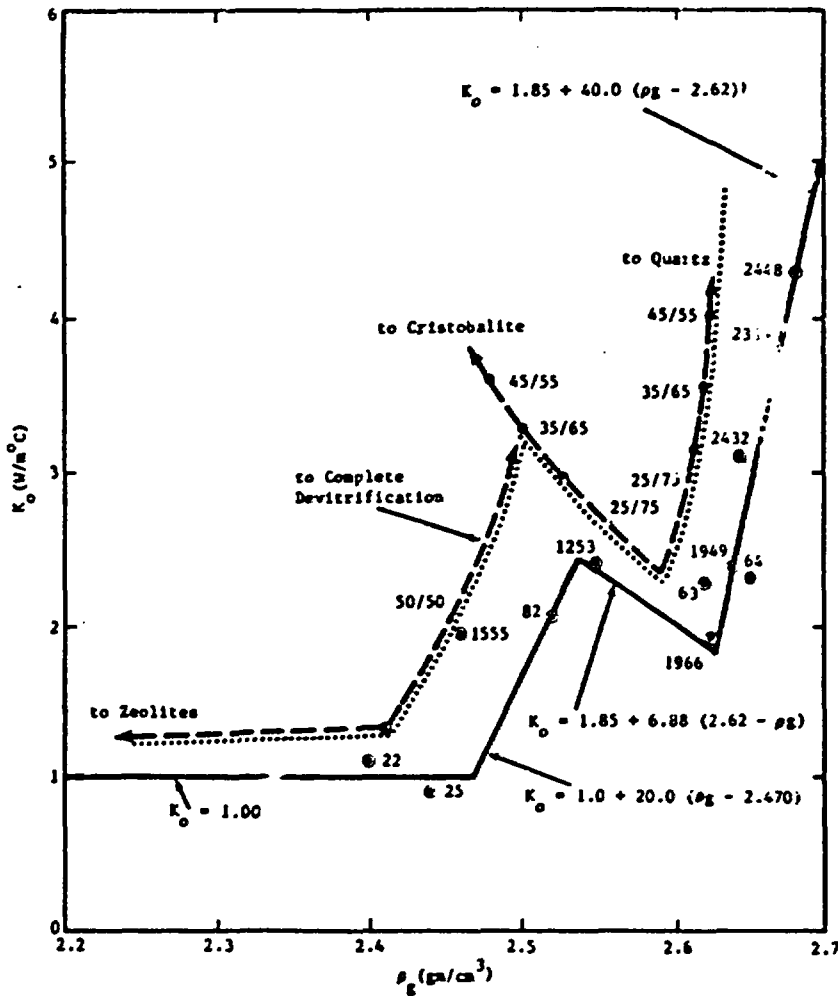


Figure 9. Extrapolated Zero-Porosity Thermal Conductivity of Measured Tuffs Versus Grain Density. (Included are: (1) Theoretical Trends Corresponding to Trends A and C and Curves II and III from Figure 8; (2) Theoretical Bounding Curve Lying Below Trends A through E of Figure (dotted line); and (3) Lower Bounding Curve Based on Experimental Data (solid line)).

Measured natural state and fully dehydrated conductivities on samples of the partially welded Bullfrog Tuff at Yucca Mountain range from 2.19 to 2.65, and 1.56 to 1.74 W/m°C, respectively. The samples have an average porosity of 22%. At an average porosity of 24%, calculated fully saturated and measured fully dehydrated conductivities of the Grouse Canyon Tuff in G-Tunnel range from 1.69 to 2.20 and 0.98 to 1.19 W/m°C, respectively.

3.3.2 Thermal Expansion

Just as temperatures resulting from waste emplacement strongly depend on rock thermal conductivity, so the stresses resulting from waste emplacement depend upon the thermal-expansion response of the host rock mass. The brief discussion given here summarizes the present state of knowledge about the thermal expansion behavior of tuffs and points out remaining research needs.

The results of a large number of ambient-pressure measurements made on small blanks are summarized in Figure 10 and described in detail in Reference 36. Measurements on devitrified and quartz-bearing tuffs ranging from 8% to 27% porosity, indicated by circles in Figure 10, are consistent and suggest a general insensitivity to both mineralogy and porosity in these samples. For eight samples, regardless of origin, the average linear expansion coefficients between ambient temperature and 100°C and between 100° and 200°C are 6.9 ± 1.5 and $11.3 \pm 2.6 \times 10^{-6} \text{ } ^\circ\text{C}^{-1}$, respectively. Individual measurements appear accurate to within $\pm 1 \times 10^{-6} \text{ } ^\circ\text{C}^{-1}$. Based on these results, it appears that the matrix thermal expansion of devitrified and quartz-rich welded tuffs is largely insensitive to detailed mineralogy.

In many cases, however, mineralogical effects seem capable of dominating expansion behavior. In Figure 10, the two squares represent the results obtained on two samples of anhydrous (0.1 to 0.3 wt% H₂O) obsidian. These two samples, mostly siliceous glass, expand continuously to at least 500°C, with no hysteresis on cooling. In contrast, all samples of devitrified tuffs studied to date show positive hysteresis on cooling.

Note that the expansion of the obsidians is less than that of the devitrified tuffs, with a temperature-independent expansion coefficient of $\sim 5 \times 10^{-6} \text{ } ^\circ\text{C}^{-1}$.

In most tuffs, however, the silicic glass is at least partially hydrated, with water contents of up to 7 wt% not uncommon. Expansion results on one densely welded sample that is almost entirely glassy, represented by an upside-down triangle in Figure 10, suggest that contraction of hydrated glass on heating in-situ to near or above the local boiling point of water could cause major contractions in the heated rock mass. Likewise, many nonwelded samples, represented by triangles in Figure 10, contain hydrated glass.

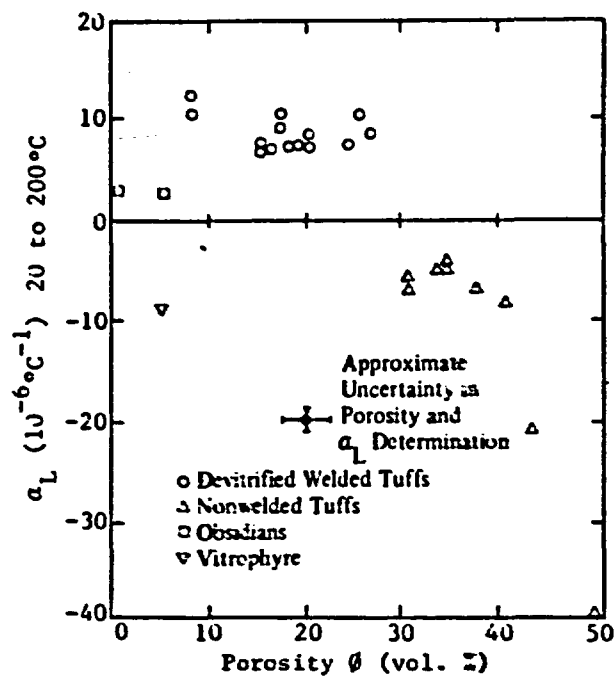


Figure 10. Average Linear Expansion Coefficient on Tuffs Between Ambient Temperature and 200°C as a Function of Porosity

Three other types of minerals can also cause complexity in thermal expansion results, however. In many samples of welded and nonwelded tuffs, small amounts of expandable clays are present. Upon dehydration

near the local boiling point of water, these clays will contract; even very small amounts of clay can result in zero net expansion after dehydration. Figure 11 shows one example of the effects of clay contraction. In this figure, sample UE25a-1-2494 is shown to contract to the zero-expansion line at near 80°C. This behavior, which is consistent in several samples at this depth, can be explained by only 35 to 40% alteration of the 2% biotite that the sample contains if it is assumed that this alteration is to expandable clay. Since many if not most silicic tuffs contain at least some biotite, alteration of this phase must be understood to within well-defined limits, since it can greatly reduce the expansion expected from otherwise simple tuffs. Expandable clays are particularly abundant in many nonwelded tuffs, including several of those included in Figure 10.

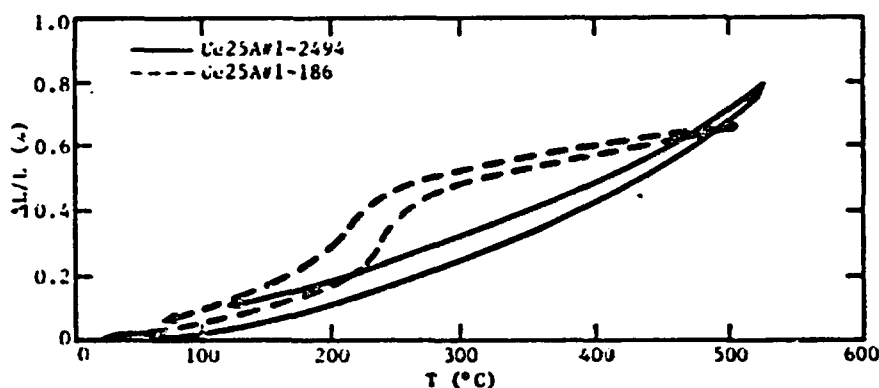


Figure 11. Linear Expansion to 500°C to Two Welded Tuffs (Sample 186 contains abundant cristobalite; Sample 2494 appears to contain a very small amount of expandable clay.)

In tuffs that are devitrified to a mixture of cristobalite and feldspars, the presence of cristobalite causes some irregularity in expansion largely at temperatures of ~200°C or above. This is shown in Figure 1 as represented by Sample UE25a-1-186, from the devitrified portion of the Tiva Canyon Member of the Paintbrush Tuff. The behavior reflects the α - β inversion of cristobalite; it should be of concern, however, only at elevated temperatures.

A final class of minerals can have a pronounced effect on thermal expansion in some cases. This group, zeolites, includes a large group of hydrated aluminosilicates, with widely varying properties. Table 3 lists the general-stability relations, differential thermal analysis (DTA) and dehydration behavior of the zeolites reported in tuffs at NTS, in the generally reported order of decreasing abundance. Except for heulandite and phillipsite, the relevant zeolites are reported to be structurally stable to temperatures $>600^{\circ}\text{C}$, and should have little effect on thermal expansion except that they will elevate fluid pressures as they dehydrate. In general, the most dominant zeolite in silicic tuffs is reported to be clinoptilolite. Recent mineralogical investigations of the tuffs at or near Yucca Mountain,^{6,7} indicate small amounts of heulandite or phillipsite in the lower portions of the devitrified Topopah Springs Member of the Paintbrush Tuffs, which is situated above the static water level. Occurrence of even small amounts of these phases, which begin to contract at temperatures at least as low as 180°C , could greatly affect the expected behavior of devitrified tuffs and either lead to decreased net expansion on heating or negative hysteresis on cooling. Care must be taken in expansion measurements of such tuffs to include large enough volumes to measure the response of any fractures that might contain heulandite.

A limited number of expansion measurements have been made under confining pressure. In the case of the Bullfrog Member of the Crater Flat Tuff, results on oven-dried samples agree fairly well with measurements made at ambient pressure. Measurements at a confining pressure of 10.3 MPa yields an average linear expansion coefficient between ambient and 200°C of $6.1 \times 10^{-6} \text{ }^{\circ}\text{C}^{-1}$, as compared with $8.9 \times 10^{-6} \text{ }^{\circ}\text{C}^{-1}$ based on unconfined measurements. The difference is probably at least partly due to closing of microcracks under pressure.³⁸

Table 3

Thermal, Thermogravimetric, and Structural Data for the Most Common Zeolites in Silicic Tuffs*

<u>Type of Zeolite and Comments</u>	<u>Differential Thermal Analysis (DTA)</u>	<u>Thermogravimetric Analysis (TGA)</u>	<u>Structural Stability**</u>
Clinoptilolite	Endotherm, 125° to 300°C	Continuous; Σ 14%	Stable to at least 750°C
Analcime (major, especially at depth)	Endotherm, 200° to 400°C	Continuous weight loss to 400°C; Σ 8.7%; dehydration reversible	Stable to 700°C
Mordenite, not uncommon	Endotherm, 25° to 300°C	Continuous; Σ 16%	Stable to at least 800°C
Erionite, minor	Endotherm, 50° to 400°C	Continuous; Σ 15%	Stable to at least 750°C
Heulandite, variable; some old literature reports clinoptilolite as heulandite; new literature suggests heulandite fairly common	Endotherm, 25° to 300°C; discrete at 350°C	Stepwise weight loss, near 100° and 250°C; Σ 17%	Transforms to heulandite "B" near 250°C; structure collapses above 360°C; some lattice contraction at 180°C the start of transformation
Phillipsite, traces	Endotherms at 100°, 200°, 300°C	Stepwise weight loss, starting near 130°C; Σ 18% @ 300°C	New structure forms at 160° to 200°C; small change, "metaphillipsite"
Chabazite, minor	Endotherm, 25° to 300°C	Continuous; Σ 23%	Stable to at least 700°C

*Modified from Reference 37

**Limited to the duration of the experiments

At present, however, only confined expansion measurements, in which there is no control of pore fluid pressures, have been made. Thus the details of responses to mineral dehydration at known fluid pressures can only be estimated. Depending upon the temperatures that are expected to result from waste emplacement, understanding of the thermal-expansion behavior of a complex series of tuffs may be required at elevated temperatures. Even if waste were emplaced in a devitrified or quartz-rich welded tuff, for example, it probably would be necessary to understand the behavior of both expandable clays and zeolites in considerable detail. Failing this level of detailed information, bounding estimates of contraction resulting from mineral dehydration can be made on the basis of measurements at ambient pressure.

3.3.3 Heat Capacity and Thermal Diffusivity

No extensive laboratory studies of heat capacity or thermal diffusivity have been undertaken. A limited number of heat capacity measurements on dehydrated samples indicate that the heat capacity of the silicates in both devitrified and glassy tuffs above 100°C is 0.20 cal/g°C, to within 0.01 to 0.02 cal/g°C. Accordingly, heat capacities for modeling studies have been estimated from the relation C_p (cal/g°C) = 0.2 (1 - ϕ) + ϕS , where ϕ is porosity and S is the saturation of the material, the heat capacity of liquid water is assumed constant at 1 cal/g°C, and that of air negligible. Increasing heat capacity of liquid water with increasing temperature and even slight bonding of water within zeolites and/or expandable clays present in tuffs should combine to make this estimate conservative.

In modeling studies to date, thermal diffusivities have been calculated from the relation

$$\bar{\alpha} = \frac{K}{\rho C_p} \quad (2)$$

where $\bar{\alpha}$ is diffusivity, K thermal conductivity, ρ density, and C_p heat capacity. A small effort is under way, however, to examine the feasibility of measuring thermal diffusivities of fully saturated and partially saturated rocks as a function of saturation.

3.4 Mechanical Properties of Tuffs (W. A. Olsson and L. W. Teufel, SNL)

Through the years, a large amount of mechanical data has been collected for NTS tuffs from Yucca Flat, Pahute Mesa, and the Area-12 tunnels, all far removed from Yucca Mountain, the current area of interest. Samples were obtained from sites of specific weapons tests and were characterized in support of those tests. Generally, the information required to extend the results to a repository environment is not available. Variables essential to long-time repository modeling were usually not measured.

The mechanical properties reported here were obtained from samples from UE25a-1 (Yucca Mountain) and from the Grouse Canyon welded tuff in G-tunnel. These studies are in direct support of the Mine Design effort described in Section 4. Variables under evaluation include confining pressure, total effective pressure, water content, strain rate, temperature, and the presence of joints (artificial).

The mechanical properties of several tuffs from Hole UE25a-1 are given in Table 4. Unless otherwise noted, all intact tests were run at a strain rate of 10^{-4} s^{-1} . All stresses and strains are referred to original dimensions.

Representative examples of unconfined (Figure 12) and confined (Figure 13) compression tests show the effects of degree of welding (porosity) and increased confining pressure. A more complete degree of welding (lower porosity) causes higher strengths and higher Young's moduli. Higher confining pressures tend to cause increased strength and increased Young's modulus. Increased ductility, in the sense of higher strains at fracture, also results from higher confining pressures. At 200°C the gross shapes of the stress-strain curves are unaffected but the peak stress is lower.

Table 4

Mechanical Properties of Tuff from Hole UE25a-1

Specimen Number	Confining Pressure (MPa)	Temperature (°C)	Maximum Stress Difference (MPa)	Young's Modulus (GPa)	Poisson's Ratio	Bulk Modulus (GPa)	Calculated Porosity (%)	P-Wave Velocity (km/s)
1692	0	RT	40.83	14.02	0.20	----	36.6	2.59
1490	0	RT	47.72	12.29	0.14	----	28.1	----
1634	20.7	RT	67.45	8.50	0.27	2.74	32.2 (est.)	----
1605	20.0	RT	26.14	7.99	0.22	1.74	29.5	----
1662	20.0	RT	70.28	9.57	0.25	6.03	34.9	----
2452	0	RT	54.69	6.37	0.05	----	20.3	2.78
2039	0	RT	32.21	7.84	0.18	----	31 (est.)	----
2491	20.7	RT	140.00	22.10	0.28	3.25	17.7	2.77
2421	20.0	RT	145.24	19.24	0.23	5.09	22 (est.)	----
2401	50.0	RT	173.93	18.74	0.19	5.52	21.9	----
1948	100.0	RT	298.97	21.95	0.20	----	19.1	----
723	0	RT	137.70	40.40	0.22	----	12.9	----
2014	0	RT	129.70	47.90	0.30	----	16.7	3.28
1985	20.7	RT	206.80	31.00	0.25	5.45	14.5	3.72
1968	20.0	RT	175.90	27.01	0.20	----	18.0	----
739	20.7	200	133.20	23.90	0.15	----	11.3	----
185	20.7	200	105.00	----	----	----	26.7	----

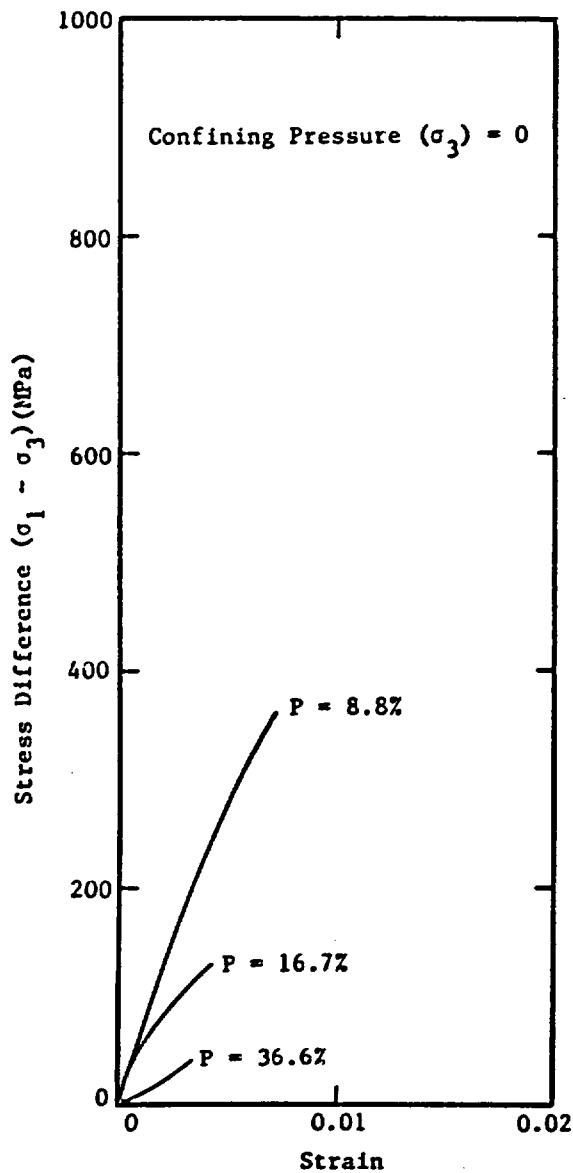


Figure 12. Representative Compressive Stress-Strain Curves for Unconfined Samples with Different Porosities (P)

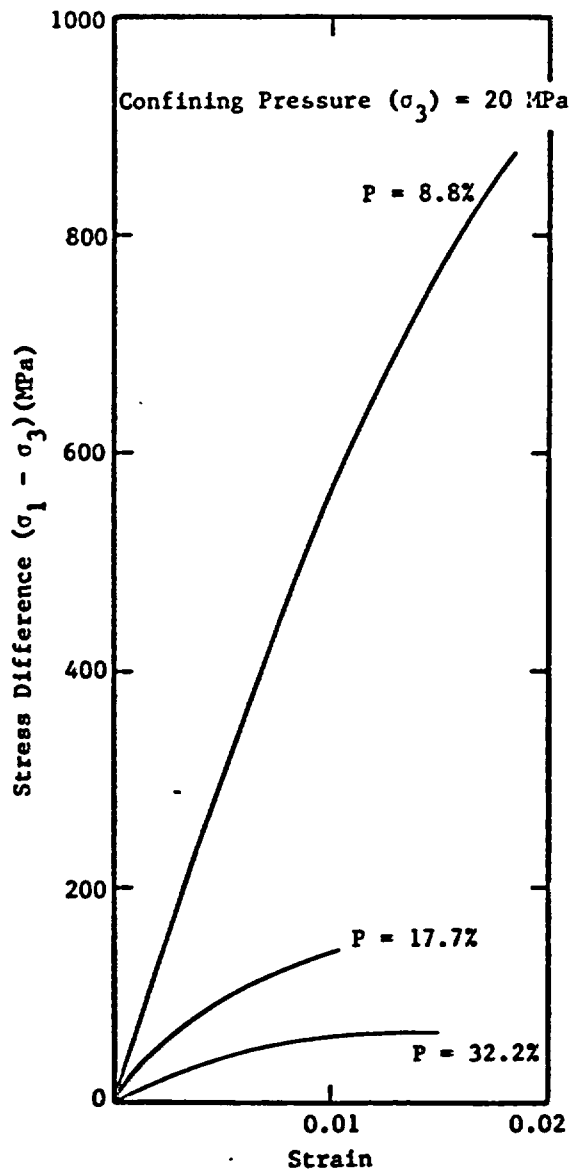


Figure 13. Representative Compressive Stress-Strain Curves Showing the Effect of Confining Pressure (20 MPa) on Samples with Different Porosities (P) (Compare with Figure 12)

By independently measuring the linear axial and transverse strains during hydrostatic loading we observed an elastic moduli anisotropy. This measure of elastic anisotropy has been plotted versus percent porosity in Figure 14. There is a definite systematic relation between degree of welding and degree of anisotropy. The welded tuff is stiffest perpendicular to bedding, and nonwelded tuff is stiffest parallel to bedding. This may complicate modeling efforts.

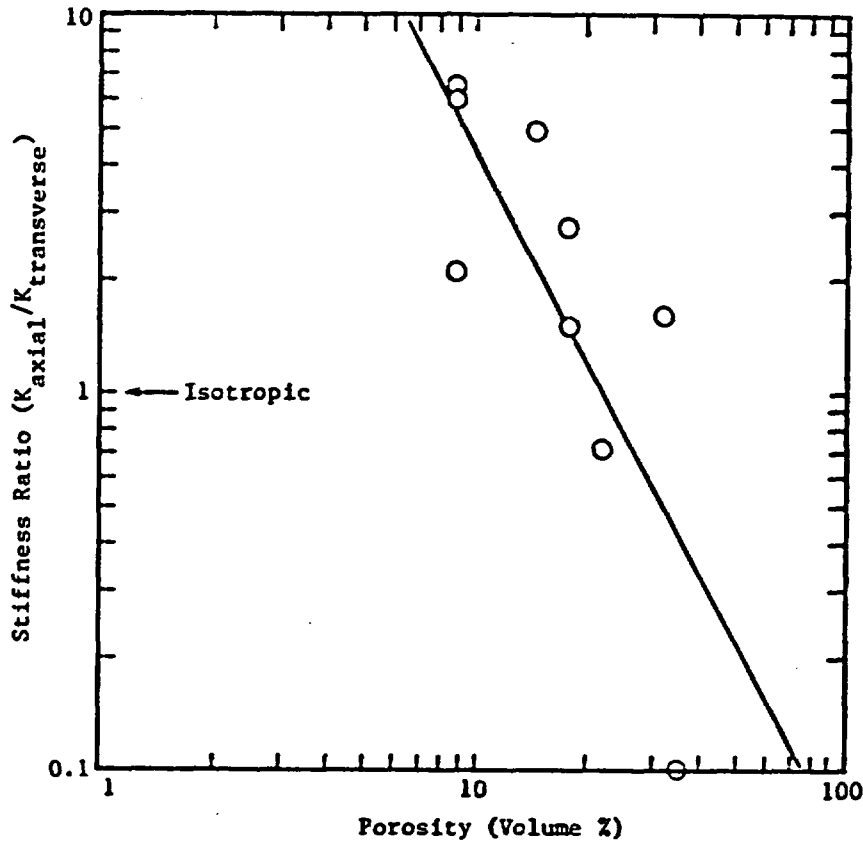


Figure 14. Anisotropy of the Elastic Moduli as a Function of Porosity. The Welded Tuff is Stiffest Perpendicular to Bedding and the Nonwelded Tuff is Stiffest Parallel to Bedding.

A significant result that helps to understand the mechanics of deformation of tuff and to correlate among the various types is that the degree of welding is reflected by the porosity. Densely welded tuffs have low porosity, and this grades uniformly to high porosity in nonwelded tuffs. Figure 15 shows peak differential stress plotted against porosity for confining pressures of 0 and 20 MPa. There is a clear, systematic relationship of power-law form that has also been found for sandstone.³⁹ The scatter of the data is considerable, but since other variables such as mineralogy may also vary with degree of welding, the correlation between strength and porosity is remarkable. The power-law relation is given by

$$\sigma_1 - \sigma_3 = AP^n \quad (3)$$

For these data, the maximum stress difference can be expressed as a function of the confining pressure and the porosity as shown by

$$\sigma_1 - \sigma_3 = \left[A_0 + \frac{A_{20} - A_0}{20} \sigma_3 \right] P^n \quad (4)$$

where A_0 and A_{20} are the values of A for 0 and 20 MPa confining pressures, respectively. The fact that strength depends on porosity, and that this dependence differs for the two confining pressures, shows that the other strength parameters such as cohesion and angle of internal friction are also functions of porosity.

Further analysis permits Mohr-Coulomb failure envelopes (necessary for input in mechanical models) to be calculated as a function of porosity. In general, agreement between the calculations and experiments has been very good. However, the in-situ state of stress may have a strong influence on the amount of deformation for a particular application that occurs before failure. Consequently in-situ stresses must be determined.

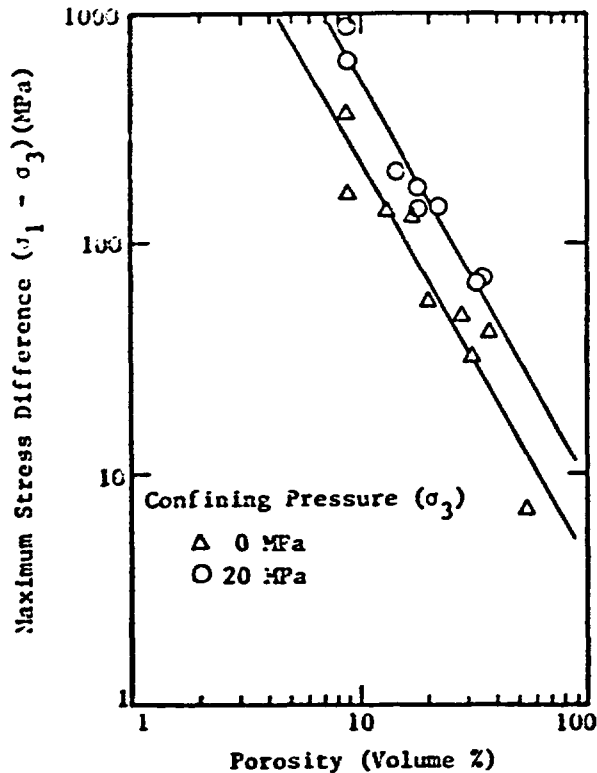


Figure 15. Compressive Strength as a Function of Porosity and Confining Pressure for Air-Dried Samples and a Strain Rate of 10^{-5} s^{-1}

Tensile fracture may be the dominant failure mechanism of brittle materials. Even in triaxial compression at low confining pressure, many extension fractures on both the microscopic to macroscopic scale have been observed. Thus, understanding tensile fracture propagation may be of fundamental importance. A limited amount of tensile strength and fracture toughness data has been obtained recently⁴⁰ for welded tuff from G-tunnel. Average values for the tensile strength, Young's modulus, and Poisson's ratio were $2.75 \pm 0.62 \text{ MPa}$, $7.43 \pm 2.30 \text{ GPa}$, and 0.17 ± 0.04 , respectively.

Brazil tensile strength also correlates with porosity as shown in Figure 16. These data were obtained before commencement of the soaking experiments on Topopah Springs welded and devitrified tuff and Bedded Tuff of Calico Hills. Note that the tensile strength cannot be determined

solely by the formation since both strength and porosity vary widely for samples from the Topopah Springs formation.

The fracture toughness as given by K_{Ic} for welded tuff from G-tunnel is $\sim 0.50 \text{ MPa m}^{1/2}$. This is a measure of the stress at the crack tip at the onset of propagation. By comparison, K_{Ic} values for Indiana limestone, Westerly granite, and rock salt are respectively 0.95, 2.60, and 0.4 $\text{MPa m}^{1/2}$. Thus, tensile fracture propagation through ash-flow tuff is relatively easy.

We have run two elevated temperature (200°C) tests on tuff, and the data are given in Table 4. Both the welded (739) and partially welded (185) specimens showed a 30% decrease in strength compared to room-temperature data. These studies have just begun, and much more work is planned.

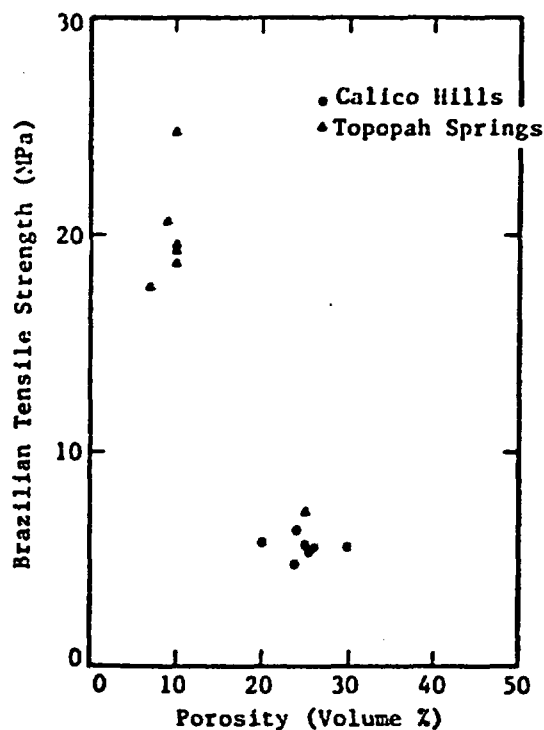


Figure 16. Brazil Tensile Strength Versus Porosity for Samples of Calico Hills and Tonopah Springs Tuff

Water can affect the properties of rock through chemical or mechanical mechanisms. The mechanical effect arises through the coupling of diffusion and deformation, which can cause nonequilibrium pore pressures and resultant alterations in strength. We have studied the effects of strain rate and degree of saturation together. Specimens of welded tuff from G-tunnel were divided into two groups. One group was saturated with tap water under a vacuum until weight was constant; the second was dried at 100°C until weight stabilized. Figure 17 shows that both the dry and wet groups demonstrate a significant strain-rate effect. Both wet and dry samples show about a 6% strength decrease per decade decrease in strain-rate. Figure 17 suggests that the water effect is not due to mechanical coupling because if pore pressures were increasing at high rates of strain, the material would exhibit anomalous weakening.

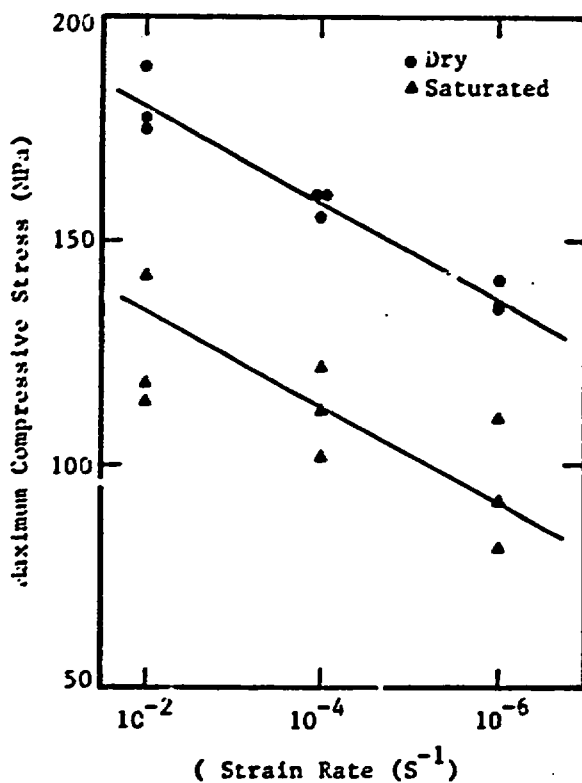


Figure 17. The Effect of Strain Rate and Water Content on the Maximum Compressive Stress of Welded Tuffs

The chemistry and physics of the weakening by water is not well understood. The concepts of stress-corrosion cracking⁴¹ or hydrolytic weakening⁴² apply to silicate rocks, and are based on a mechanism of hydration of SiO bonds at crack edges or dislocation cores. The stress-corrosion theory may be more applicable under conditions to be found near a repository. Hydrolytic weakening has been observed in a regime of very high temperature (>380°C) and leads to increased dislocation mobility and consequent strength reduction. It may occur at lower temperatures after extended periods of time. Stress corrosion, although certainly temperature-dependent, significantly affects crack propagation at room temperature.

The compressional or P-wave velocity nondestructive test can provide useful information. Microstructural damage is known to reduce P-wave velocity, and this phenomenon has been used by mining research workers to gain insight into the amount of damage caused by blasting, for instance. Because the P-wave velocity is proportional to the Young's modulus and inversely related to the density, one expects the velocity to be a function of porosity. Data obtained on material from Yucca Mountain and G-tunnel⁴³ shows a clear trend. As expected, P-wave velocity increases as porosity decreases. Comparison to theoretical predictions will be done after more testing.

The shear strength of jointed rock has also been considered. Investigations have concentrated on the properties of a single joint, which forms the weakest and therefore deciding link in the stability of a rock mass. Limiting the scope of interest to a single element of a discontinuous rock mass provides, of course, only fundamental empirical information. However, it also determines and explains the behavior of the entire system since the stability of the rock mass depends on the behavior of individual joints as well as joint interactions that can be adequately modeled, once the behavior of a single joint is determined.

We determined the shear strength in triaxial compression of a simulated joint of welded tuff from G-tunnel as a function of confining pressure, displacement rate, and water saturation. Joints are simulated by

using a right circular cylinder with a polished precut that is inclined at 35° to the cylinder (load) axis. Room-temperature tests were conducted at confining pressures from 5 to 40 MPa, axial displacement rates from 10⁻² to 10⁻⁶ cm/s, and water saturation of 0% (dry) and 100%.

The shear strength of the simulated joint in welded tuff fits the linear relation

$$\tau = \mu\sigma \quad (5)$$

where τ is the shear stress, μ is the coefficient of friction, and σ is the normal stress.

Accordingly, the coefficient of friction at the initiation of slip was independent of the normal stress, with a value of 0.64 at a displacement rate of 10⁻⁴ cm/s. Similar results were obtained for partially welded tuff from Yucca Mountain at a displacement rate of ~10⁻³ cm/s ($\mu = 0.59$). The independence of μ on the confining pressure and the corresponding normal stress across the sliding surface is consistent with the rock-friction literature as reviewed by Byerlee.⁴⁴

To determine the effect of displacement rate on the coefficient of friction, a series of dry, room-temperature tests were conducted at 10 MPa confining pressure and constant axial displacement rates from 10⁻² to 10⁻⁶ cm/s. With decreasing displacement rate the coefficient of friction increased from 0.62 at 10⁻² cm/s to 0.66 at 10⁻⁶ cm/s as shown in Figure 18. These results are consistent with the work of Dieterich⁴⁵ and Teufel and Logan,⁴⁶ who attributed the velocity dependence of friction to time-dependent growth of asperity contacts by creep. An increase in the area of individual asperity contacts at any given normal stress increases the real area of contact and hence the shear strength of the sliding surface.

The coefficient of friction, μ , of a water-saturated precut is also independent of normal stress and linear with respect to τ/σ . However, μ for the water-saturated precut is 9% greater than for dry precuts, with a value of 0.70.

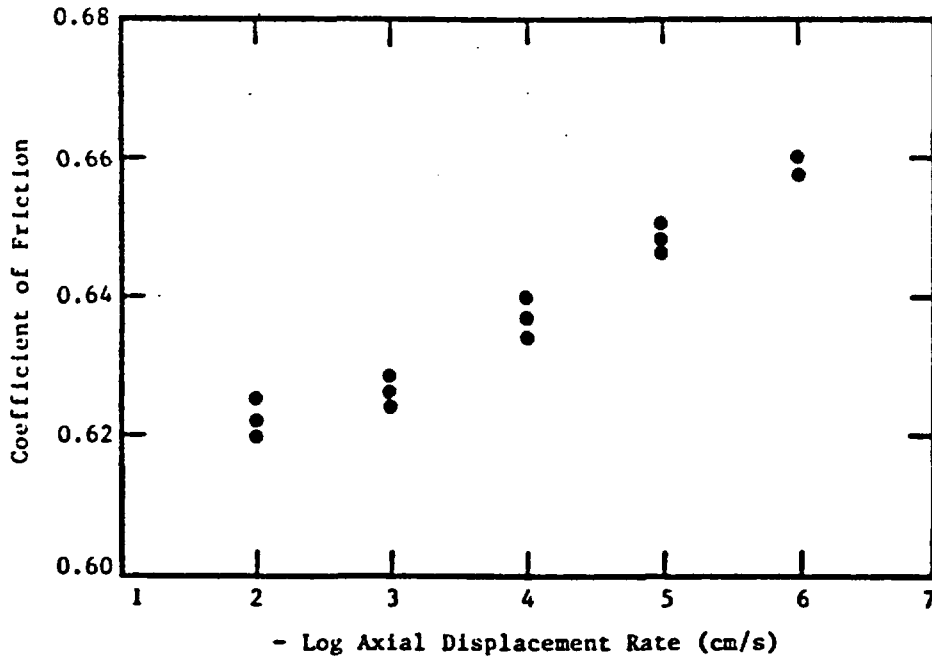


Figure 18. Coefficient of Friction (35°C Saw cut) Versus Displacement Rate for Dry Samples and a Confining Pressure of 10 MPa

The increased frictional resistance of welded tuff due to water saturation is enhanced as the displacement rate decreases (Figure 19). As the displacement rate decreases from 10^{-2} to 10^{-6} cm/s, the coefficient of friction increases from 0.67 to 0.74. In comparison to dry tuff, μ for the wet tuff is 7% greater at 10^{-2} cm/s and 11% greater at 10^{-6} cm/s. The increased velocity-dependence of the frictional resistance of the wet tuff is attributed to time-dependent hydrolytic weakening and stress corrosion of asperity contacts on the sliding surface, which increases the real area of adhesive contact. The observed time-dependent increase in the frictional strength of simulated joints and the time-dependent decrease in the failure strength of intact tuff suggests that, for long time durations, the strength of jointed tuff rock mass may increase sufficiently to approach that of the intact rock.

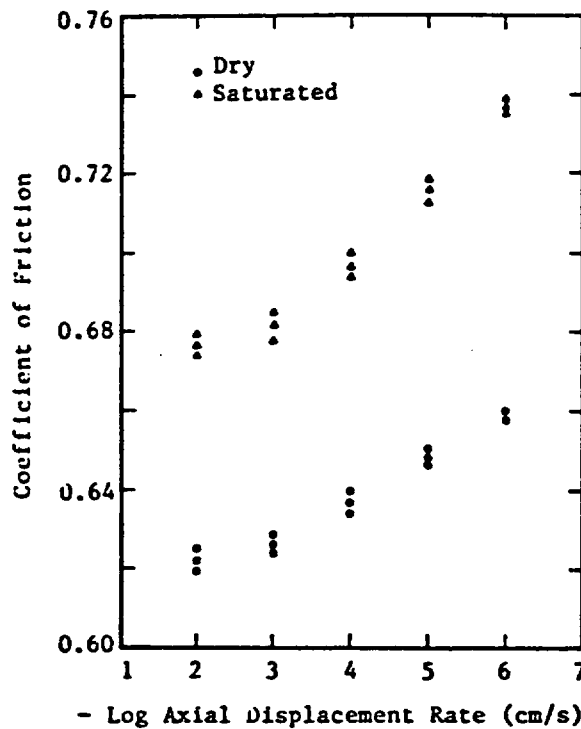


Figure 19. The Effect of Water on Increasing the Coefficient of Friction (35° Saw cut) as the Displacement Rate Decreases. (Confining pressure was 10 MPa)

To date, these studies have established a clear relation between strength and porosity, and a definite effect of water content (temperature) and strain (displacement) rate on strength and coefficient of friction. Future studies will expand on those reported here, in addition to determination of pore pressure effects, joint normal and shear modulus, creep effects, joint and matrix permeability as a function of time, temperature and normal stress, and suspected mineralogical effects (soak tests) on mechanical properties.

3.5 Radiation Effects on Tuff (J. K. Johnstone, SNL)

Radiation effects are restricted to the very near field; consequently, these studies are limited to welded tuff. Samples are being prepared to measure the effects of γ radiation on density, weight loss, thermal expansion, thermal conductivity, mechanical properties (unconfined, axial

compression), sorption behavior, and mineralogical alteration. Samples will be irradiated in both saturated and dry states with duplicates as unexposed controls. The irradiation facility contains a source that is 10^7 rad/h (~ 0.7 MCi) ^{60}Co (1.2 MeV γ). The ambient temperature in the exposure cavity is 90°C . The total exposure will be 10^{10} rad. So far we have no results.

Future tests may include combinations of components including simulated waste forms, canister materials, and engineered barriers.

3.6 Behavior of Water in Tuff

The two main sources of water in tuffs are pore water and mineralogical water such as that contained in zeolites, hydrated glass, and clay. Each source is capable of contributing large quantities of water. The unknown effects of water in tuff were raised as an issue before the NAS during the last briefing. Since that time, two studies were undertaken to characterize the behavior of water under different stimuli.

3.6.1 Water Loss by Drying from Welded Tuff (G. R. Hadley, SNL)

Water transport through porous rock can occur as a flow of liquid water or water vapor as well as by diffusion of water vapor through air. Although much is known about the first process, the role of the two other processes for geologic materials has been largely ignored. Drying theories have been developed and applied in several other areas, but until recently the loss of water from porous rock due to drying has not been of great interest. Expected conditions in a waste-disposal scenario, however, make evaporative drying an important mechanism to consider.

A set of preliminary experiments has been conducted in which water-loss rates due to drying in dry nitrogen were measured for tuff core sections (4.7 cm dia x 6 cm long) at temperatures from 25° to 150°C . A complete description of the experiments is found in Reference 47.

Results for the drying rate at room temperature are shown in Figure 20, together with model predictions. For this particular run, over

90% of the pore water was lost from the sample within 72 hours. The rest was later removed by heating. Other runs at elevated temperatures (up to 150°C) show even higher loss rates and consequently faster dehydration.

Two models were formulated in an attempt to understand the drying process more fully. Both models assume two single-phase regions (one liquid and one vapor) separated by a well-defined moving front (Figure 21). In one case, the vapor region is treated as a Darcy flow through the porous rock driven by the higher partial pressure of water vapor at the front. This model has proved effective in describing the motion of water vapor through rock salt in other tests. The second model assumes that the vapor region consists of both water vapor and air, with molecular diffusion the dominant mode of water transport.

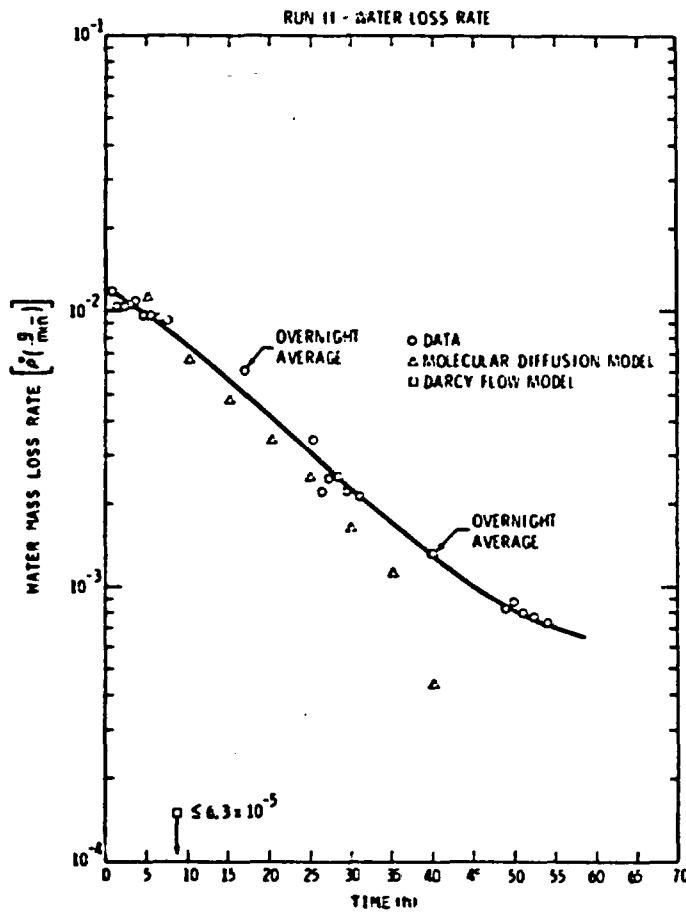


Figure 20. Results of Drying Welded Tuff at Room Temperature

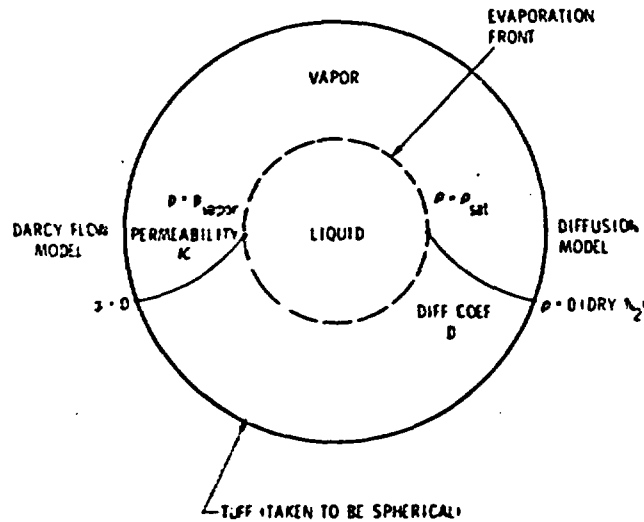


Figure 21. Schematic of Models Used to Explain Drying Behavior

The Darcy flow model requires the material permeability as input. For the present experiments, the permeability was chosen to fit the high-temperature data (not presented here). As can be seen in Figure 20, the Darcy flow-model prediction is several orders-of-magnitude low for the room-temperature case. On the other hand, the diffusion model fits the data reasonably well until late times. By then most of the water is gone and the major mechanism might change from being front-controlled to some other unknown phenomenon.

One obvious application of this research is for drying drill holes, mine pillars, etc, when exposed to a drying atmosphere. The results seem to indicate significant drying over a period of days, the exact rate depending on the geometry of the exposed rock and the humidity of the drying atmosphere.

Another important application is the determination of water collected during waste emplacement (or heater experiments). Whenever the humidity in a heated chamber drops below 100%, vapor from the hot rock may diffuse into the chamber and recondense. Because tuff contains a sizable

volume percent of water, significant amounts of water may accumulate over time. If the process is evaporation-front-controlled, preliminary calculations suggest that the rate of water release may decrease only slowly or not at all as the front recedes into the formation.

Experiments are necessary that include better diagnostics in order to more fully understand the transport process. Specific questions to be answered include:

- Is the water-loss rate controlled by a well-defined evaporation front?
- If a front exists, is its motion governed by mass balance or energy balance?
- What role does capillarity play in the transport process?

Experiments are being planned that will try to answer these questions. Gamma-ray absorption seems the most promising technique for measuring saturation as a function of position and time. Its use should allow adequate spatial resolution to investigate front motion.

3.6.2 In-Situ Tuff Water-Migration/Heater Experiment (J. K. Johnstone, SNL)

An in-situ experiment in the welded Grouse Canyon Tuff is under way. The experiment serves as an initial assessment of water behavior in a deep underground environment (>400 m) in response to a thermal source. The rock is 95 to 99% saturated (20 to 25 vol% water) and is well above the water table. While G-tunnel is not a potential repository site, the Grouse Canyon Tuff has physical, thermal, and mechanical properties very similar to those in tuffs now under consideration. In addition to an initial evaluation of water behavior, the experiment supports computer code and instrumentation development and attempts to measure in-situ thermal properties. A complete description of the experiment is contained in Reference 48.

The experiment is composed of six satellite holes arranged at three radii concentrically about a central heater hole as shown in Figure 22. Three holes are designed to measure water behavior, two to measure in detail the thermal profiles, and one to measure thermally induced stresses. In addition, a hole aligned as nearly perpendicular to the heater axis and along the midplane as possible is included for a laser interferometer for measuring displacement. The radial distance of the holes from the heater was selected after evaluation of the pretest thermal and thermomechanical modeling results and current drilling capabilities. Each hole is located so that it is not shadowed from the heater by another hole. All the holes were 150Z-cored during drilling and, where possible, visually scanned with a borehole TV camera.

The instrument "cavity" in each of the experiment holes is arranged as symmetrically as possible at the midplane of the heater, as shown schematically in Figure 23. Two of the water-migration holes were located so that joints intersect the water collection cavity, and the other hole so that joints do not intersect the water-collection cavity.

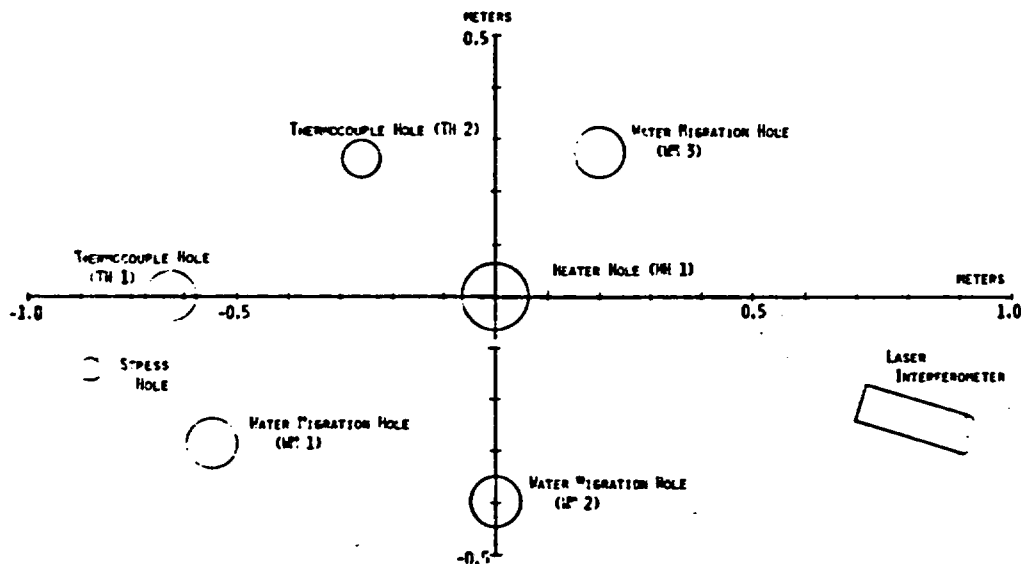


Figure 22. Experimental Hole Array

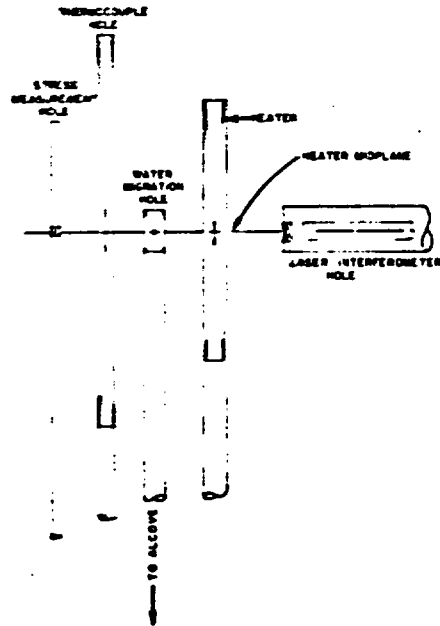


Figure 23. Schematic of Symmetrical Orientation of the Experimental Holes ~~around the Heater Midplane~~

Since the welded tuff lies in the ceiling over G-tunnel, all of the drill holes except the laser interferometer hole were oriented at 20° above horizontal (Figure 24). As a result, the water drained away from the heater and prevented the refluxing observed in other tests.

An electrical heater, 1.2 m long x 10.2 cm OD, and operated between 760 and 1000 W for 63 days, was used for the experiment. Because of the near horizontal orientation, the heater was designed to minimize convection currents. The maximum temperature at the heater hole rock wall was ~240°C.

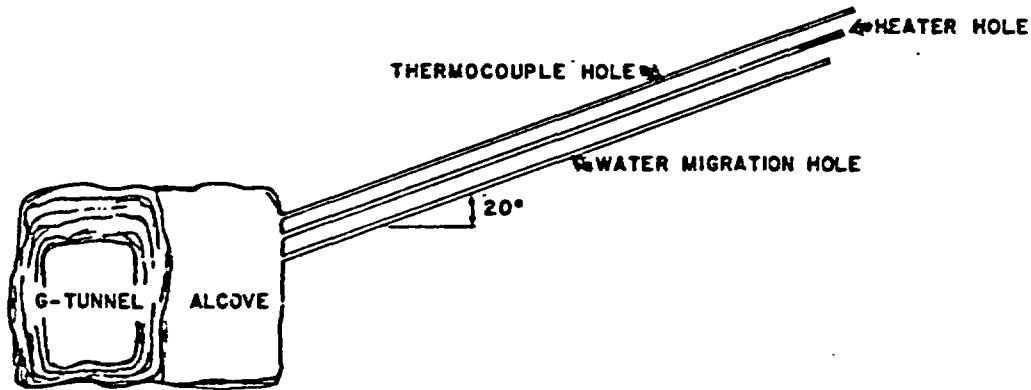


Figure 24. Vertical Orientation of the Experimental Holes in Relation to the Alcove and G-Tunnel

Water was collected continuously during the heated phase of the experiment in the heater hole and in two of the three water-migration holes. The water-collection rates are shown in Figure 25. The total amount of water collected was ~60 L from the heater hole, ~3.6 L from WM-2, and ~1.5 L from WM-1. Water generation ceased abruptly when the heater power was shut off. The water collected is undergoing chemical analysis.

Preliminary analysis suggests that around the heater hole, water movement is by vapor diffusion into the hole. Water migration into the satellite holes appears to be by Darcy flow driven by the high partial pressure of water at the vaporization front.

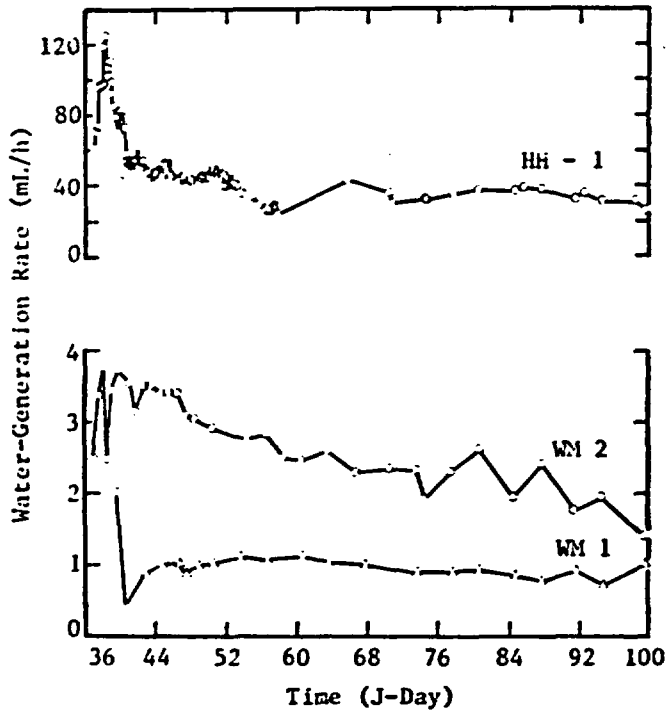


Figure 25. Water-Collection Rates for the Heater Hole (HH-1) and Two of the Water-Migration Holes (WM 1, WM 2) as a Function of Julian (J) Days

In addition to the water data, detailed information was obtained on the thermal profiles and thermally induced stress and displacement. All these data are currently undergoing evaluation. Detailed posttest activities are in progress, including permeability testing, TV examination of the holes, corebacks, mineralogical examination, and instrumentation evaluation.

4. MINE DESIGN WORKING GROUP (L. D. Tyler and B. S. Langkopf, SNL)

The main objectives of the Mine Design Working Group are to

- Define the anticipated environment for a repository in welded tuff located above or below the water table
- Identify model needs and critical data needs for confident design in using welded tuff as the host rock for a high-level waste (HLW) repository
- Develop conceptual test plans for in-situ tests designed to resolve the issues identified above
- Integrate the results of the in-situ tests and both laboratory and model studies into an engineering design data package for use in completing a conceptual design

The Mine Design Working Group consists of representatives from Sandia National Laboratories, Los Alamos Scientific Laboratory, RE/SPEC, Inc., and Texas A&M University.

A base case has been established for a repository in welded tuff below the water table in Yucca Mountain. Scoping calculations are under way using available host-rock data and models, along with reasonable assumptions (where necessary) to complete a timely estimate. The tuff properties and stratigraphy used in the modeling are based on information from UE25a-1. Inadequate models and/or data will be identified. The calculation will be iterative. Feedback is required in several stages of the calculation to maintain internal consistency; for example, if substantial opening of fractures is predicted, then the impact on the calculated temperature distribution must be evaluated. The base-case calculation is outlined in more detail below.

- Initial Assumptions -- As already stated, a basis was defined that include canister geometry, thermal power, and implantation density and geometry. Engineered barriers will be considered later. If, in the course of the calculation, it is found that the basis is for some reason untenable, a new basis will be defined.

- Characterization of the Mine -- A mine layout with sufficient specification to allow subsequent thermal, mechanical, and chemical characterization was established. Practical factors such as mining and mine-stabilization methods will be considered because they affect mine geometry and the types of materials, respectively, that will be interacting to establish the mine's chemical environment. Ventilation requirements will be considered because they impact heat transfer and rock drying. Rate of water inflow, which affects heat transfer and the chemical environment, will be considered.

- Thermal Analysis -- The temperature distribution at representative points within the repository will be determined as a function of time. Approximate temperature histories will be determined for the local (canister well), near-field (mine floor and pillars), and far-field (overlying rock strata) environments. In all cases, the effects of convecting steam or water will be considered in addition to thermal conduction.

- Mechanical/Structural Analysis -- The anticipated displacement and rock failure as a function of time at representative positions will be scoped. Calculated temperatures will be used to estimate expected thermal stresses. These will be used, along with available constitutive relations (probably simple elastic behavior) and strength data, to calculate stress, displacement, and any failure at representative points in

the repository. (Some analysis of the sensitivity of this output to assumed constitutive relations and strength should be possible.) As already discussed, if any substantial fracturing is predicted, its effect on heat transfer will be evaluated and new temperature histories will be calculated if warranted.

- Chemical Analysis -- The chemical and radiation environment will be identified at each representative repository point. Chemical thermodynamics or kinetics calculations will not be performed.

After the analysis of the base case is completed, work will begin on evaluating how the repository environment would be modified if the repository is located above the water table. A major difference now anticipated for any such repository is change in the heatup history. It is possible that the results of these scoping studies alone will clearly indicate a preferable location; in any event, data and model needs will be identified. A preliminary estimate of the anticipated repository environment will also be completed.

Three meetings of the Mine Design Working Group have been held as of the end of April, 1980. At present the working group is using the results of the completed conductive heat-transfer scoping calculations as input for the thermomechanical scoping calculations.

4.1 Thermal Scoping Studies

Initial heat-transfer calculations were used to develop an understanding of the thermal environment of a repository in welded tuff for

- Boiling conditions (hydrostatic and atmospheric pressure)
- Gross thermal load (GTL) (25 to 150 kW/acre)
- Canister pitch* (function of GTL)

*Linear spacing

- Extraction ratio* (ER) (10 to 30%)
- Thermal property changes due to water boiling.

Both spent fuel and reprocessed HLW were considered. The initial conditions used in most of the modeling are shown in Figures C1 and C2 and Tables C1-C4 in Appendix C.

The purpose of the very near-field calculations was to determine the thermal environment of the canister and surrounding rock for different heat loads. The room-and-pillar calculations were to determine the thermal environment of the room and pillar caused by different gross thermal loadings and extraction ratios. The far-field calculations were to determine the responses of the far-field stratigraphy to different gross thermal loadings.

An upper limit GTL of 100 kW/acre at a 20% ER has been established as a reference condition for both spent fuel and high level waste. Scoping calculations were done using the boiling limits of atmospheric pressure (i.e., 100°C) and hydrostatic pressure (i.e., 225°C for the static water level). This reference condition will be reassessed as additional studies are completed. Results from the thermal calculation for a GTL of 75 kW/acre at an ER of 20% are presented below for both spent fuel and HLW.

4.1.1 Spent-Fuel Results

Results** of the 75 kW/acre GTL calculation for the very near field are shown in Figures 26 and 27. Figure 26 shows temperature histories for selected points at the midplane of the spent-fuel canister for an ER of 20%, GTL of 75 kW/acre, and 100°C boiling temperature. Figure 27 shows the spatial temperature distribution through the repository at the midplane of the spent-fuel canister at the time when the canister temperature

*Ratio of the room width to the sum of the room + pillar width.

**These results assume an ambient rock temperature of 55°C at the repository depth. Recent field work indicates a lower ambient temperature approaching 35°C.

peaks; boiling was assumed to occur at 100°C. Figure 28 illustrates temperatures of the floor and ceiling centerlines, and room midheight with time for the room-and-pillar calculation of 75 kW/acre and 100°C boiling. The far-field temperature profiles along the vertical centerline for a 75 kW/acre repository are given in Figure 29. The far-field calculations indicate that the radial temperatures outside the repository boundary for GTL below 150 kW/acre will be <100°C.

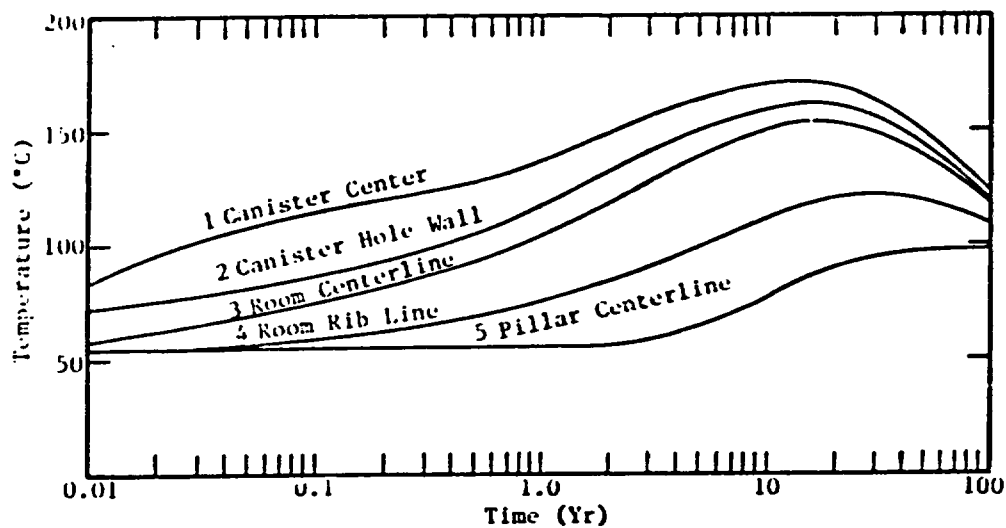


Figure 26. Temperature History at Selected Points Through Midplane of Spent-Fuel Canister for ER of 20%, GTL of 75 kW/Acre, and Boiling of Porewater (Ambient Rock Temperature of 55°C)

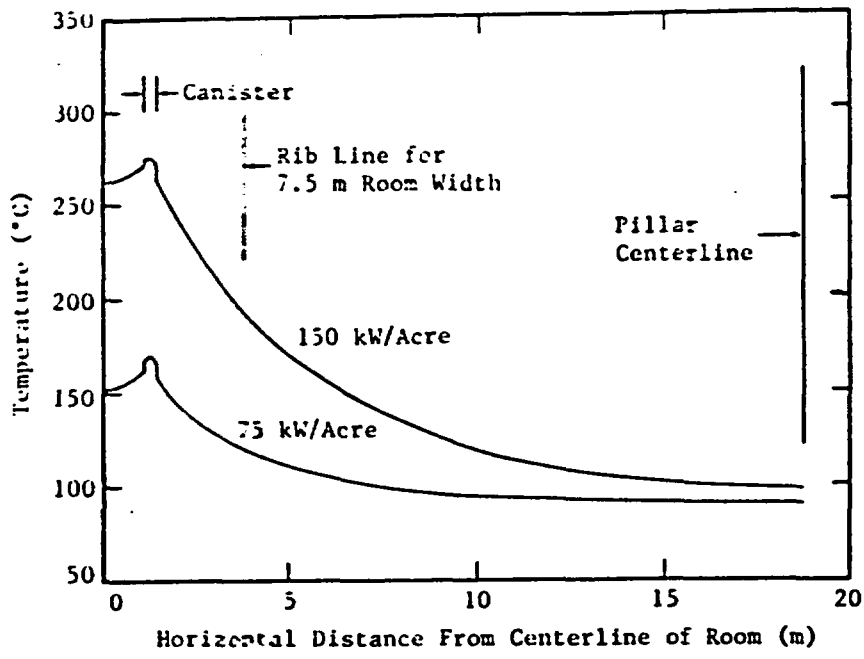


Figure 27
 Spatial Temperature
 Distribution Through
 Midplane of Spent-Fuel
 Waste Canister
 (Ambient Rock Temper-
 ature of 55°C)

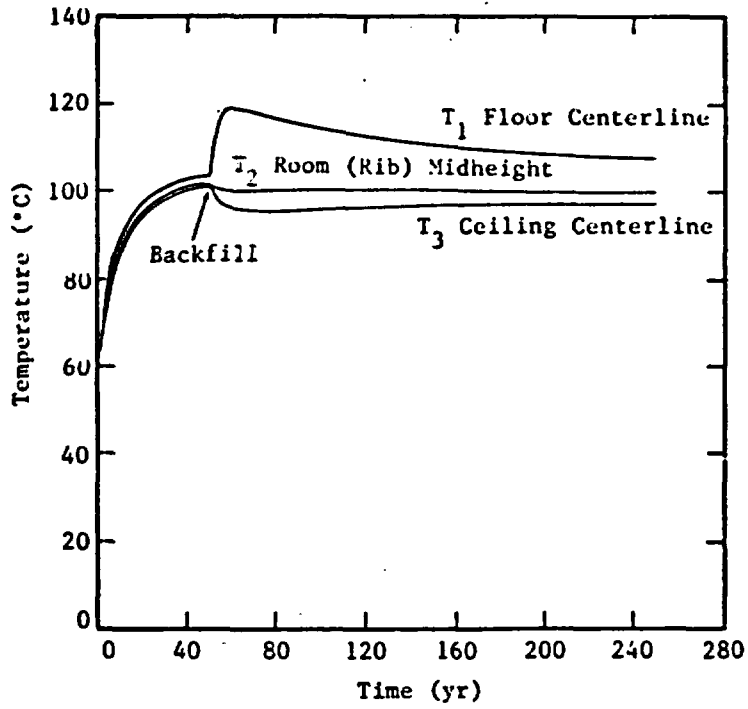


Figure 28
 Time-Temperature History
 for Three Room Locations
 for ER = 0.7,
 GTL = 75 kW/Acre,
 100° Boiling, and
 Saturated Backfill
 (Ambient Rock Temper-
 ature of 55°C)

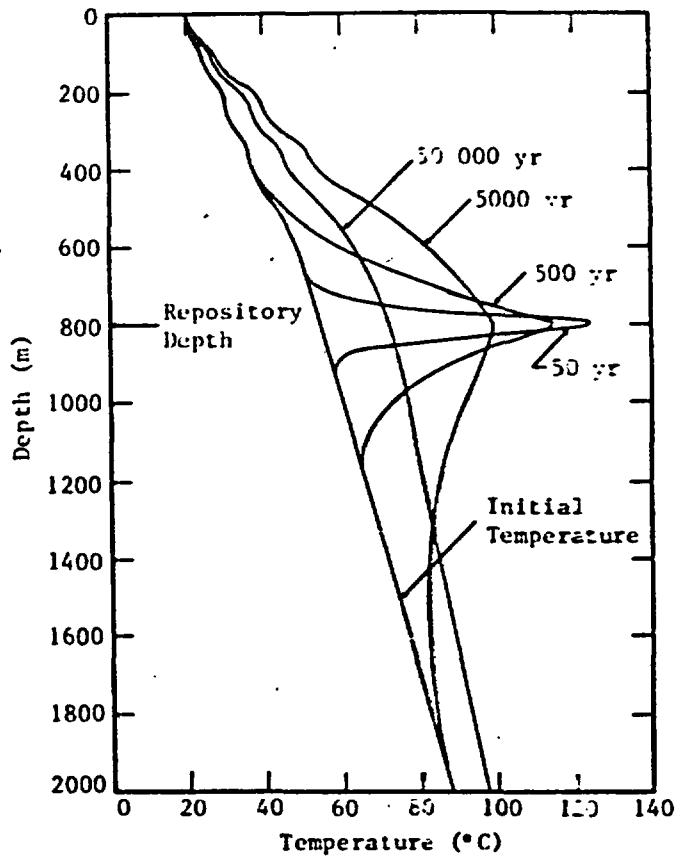


Figure 29. Far Field Temperature Profile Along the Vertical Centerline for GTL of 75 kW/Acre

4.1.2 High-Level Waste Results

Representative examples of results* from the H₂W computer modeling studies are also included as figures. Results of the very near-field calculations are summarized in Figures 30 and 31. These figures show maximum canister and tuff temperatures (at the canister centerplane) as a function of tuff thermal conductivity, assuming 100°C boiling for different canister powers. Figures 32 and 33 show the floor and pillar centerline peak

*Ambient rock temperature conditions the same as for spent-fuel calculations (see footnote, p88).

temperatures for different GTL (also included are different boiling temperatures, extraction ratios, initial temperatures, and types of backfill); these figures are the results from the room-and-pillar calculations. The room mid-height temperatures are 5°C or less higher than the pillar center-line temperatures. Figure 34 is from a far-field calculation. It illustrates the temperatures at depth for various times for a 75 kW/acre case.

Two observations follow from the thermal scoping calculations:

- a. When the before-and-after boiling thermal conductivities in the very near field are varied by +20%, and these variations are combined in different ways, the results do not vary more than +10%
- b. The use of unsaturated instead of saturated backfill does not significantly affect the thermal results of room-and-pillar spent-fuel and HLW calculations.

4.2 Thermomechanical and Hydrethermal Scoping Studies

Thermomechanical scoping studies are presently under way. These studies will use the same initial conditions as the thermal studies, but will add mechanical properties such as thermal expansion, Poisson's ratio, Young's modulus, and in-situ stress. The first calculations in these studies will be far-field and room-and-pillar calculations for HLW and spent fuel. A two-dimensional jointed-material model will be used for these calculations. As a result of initial thermal calculations and available thermal criteria, the thermomechanical studies will use a more limited range of GTL (25, 50, 75, and 100 kW/acre). In order to reduce the number of calculations required, the room-and-pillar calculations will use a 20% ER and a 100°C boiling temperature.

In the second step of the mechanical scoping studies, a three-dimensional jointed-material model will be used to perform calculations for the very near-field, room-and-pillar, and far-field environments.

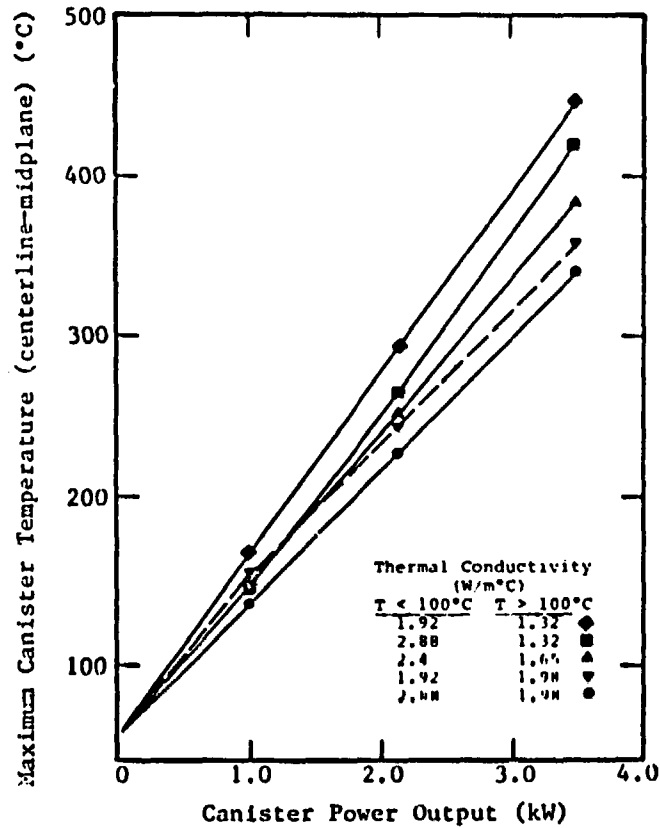


Figure 30. Effect of Tuff Conductivity on Maximum Canister Temperature (Time = 2 yr, 75 kW/acre, ER = 20%, Ambient Rock Temperature = 55°C)

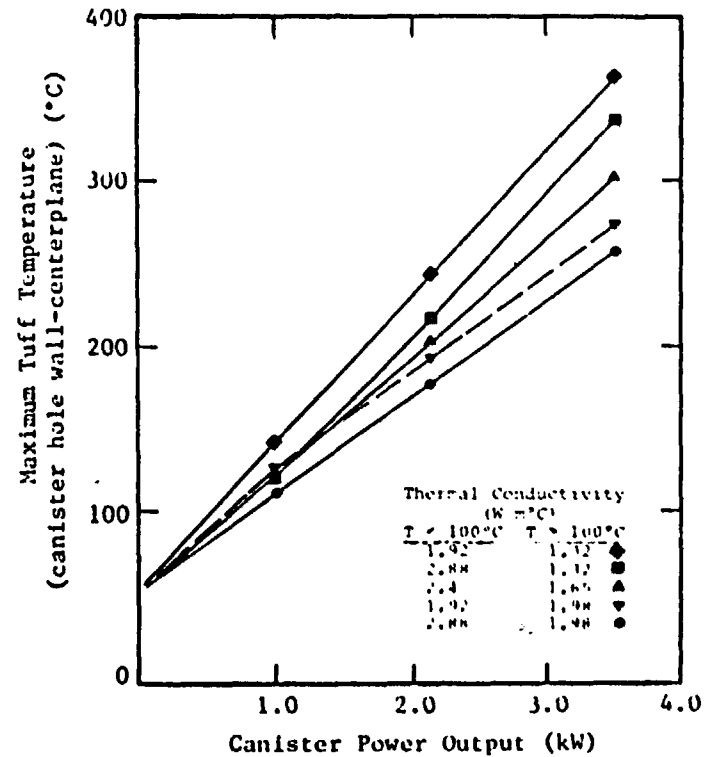


Figure 31. Effect of Tuff Conductivity on Maximum Tuff Temperature (Time = 2 yr, 75 kW/acre, ER = 20%, Ambient Rock Temperature = 55°C)

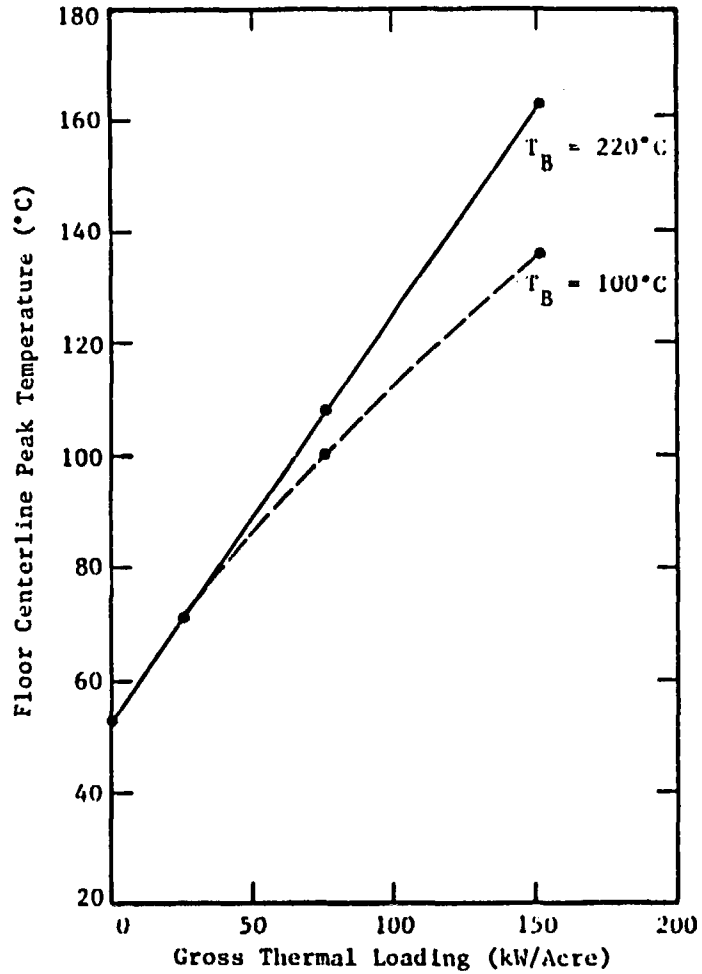


Figure 32. Peak Floor Temperature vs GTL
(Ambient Rock Temperature = 55°C)

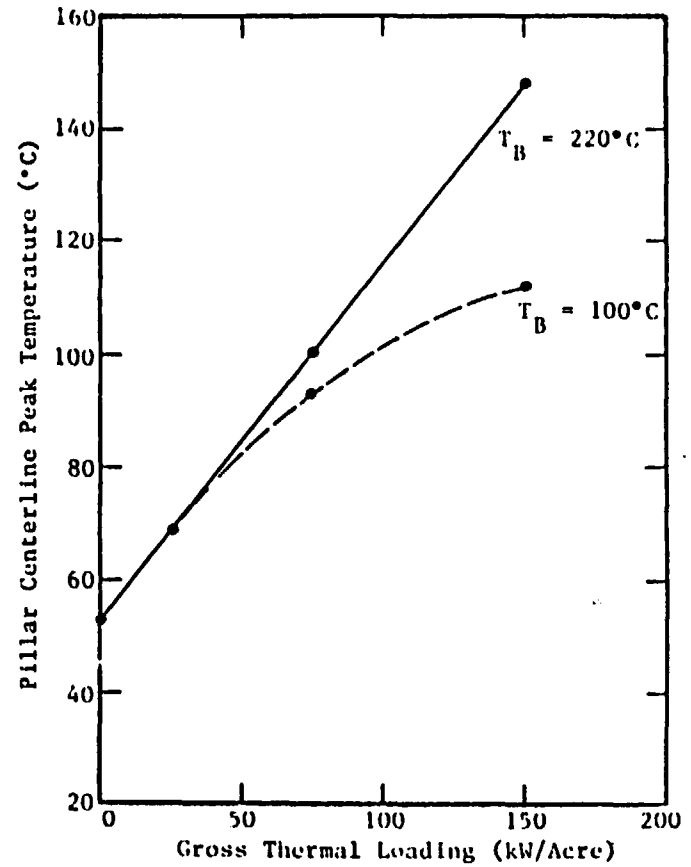


Figure 33. Peak Pillar Centerline
Temperature vs GTL (Ambient
Rock Temperature = 55°C)

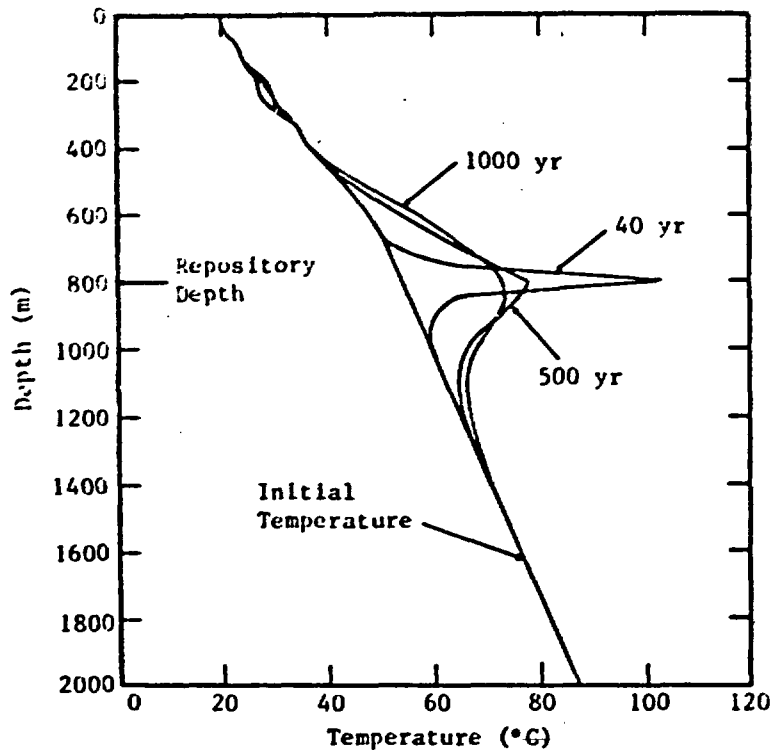


Figure 34. Temperature Profile Along the Vertical Centerline for HLW and 75 kW/Acre GTL

Calculations of hydrologic effects at Yucca Mountain are also under way. Preliminary indications are that the far-field effects of hydrothermal transport would be minor. This is especially true if in-situ boiling is assumed to occur at the hydrostatically controlled temperature, since, even for thermal loadings in excess of 100 kW/acre, no boiling is predicted under this assumption.

As regards very near-field considerations, in addition to the limit established previously (i.e., 100 kW/acre), it must be kept in mind that the use of engineered barriers will, if anything, require further reduction of GTL resulting in temperatures so low that fluid pressurization, vaporization, and transport will be further restricted.

4.3 Future Studies

As studies progress, data needs and basic assumptions of the phenomena modeled will be evaluated. Uncertainty in available data may require sensitivity analyses to determine if the uncertainty is critical, followed by or in conjunction with laboratory and in-situ experiments designed to acquire the needed data. Additional computer modeling may be required after completing laboratory and in-situ experiments. Some of the concerns to be addressed include:

- Far-field hydrothermal circulation effects
- Very near-field hydrothermal circulation effects
- Pressurization as a result of boiling water
- Radiation effects
- Engineered barriers
- Phase transitions of water
- Mine ventilation (and/or blast cooling)
- Recharge of the mine

5. IN-SITU (FIELD) EXPERIMENTS

5.1 Underground Rock-Mechanics Laboratory (J. K. Johnstone, SNL)

Planning is currently under way to mine a rock-mechanics laboratory in the welded Grouse Canyon Tuff in G-tunnel. The usable portion of the welded unit in the proposed vicinity of the laboratory is 12 to 15 m thick.

The underground rock-mechanics laboratory is a major facility in support of Mine Design activities. As discussed previously, the Mine Design Working Group is currently evaluating a mine opening in tuff in an attempt to identify deficiencies and unknowns in existing data and models. The working group will then formalize the rock-mechanics plan for in-situ experiments. We expect to

- Study the effects of joints and matrix water release on the thermal and mechanical response of the rock mass
- Verify jointed-rock models currently under development
- Determine rock mass thermal conductivity
- Determine in-situ permeability during heating
- Verify predicted thermal and mechanical response for specific canister spacing and room geometry
- Generally evaluate the application of laboratory data to a field environment.

5.2 Nuclide-Migration Field Experiments (B. R. Erdal, LASL)

In order to estimate the concentrations and travel times to discharge areas for radionuclides that may leave a repository, predictive models must be developed based on understanding the dynamic processes that occur at each location in the total repository-rock system. These models must

include appropriate chemical equilibrium and rate expressions that adequately describe the various chemical phenomena involved; i.e., dissolution, complexation, precipitation, ion exchange, surface adsorption, hydrolysis, coprecipitation, formation of solid solutions, colloid and polymer formation, etc. Knowledge of the regional hydrologic regime must then be superimposed on the chemistry. This includes effects such as hydrodynamic dispersion, distance, pore/fluid velocity, and saturated or unsaturated flow. For many rocks, including tuff, there is the additional complication of having flow that is dominated by the hydrology and mineralogy of a fracture system. In this case it is particularly important to establish reliable bounds for fracture dimensions and fluid velocities. Mathematical methods must be developed to handle all the processes that occur in a three-dimensional system of this type. These models must be verified by selected tests specifically designed to address this problem.

Transport of radionuclides through fractured systems is a relatively new field for which much research will be required before it is understood as well as the more familiar porous media. Two methods of approach to transport in fractured media have been proposed. In the first approach, one relies upon the observed regularity of many fracture systems to consider the rock mass as a network of interconnected discrete fractures, and each fracture must be separately identified. The other approach treats the rock mass as a porous medium in which the hydraulic characteristics of the fractures are averaged. The first approach is reasonably applied only in the near field, where the detailed identification of fracture flowpaths is sometimes feasible. A mixed fracture-porous medium model may be appropriate for the intermediate case where only the largest fractures are of concern. In the far-field, only a strictly porous medium model will probably be feasible.

In considering groundwater flow and radionuclide retention in the complex flow systems that can occur in rock, serious problems may arise in determining (1) if laboratory studies are being performed under conditions appropriate to natural systems, and (2) if models of nuclide transport derived from laboratory results correctly handle nuclide movement under

natural conditions. These questions can be answered only by increasingly more complex laboratory and field tests at depth.

A project to address these problems has recently begun with support from the Office of Nuclear Waste Isolation. The project will be carried out jointly by the Los Alamos Scientific Laboratory, Sandia National Laboratories, and Argonne National Laboratory. The work has three principal objectives:

- Develop the experimental, instrumental, and safety techniques necessary to conduct controlled small-scale field radionuclide-migration experiments
- Use these techniques to define radionuclide migration through rock by performing generic field experiments at depth under closely controlled conditions
- Determine whether available lithologic, geochemical, and hydraulic properties, together with existing or developed transport models are sufficient and appropriate to describe real field conditions (i.e., to scale from laboratory studies to bench-size studies to field studies.)

The tests will be performed in bedded tuff exposed in G-tunnel at WTS. The location was selected because of the following factors:

- Formations are accessible at depths that will allow comparison of laboratory results with field measurements and testing of models
- Support facilities already exist
- Mining and drilling costs and time should be reduced since the equipment and subcontractors are onsite
- Mining in G-tunnel/bedded tuff is relatively easy

Since G-tunnel is not a potential nuclear waste repository, the proposed experiments will not compromise the integrity of an actual site.

The field experiment is composed of several key elements. The first is detailed characterization of the groundwater in tuff. This will be

carried out on several tuffaceous wells, seeps in G-tunnel and rock equilibration experiments. Two nuclide migration experiments will be performed, using the appropriate groundwater. The first uses stable or short-lived nuclides, and the second uses longer-lived radionuclides, including actinides. The experimental fracture will be recovered after each experiment. The first experiment serves as a demonstration of the experimental procedure and of safe operating and mineback/fracture recovery procedures before commencement of the second, actinide-containing experiment. Detailed postflow analyses of the rock, solution-rock interactions, radionuclide distributions, etc, will be made. They are essential for correlating the migration of nuclides under actual conditions with laboratory and modeling studies.

The fundamental question being addressed is: If the physical and chemical properties of a rock and a solution are measured in the laboratory, can accurate models of radionuclide migration through that rock in the field be formulated? The specific results using G-tunnel tuff may not directly apply to radionuclide migration in other lithologic varieties of tuff, but methods of formulating models that describe field behavior and the understanding of which laboratory data are important will apply. The generic experimental, instrumental, and safety techniques developed for the field tests can be applied to other field experiments and will be useful for planning large-scale field tests.

6. CONCLUSIONS

The following preliminary conclusions are based on work completed to date on the ongoing studies described herein.

1. No single property or group of properties that would disqualify tuff as a potential repository medium has emerged.
2. At least one property--thermal conductivity--suggests potential limitations on repository thermal loadings. Thermal conductivity of tuffs is a complex problem that depends on porosity, water content, fracture frequency, and mineralogy. Although there are currently no criteria against which to evaluate thermal conductivity, initial modeling results indicate that reasonable limitations on repository thermal loadings can minimize potential difficulties.
3. We have demonstrated that there are minerals in the varieties of tuffs at NTS, particularly nonwelded tuff, that exhibit excellent sorptive properties for cations and that should provide a natural barrier against migration to the biosphere. These studies are continuing.
4. Extensive variation in tuff properties has been demonstrated. However, initial correlations of properties with porosity, grain density, mineralogy and water content have established the framework for future development of a substantial capability for predicting

properties. These relationships are in their infancy at present, but appear very promising.

5. Currently the majority of studies are laboratory-oriented. A substantial expansion of field and modeling activities, as well as laboratory studies, is required to meet the 1985 deadline for selecting a medium.

7. UNRESOLVED ISSUES

7.1 Water and Joint Effects on Tuff Properties and Models

The effects of water and joints on the properties of tuff, especially in an at-depth environment, remains the major unresolved issue. The studies so far show that the presence or absence of either water or joints has a major effect on thermal and mechanical properties. Current state-of-the-art thermal and thermomechanical models are only just beginning to account for joints and variable water content. Initial experiments imply that welded tuff may easily dry in a mine environment, while the water in the rock surrounding a hot-waste canister may migrate into the canister hole. Our current inability to characterize the in-situ joint properties (length, aperture, orientation, frequency, filling, degree of mineralization, etc) may prove to be a significant problem.

Effects of radiation on saturated tuff are unknown. Laboratory studies, field tests, and model development will continue to address the water and joint problems. Much of the direction of this work will come from the analytical results of the Mine Design Working Group.

7.2 Sorptive Properties and Transport or Retardation

Our ability to model the total geochemical system involved in transport of radionuclides from a repository to the biosphere is severely limited for any rock type, including tuff, being considered for a repository. This lack of understanding creates a significant uncertainty in estimating the adequacy of a geologic medium to retard migration. Unresolved issues that still require much work include

- The complex chemistry of lanthanides and actinides (e.g., plutonium and americium) in neutral to slightly basic groundwaters

- The effect of probable reducing conditions on elements that can exist in several oxidation states (e.g., plutonium, technetium, uranium)
- The apparently poor sorptive properties of tuffs (and many other rocks) for anions

Laboratory investigations to identify these and other parameters are being made. A field test of nuclide (representative fission products and actinides) migration in a single fracture in tuff is being performed. In addition to the development of techniques for such tests, a purpose of this experiment is to test the state-of-the-art of extrapolating laboratory results and applying models to real situations. Efforts are being made to develop a predictive model for tuff that incorporates the dynamic and equilibrium processes occurring at each location in the total repository-rock-groundwater system.

7.3 Creep

No information is available on creep behavior of tuff. Current studies suggest that creep may be a factor in mine opening stability during the operating phase of a repository. Studies are under way to evaluate this phenomenon.

7.4 Mineralogy and Petrology

The effect of vertical and lateral variability on the thermophysical properties of tuff remains an issue. The complexity of this variability has been demonstrated. Dehydration of zeolites during possible heating could affect the thermal and mechanical properties. Initial studies show promise in developing relations to predict various properties as a function of porosity, grain density, and/or mineralogy. Such relationships are essential for model development. Evaluation of the lateral and vertical variability continues with the drilling of the current USW-G1 hole at Yucca Mountain.

Tuff as a medium is complex and it occurs in complex blocks. Continued characterization and correlation of the mineralogical variation with properties is necessary for future modeling.

References

1. Letter from E. F. Gloyna, Chairman of the Committee on Radioactive Waste Management, to S. Meyers, Director of the Office of Nuclear Waste Management, US DOE, April 23, 1979.
2. R. L. Smith, Ash Flows, Geol Soc Amer Spec Paper 67, 1960a.
3. R. L. Smith, Zones and Zonal Variations in Welded-Ash Flows, US Geol Surv Prof Paper 354-F, 1960b, pp 138-143.
4. R. L. Smith and R. A. Bailey, "Resurgent Cauldrons," Geol Soc Amer Mem 116, 1968, pp 613-662.
5. A. O. Shepard and H. C. Starkey, Effect of Cation Exchange on the Thermal Behavior of Heulandite and Clinoptilolite, US Geol Surv Prof Paper 475-D, 1964.
6. G. H. Heiken and M. L. Bevier, Petrology of Tuff Units from the J-13 Drill Site, Jackass Flats, Nevada, LA-7563-MS (Los Alamos, NM: Los Alamos Scientific Laboratory, 1979).
7. M. L. Sykes, G. H. Heiken, and J. R. Smyth, Mineralogy and Petrology of Tuff Units from the UE25a-1 Drill Site, Yucca Mountain, Nevada, LA-8139-MS (Los Alamos, NM: Los Alamos Scientific Laboratory, 1979).
8. P. W. Lipman and E. J. McKay, Geologic Map of the Tonopah Spring SW Quadrangle, Nye County, Nevada, US Geol Surv Map GQ-439, 1965.
9. F. M. Byers, W. J. Carr, P. P. Orkild, W. D. Quinlivan and K. A. Sargent, Volcanic Suites and Related Cauldrons of the Timber Mountain - Oasis Valley Caldera Complex, Southern Nevada, US Geol Surv Prof Paper 919, 1976.
10. R. F. Marvin, F. M. Byers, Jr., H. H. Mehnert, P. P. Orkild and T. W. Stern, Radiometric Ages and Stratigraphic Sequence of Volcanic and Plutonic Rocks, Southern Nye and Western Lincoln Counties, Nevada, Geol Surv Amer Bull 81, 1970, pp 2657-2676.
11. P. P. Orkild and F. Maldonado, C. - Jackass Flats and Rock Valley, US Geol Surv unpublished land-use report, 1978.
12. Personal communication with B. Crowe, Los Alamos Scientific Laboratory, Los Alamos, NM.
13. J. R. Boles, "Composition, Optical Properties, Cell Dimensions and Thermal Stability of Some Heulandite Group Zeolites," Am Min, 57:1463-1493, 1972.

14. A. C. Doyle and G. L. Meyer, Summary of Hydraulic Data and Abridged Lithologic Log of Groundwater Test Well 6 (J-13), Jackass Flats, Nevada Test Site, Nye County, Nevada, US Geol Surv Tech Ltr NTS-50, 1963.
15. Personal communication with B. Crowe, Los Alamos Scientific Laboratory, Los Alamos, NM.
16. P. W. Lipman, R. L. Christiansen, and J. T. O'Connor, A Compositionally Zoned Ash-Flow Sheet in Southern Nevada, US Geol Surv Prof Paper 524-F, 1966, pp F1-F47.
17. K. A. Sargent, D. C. Noble, and E. B. Ekren, "Belted Range Tuff of Nye and Lincoln Counties, Nevada," Changes in Stratigraphic Nomenclature, US Geol Surv Bulletin 1224-A, 1964, pp 32-36.
18. L. V. Benson, Mass Transport in Vitric Tuffs of Rainier Mesa, Nye County, Nevada, NVO-1253-10 (Reno, NV: Water Resources Center, Desert Research Institute, University of Nevada, October 1979).
19. J. G. Liou, "Analcime Equilibria," Lithos, 4:389-402, 1971.
20. I. J. Winnograd and W. Thoradson, Hydrogeologic and Hydrochemical Framework, South Central Great Basin, Nevada-California, with Special Reference to the Nevada Test Site, US Geol Surv Prof Paper 712-G, 1975.
21. K. Wolfsberg, B. P. Bayhurst, B. M. Crowe, W. R. Daniels, B. R. Erdal, F. O. Lawrence, A. E. Norris, J. R. Smyth, Sorption-Desorption Studies on Tuff I. Initial Studies with Samples from the J-13 Drill Site, Jackass Flats, Nevada, LA-7480-MS (Los Alamos, NM: Los Alamos Scientific Laboratory, 1979).
22. E. N. Vine, R. D. Aguilar, B. P. Bayhurst, W. R. Daniels, S. J. DeVilliers, B. R. Erdal, F. O. Lawrence, S. Maestas, P. Q. Oliver, J. L. Thompson, and K. Wolfsberg, Sorption-Desorption Studies on Tuff II. A Continuation of Studies with Samples from Jackass Flats, Nevada and Initial Studies with Samples from Yucca Mountain, Nevada, LA-8110-MS (Los Alamos, NM: Los Alamos Scientific Laboratory, 1980).
23. B. R. Erdal, W. R. Daniels, D. C. Hoffman, F. O. Lawrence, and K. Wolfsberg, "Sorption and Migration of Radionuclides in Geologic Media," Vol. 1 of Scientific Basis for Nuclear Waste Management, ed G. J. McCarthy (New York: Plenum Press, 1979).
24. B. R. Erdal, B. P. Bayhurst, B. M. Crowe, W. R. Daniels, D. C. Hoffman, F. O. Lawrence, J. R. Smyth, J. L. Thompson, and K. Wolfsberg, "Laboratory Studies of Radionuclide Transport in Geologic Media," in Proceedings of the International Symposium on the Underground Disposal of Radioactive Wastes, Otaniemi, Finland, 1979 (to be published).

25. B. R. Erdal, B. P. Bayhurst, W. R. Daniels, S. J. DeVilliers, F. O. Lawrence, E. N. Vine, and K. Wolfsberg, "Parameters Affecting Radionuclide Migration in Geologic Media," Vol. 2 of Scientific Basis for Nuclear Waste Management, ed C. J. Northrup (New York: Plenum Press, to be published).
26. J. L. Thompson and K. Wolfsberg, Applicability of Micro-Autoradiography to Sorption Studies, LA-7609-MS (Los Alamos, NM: Los Alamos Scientific Laboratory, 1978).
27. J. R. Smyth, J. L. Thompson, and K. Wolfsberg, "Microautoradiographic Studies of the Sorption of U and Am on Natural Rock Samples," Radioactive Waste Management 1 (in press).
28. K. L. Erickson, "Preliminary Rate Expressions for Analysis of Radionuclide Migration Resulting from Fluid Flow Through Jointed Media," Vol. 2 of Scientific Basis for Nuclear Waste Management, ed C. J. Northrup (New York: Plenum Press, to be published).
29. K. L. Erickson, A Fundamental Approach to the Analysis of Radionuclide Transport Resulting from Fluid Flow Through Jointed Media, SAND80-0457 (Albuquerque, NM: Sandia National Laboratories, to be published).
30. F. Helfferich, Ion Exchange (New York: McGraw-Hill, 1962).
31. J. Rosen, "Kinetics of a Fixed-Bed System for Solid Diffusion into Spherical Particles," J Chem Physics, 37:387 (1952).
32. J. Rosen, "General Numerical Solution for Solid Diffusion in Fixed Beds," Ind Engr Chem, 46:1590 (1954).
33. A. R. Lappin, Thermal Conductivity of Silicic Tuffs: I. Predictive Formalism and Comparison with Preliminary Experimental Results, SAND80-0679 (Albuquerque, NM: Sandia National Laboratories, in preparation).
34. E. C. Robertson and D. L. Peck, "Thermal Conductivity of Vesicular Basalt from Hawaii," J Geophys Res, 79:4875-4888 (1974).
35. E. C. Robertson, Thermal Conductivity of Rocks, USGS Open File Report 79-356, 1979.
36. A. R. Lappin, Preliminary Thermal Expansion Screening Data for Tuffs, SAND78-1147 (Albuquerque, NM: Sandia National Laboratories, March 1980).
37. D. W. Breck, Zeolite Molecular Sieves (New York: John Wiley and Sons, 1974).

38. H. W. Cooper and G. Simmons, "The Effects of Cracks on Thermal Expansion of Rocks," Earth Plan Sci Lett, 36:404-412 (1977).
39. D. E. Dunn, L. J. La Fountain, and R. E. Jackson, "Porosity Dependence and Mechanism of Brittle Fracture in Sandstone," J Geophys Res, 78:2403-2417 (1973).
40. R. Weisinger, L. S. Costin, and T. J. Lutz, " K_{IC} and J-Resistance-Curve Measurements on Nevada Tuff," Exper Mech 20 (2):68-72 (1980).
41. R. J. Martin III, "Time-Dependent Crack Growth in Quartz and Its Application to the Creep of Rocks," J Geophys Res, 77(8):1406-1419 (1972).
42. D. Griggs, "Hydrolytic Weakening of Quartz and Other Silicates," Geophys J. R. Astro Soc, 14:19-31 (1967).
43. N. R. Warpinski et al, Hydraulic Fracture Behavior at a Geologic Formation Interface: Pre-Mineback Report, SAND78-1578 (Albuquerque, NM: Sandia National Laboratories, 1978).
44. J. D. Byerlee, "Friction of Rocks," Pageoph, 14:615-627 (1978).
45. J. H. Dieterich, "Time-Dependent Friction and the Mechanics of Stick-Slip," Pageoph, 116:790-807 (1978).
46. L. W. Teufel and J. M. Logan, "Effect of Displacement Rate on the Real Area of Contact and Temperatures Generated During Frictional Sliding of Tennessee Sandstone," Pageoph, 116:840:865 (1978).
47. J. R. Hadley and J. E. R. Turner, Evaporative Water Loss from Welded Tuff, SAND80-0201 (Albuquerque, NM: Sandia National Laboratories, to be published).
48. J. K. Johnstone, In-Situ Tuff Water Migration/Heater Experiment: Experimental Plan, SAND79-1276 (Albuquerque, NM: Sandia National Laboratories, to be published).

APPENDIX A

**Correlation of Sorptive Properties of Tuff
With Mineralogy**

Status Report

CORRELATION OF SORPTIVE PROPERTIES OF TUFF WITH MINERALOGY

K. Wolfsberg and E. N. Vine

We have re-evaluated our correlation of sorptive data with mineralogy. This re-evaluation is based on the mineralogic composition data¹ obtained by LASL Group G-9 with the new Siemens X-ray diffraction spectrometer. Included in our sorption data are both published and unpublished results.²⁻⁵

If most of the tuff samples studied are classified as either devitrified or zeolitized based on mineralogic composition, we find that sorption data falls into groups with relatively small ranges for individual elements in each class. Of the thirteen samples studied, five are in the category of zeolitized tuffs (>20% clinoptilolite or heulandite), five are devitrified tuffs (principally quartz, cristobalite, or feldspars with <10% zeolites or clays), and three contain 10 or 15% clay or zeolites. We summarize the results for the three categories in Tables A1-A3. The data for the elements for which the mechanism of sorption-desorption is most likely via ion exchange--cesium, strontium, and barium--correlate well for the zeolitized and devitrified tuffs.

Data for cerium and europium have much larger ranges, indicating that other factors must be involved. Most likely the special problems³ that are found for americium and plutonium in slightly basic solutions are also present for the lanthanides.

The three tuff samples in Table A3 do not fit into any clear pattern for samples containing clays, low amounts of zeolites, or glass. The two vitric tuffs which contain zeolites seem to correlate well with the other zeolitic tuffs in Table A1. More sensitive clay analyses are being performed by LASL Group G-9. We will do additional experiments with appropriate samples selected by LASL Groups G-9 and CNC-11 to try to clarify the roles of clays and glasses in sorption. Perhaps enrichment in the desired mineral fraction will be possible.

The sorption ratios listed in Tables A1-A3 are average values for contact times ranging from 1 to 12 weeks. Values for sorption of technetium and uranium under both the ambient atmosphere and under nitrogen (≤ 0.2 ppm oxygen, ≤ 20 ppm carbon dioxide) are also given.

To give a meaning to sorption ratios, we list in Table A4, the fraction of a nuclide in solution in equilibrium for several R_d values and for solution to solid ratios of 20 (the condition of our experiments) and 0.33 (saturated condition for a porous tuff).

References.

1. J. Smyth and F. Caporuscio, unpublished data (1980).
2. K. Wolfsberg, B. P. Bayhurst, B. M. Crowe, W. R. Daniels, B. R. Erdal, F. O. Lawrence, A. E. Norris, J. R. Smyth, Sorption-Desorption Studies on Tuff I. Initial Studies with Samples from the J-13 Drill Site, Jackass Flats, Nevada," Los Alamos Scientific Laboratory report LA-7480-MS (1979).
3. E. N. Vine, R. D. Aguilar, B. P. Bayhurst, W. R. Daniels, S. J. DeVilliers, B. R. Erdal, F. O. Lawrence, S. Maestas, P. Q. Oliver, J. L. Thompson, and K. Wolfsberg, "Sorption-Desorption Studies on Tuff II. A Continuation of Studies with Samples from Jackass Flats, Nevada and Initial Studies with Samples from Yucca Mountain, Nevada," Los Alamos Scientific Laboratory report LA-8110-MS (1980).
4. B. M. Crowe (Compiler), "Research and Development Related to the Nevada Nuclear Waste Storage Investigations, October 1 - December 31, 1979," Los Alamos Scientific Laboratory report LA-8309-PR (1980).
5. E. N. Vine, unpublished data (1980).

TABLE A1
ZEOLITIZED TUFF

	<u>JA-18</u>	<u>YM-38</u>	<u>YM-42</u>	<u>YM-49</u>	<u>YM-48</u>	<u>Range or Value</u>
Composition, Percent						
Montmorillonite		2-5	tr	tr	tr	0-5
Illite/Muscovite						
Clinoptilolite	20-30	40-60	20	50-70	10-20	10-70
Quartz	5-10	5-10	35-40	10-15		0-40
Cristobalite		15-30		10-15		0-30
Alkali Feldspar	5-10	20-30	40	10-20	20-30	5-40
Calcite						
Glass	50-70				40-70	0-70
Average Sorption Ratio, ml/g						
Cs, Sorption	16 000 ^a	8 600	19 000	29 000	17 000	8 600-29 000
Cs, Desorption		13 000		33 000	27 000	13 000-33 000
Sr, Sorption	20 000	12 000	4 000	2 700	1 800	1 800-20 000
Sr, Desorption		20 000		3 900	2 700	2 700-20 000
Ba, Sorption	130 000	66 000	96 000	33 000	15 000	15 000-130 000
Ba, Desorption		190 000		51 000	34 000	34 000-190 000
Ce, Sorption	2 000	830		550	1 900	550-2 000
Ce, Desorption		3 800		1 200	13 000	1 200-13 000
Eu, Sorption	1 500	2 300		1 200	2 500	1 200-2 500
Eu, Desorption		8 700		2 100	8 100	2 100-8 700
Am, Sorption	180					180
Am, Desorption	1 100					1 100
Pu, Sorption	120					120
Pu, Desorption	340					340
Tc (air), Sorption				0.21	0.15	0.2
Tc (air), Desorption				2.0	1.7	2.
Tc (N ₂), Sorption		13.3				13.
Tc (N ₂), Desorption		118.				118.
U (Air), Sorption	2.3	5.1				2.3-5.1
U (Air), Desorption	15.2	14.6				15.
U (N ₂), Sorption		15.1				15.
U (N ₂), Desorption		56.9				57.
I, Sorption	0.					0.

^aFrom Table XVII, Ref. 2. The value 6 000 listed in Table XXXII, Ref. 2 and Table XXXVIII, Ref. 3 should read 16 000.

TABLE A2
DEVITRIFIED TUFF

	<u>JA-32</u>	<u>YM-22</u>	<u>YM-54</u>	<u>YM-45</u>	<u>YM-46</u>	<u>Range or Value</u>
Composition, Percent						
Montmorillonite						
Illite/Muscovite	5-10					0-10
Clinoptilolite						
Quartz	40-50	40-60	50-70	40-60	50	40-60
Cristobalite		10-20	tr	tr		0-20
Alkali Feldspar	30-40	20-30	20-40	30-50	45	0-50
Calcite						
Glass						
Average Sorption Ratio, ml/g						
Cs, Sorption	150	340	250	530	870	150-870
Cs, Desorption	440	400	310	630		310-630
Sr, Sorption	57	53	90	190	190	53-190
Sr, Desorption	56	63	97	200		56-200
Ba, Sorption	430	980	620	1 200	1 500	430-1 500
Ba, Desorption	440	1 000	660	1 300		440-1 300
Ce, Sorption	80	1 400	140	730	15 000	80-15 000
Ce, Desorption	400	6 100	990	5 700		400-15 000
Eu, Sorption	90	1 400	500	1 600	7 500	90-7 500
Eu, Desorption	800	3 600	1 800	7 300		800-7 300
Am, Sorption	130					130
Am, Desorption	2 200					2 200
Pu, Sorption	110					110
Pu, Desorption	1 100					1 100
Tc (air), Sorption		0.3				0.3
Tc (air), Desorption		1.2				1.2
Tc (N ₂), Sorption			26.	7.7		8.-26.
Tc (N ₂), Desorption			18.	79.		18.-79.
U (air), Sorption	2.2	1.6	1.6			1.6-2.2
U (air), Desorption	8.0	6.0	12.8			6-13.
U (N ₂), Sorption	0.5	1.5				0.5-1.5
U (N ₂), Desorption	1.8	13.7				2.-14.
I, Sorption	0.					0.

TABLE A3
OTHER SAMPLES

	<u>JA-37</u>	<u>YM-5</u>	<u>YM-30</u>
Composition, Percent			
Montmorillonite	10	10	
Illite/Muscovite			
Clinoptilolite	tr		15
Quartz	40-50	0-5	30
Cristobalite		0-5	20
Alkali Fledspar	30-40	15	35
Calcite	tr		
Glass		70	
Average Sorption Ratio, ml/g			
Cs, Sorption	290	6 000	1 300
Cs, Desorption	310		
Sr, Sorption	620	480	270
Sr, Desorption	850		
Ba, Sorption	750	1 100	3 500
Ba, Desorption	920		
Ce, Sorption			
Ce, Desorption			
Eu, Sorption	6 000		
Eu, Desorption	130 000		
Am, Sorption	670		
Am, Desorption	1 700		
Pu, Sorption	500		
Pu, Desorption	8 200		
Tc (air), Sorption			
Tc (air), Desorption			
Tc (N ₂), Sorption			
Tc (N ₂), Desorption			
U (air), Sorption	4.2		
U (air), Desorption	8.4		
U (N ₂), Sorption			
U (N ₂), Desorption			
I, Sorption	0.		

TABLE A4
 FRACTION IN SOLUTION

R_d (ml/g)	Solution/Solid	
	20	0.33
20	5.0×10^{-1}	1.6×10^{-2}
100	1.7×10^{-1}	3.3×10^{-3}
600	3.2×10^{-2}	5.5×10^{-4}
10 000	2.0×10^{-3}	3.3×10^{-5}

APPENDIX B

**Crushed Rock Columns:
A Comparison With Batch Measurements**

Status Report

CRUSHED ROCK COLUMNS A COMPARISON WITH BATCH MEASUREMENTS

E. N. Vine and B. P. Bayhurst

I. MEASUREMENTS

The migration of radionuclides through crushed rock columns of tuff, granite, and argillite has been studied. The geologic materials chosen were those on which batch sorption ratio (R_d) measurements had previously been made in order to provide a comparison with results obtained on the columns. The waters used for infiltration were described in Refs. 1 (tuff), 2 (argillite), and 3 (granite). A description of the columns themselves and the water delivery system(s) have also been previously reported (Refs. 1 and 4).

A summary of the crushed rock columns studied and of the parameters measured is given in Table B1.

Each column was characterized in terms of the total column volume V (the size of the column calculated from column dimensions), the free column volume FCV (measured and used to calculate the effective column porosity), the dry bulk density, the particle size, and the flow rate. Flow rates were determined by weighing the eluate sample delivered in a known time period. Upward-flow columns had relatively constant flow rates with a given syringe and pump setting, while gravity-flow columns tended to decrease in flow rate before a steady flow was established. Upward-flow rates ranged from 0.041 to 0.082 ml/h with one column run at ~4 to 5 ml/h. (A flow rate of 0.045 ml/h for a 2.1-cm-long 0.5-cm diameter column with a free column of 0.224 ml corresponds to a flow velocity of ~37 m/y.)

The free column volumes of approximately one-third of the columns studied were determined by use of both HTO and $^{131}\text{I}^-$. In the iodide case, the ^{131}I breakthrough (leading edge) curve and the rinse (trailing edge) were both used. There was essentially no difference in the values obtained with HTO or with $^{131}\text{I}^-$, and all measurements for a given column were averaged irrespective of the method used. For example, the FCV for a YM-54 column obtained with iodide

(breakthrough) was 0.177 ml and with HTO was 0.182 ml. On the YM-22 column, the iodide breakthrough method gave 0.249 ml and the iodide rinse gave 0.239 ml. The values for the CS-5 and CS-7 granite columns, the CN-1 and CN-2#1 argillite columns, and the JA-18, JA-37, and YM-45 tuff columns were measured using ^{131}I only. However, since a small retardation factor (2 to 6 ml/g) had recently been measured (Ref. 5) for "iodide" on argillite, columns CN-2#2 and CN-3 were run with both tritium and ^{131}I (as well as technetium). The tritium data have been analyzed for only one of these columns; however the breakthrough curve was identical to that obtained for ^{131}I .

Several parameters have been investigated, to a limited extent, with crushed rock columns. Flow rates were varied from 0.082 ml/h to 18 ml/h on three JA-32 tuff columns loaded with ^{85}Sr . Argillite columns, with $^{95\text{m}}\text{Tc}$, ^{131}I , and HTO, were run under controlled atmosphere conditions (≤ 0.2 ppm oxygen, ≤ 20 ppm carbon dioxide) as well as in normal atmospheric conditions. The effect of the cesium ion concentration on tuff was also investigated. Two YM-54 columns were loaded with ^{137}Cs in a 5- to 15- μl spike at a concentration of $\sim 10^{-6}$ M. Another YM-54 column was also run with a continuous feed of ^{137}Cs at a concentration comparable to that of the batch measurements, $\sim 10^{-9}$ M, to see if the R_d value of cesium increased with the decreased cesium ion concentration.

II. DATA COLLECTION AND ANALYSIS

Methods of sample collection, detection of radioisotopes, data analysis, and equations for calculation of retardation factors and corresponding distribution coefficients (R_d) have previously been described (Refs. 1 and 4).

III. RESULTS AND CONCLUSIONS

A description of the crushed rock columns studied is given in Table I. The calculated column distribution coefficients for the isotopes ^{85}Sr , ^{137}Cs , and ^{133}Ba are given in Tables B2, B3, and B4, with data from batch sorption measurements for comparison.

Several kinds of elution behavior have been observed: symmetric peaks where fifty percent of the activity eluted corresponds closely to the peak of the elution curve, asymmetric peaks, and "no peaks" - but instead a slow, usually uniform elution of activity. Plots of elution curves having symmetric and asymmetric peak shapes have been given in Refs. 1 and 4. With the exception of JA-18

TABLE B1
CRUSHED ROCK COLUMNS

Geologic Materials	Isotopes Studied	Column Size (cm ³)	Porosity (%)	Density (g/cm ³)	General Comments
Tuff:					
YH-54#1	⁸⁵ Sr, ¹³³ Ba, ¹³⁷ Cs	0.295	79.3	0.98	10 ⁻⁶ M ¹³⁷ Cs
#2	¹³⁷ Cs	0.294	61.2		10 ⁻⁹ M ¹³⁷ Cs
#3	⁸⁵ Sr, ¹³³ Ba, ¹³⁷ Cs	0.511	66.9		10 ⁻⁶ M ¹³⁷ Cs
YH-38#1	⁸⁵ Sr	0.785	39.9	0.90	Activity decayed before it was eluted
#2	¹⁴¹ Ce	0.266	35.7		Activity decayed before it was eluted
#3	¹³⁷ Cs	0.390	39.0		Fast flow rate (4.5 ml/h)
JA-32#1	⁸⁵ Sr	0.830	54.9	0.89	
#2	⁸⁵ Sr	0.432	67.8		Fast flow rate (18 ml/h)
#3	⁸⁵ Sr	0.353	63.5		
JA-18#1	⁸⁵ Sr, ¹³⁷ Cs	0.251	56.2	0.98	
#2	¹⁴¹ Ce, ¹⁵² Eu	0.239	47.7		
JA-37	⁸⁵ Sr, ¹³⁷ Cs	0.342	44.4	0.95	
YH-22	⁸⁵ Sr, ¹³³ Ba, ¹³⁷ Cs	0.373	65.4	1.16	
YH-45	¹⁴¹ Ce	0.264	31.8	1.08	Activity decayed before it was eluted
YH-54#4	²³⁷ U	0.353	48.7	1.09	
Argillite:					
CN-1	⁸⁵ Sr, ¹³⁷ Cs	0.382	59.2	1.15	
CN-2#1	⁸⁵ Sr, ¹³⁷ Cs	0.386	64.4		
CN-2#2	^{95m} Tc, ¹³¹ I	0.616	82.0		
CN-3	^{95m} Tc, ¹³¹ I	0.732	77.9		<0.2 ppm oxygen conditions
Granite:					
CS-7	⁸⁵ Sr, ¹³³ Ba, ¹³⁷ Cs	0.412	59.2	1.26	Slow "peakless" elution of ¹³⁷ Cs
CS-5	⁸⁵ Sr, ¹³³ Ba, ¹³⁷ Cs	0.422	59.7	1.25	Slow "peakless" elution of ¹³⁷ Cs

TABLE B2
⁸⁵Sr: A COMPARISON OF BATCH AND COLUMN R_d VALUES

Column	R _d (ml/g)		Comments
	Batch	Column	
CS-5	14	8.5	
CS-7	18	15	
YM-22	50	30	
JA-32	56	42	
YM-54	84	44	
CN-1	138	43	
CN-2#1	156	52	
JA-37	300	106	
JA-18	16000	381(9%)	23% removed, 9% of which was in a peak
YM-38#1	12000	>460	Activity decayed prior to eluting

TABLE B3
¹³⁷Cs: A COMPARISON OF BATCH AND COLUMN R_d VALUES

Column	R _d (ml/g)		Comments
	Batch	Column	
YM-54	247	97	Peak, with 90% ¹³⁷ Cs; average of 3 columns
YM-22	287	122	Peak, with 95% ¹³⁷ Cs (broad peak)
CS-7	328	>606	20% removed in 314 ml (52 weeks)
CS-5	347	>665	8% removed in 352 ml (52 weeks)
JA-37	740	>560	3.6% removed in 182 ml (26 weeks)
CN-2#1	1580	>520	0% removed in 235 ml (40 weeks)
CN-1	1830	>570	0% removed in 243 ml (40 weeks)
YM-38#3	8600	"21900"	50% removed in 7680 ml (no peak was observed)
JA-18	6600-15000		13% removed in 200 ml (27 weeks)

TABLE B4
¹³³Ba: A COMPARISON OF BATCH AND COLUMN R_d VALUES

Column	R _d (ml/g)	
	Batch	Column
CS-5	154	32
CS-7	175	44
YM-54	620	124
YM-22	899	355

and YM-38 tuff columns (see Table B2), the elution curves of ⁸⁵Sr have fallen into the first category, "symmetric peaks", with the column R_d value being one to three times lower than the corresponding batch R_d value. Three JA-32 columns were loaded with ⁸⁵Sr to compare the effect of varying the flow rate from 0.082 ml/h to 18 ml/h. The effect of flow rate on the calculated distribution coefficients was negligible.

The YM-38#1 column was loaded with ⁸⁵Sr before the batch R_d measurement (12000 ml/g) was completed. None of the strontium (T_{1/2} = 65.2 d) was eluted before the activity decayed. A Polaroid film exposed to the YM-38 column several months after elution was started indicated that the ⁸⁵Sr remained in the top quarter of the column. The JA-18 column was the only other one loaded with ⁸⁵Sr for which a large batch R_d value (16000 ml/g) had been measured. The strontium on this column was eluted at a rate of ~0.07%/d for ~72 days, then a small, sharp peak (R_d = 381 ml/g) containing 9% of the total activity was observed. Elution of the JA-18 column has continued for 95 d since the peak was observed, and the slow, uniform "leaking" has resumed. The JA-18 material is a highly glassy tuff and the slow elution may be due to a gradual dissolution of the glass. This, however, would not explain the weak, sharp peak which seems to indicate that more than one "sorption" mechanism exists. The JA-18#1 and YM-38#3 columns were also loaded with ¹³⁷Cs and the same slow "leaking" without a sharp peak, was observed. Besides dissolution of the glass, the slow elution of ⁸⁵Sr and ¹³⁷Cs might also be the result of exchange of the sorbed radioactive species with stable isotopes in the pre-treated waters used, which contain ~10⁻⁹M cesium and ~6 x 10⁻⁷M strontium.

Other cesium column data are given in Table B3. The most straightforward results are from tuff columns of YM-54 (3 columns) and YM-22 (1 column), where the batch distribution coefficients are fairly small and values from desorption and sorption experiments are approximately equal. They are the only columns containing cesium analyzed to date where elution of the activity occurred in a peak. The three YM-54 columns were run at two ^{137}Cs concentrations, 10^{-6}M and 10^{-9}M , to see if the R_d value calculated for cesium was affected by the cesium ion concentration. No effect was observed. On two granite columns a slow elution of ^{137}Cs began at about day 48 and has continued for one year. On argillite, after 40 weeks, no ^{137}Cs has been eluted from either of two columns; however, the cesium batch R_d values on argillite are approximately five times larger than those for granite, and a similar slow elution behavior may still occur. On the JA-37 column, elution of ^{137}Cs began on day 95 and the activity has increased from 25 to 500 dpm/ml. In 184 d, 3.6% of the total cesium has been removed.

Since tuff columns loaded with ^{85}Sr had indicated that retardation factors were independent of flow rate, ^{137}Cs was loaded onto a YM-38 column and run at a fast (4-5 ml/h) flow rate. The ^{137}Cs was not detected until 1150 ml had been passed through the column. Since then, 10.3% of the total ^{137}Cs has been eluted in 3250 ml, in slowly increasing amounts. (If the average flow rate used on the majority of columns had been used in this case then about ten years would have been required to collect the total of 4400 ml eluted to date.) Although a sharp peak will probably never be observed, and the mathematical expressions relating distribution coefficients with retardation factors are not valid for such cases, one can calculate a "lower limit" column R_d value of $>12\,500\text{ ml/g}$ from the volume eluted to date. This is a value well above that obtained from batch measurements (8600 ml/g) and is indicative of the "complications" revealed by flow experiments.

All of the columns run to date with ^{133}Ba have shown peaks, followed in some cases by a gradual elution of activity. The R_d values calculated from the columns are given in Table B4; they are 2.5 to 4.8 times lower than the corresponding batch R_d values. It is also apparent from Table B4, that only materials with relatively low distribution coefficients for barium have been used in columns. Thus, the more complicated situations, better revealed by high R_d values, have not yet been studied with barium. On columns of YM-54 and YM-22 with batch R_d values of 620 and 899 ml/g, respectively, the batch sorption and desorption ratios were found to be equal, implying a reversible interchange of

ions. For "comparable" batch sorption R_d numbers (see Table B3) with cesium on columns of granite, JA-37, and argillite, simple peaks were not observed. This was perhaps due to the fact that the desorption R_d values were at least a factor of two larger than the sorption R_d values. This could suggest that more than one species and/or mechanism with different rates of reaction is present during sorption (and absent in batch desorption measurements) or that weathering in the batch studies and mineral alteration is affecting sorption vs. desorption. For the granite columns (batch desorption values were about twice those for sorption) the peaks of the barium elution curves represented less than half of the total activity and were followed by a slow, uniform, elution.

Other isotopes studied, but not indicated in Tables B2-B4, were ^{141}Ce , ^{95m}Tc , ^{237}U , and ^{131}I . The cerium which was loaded on a YM-45 tuff column (batch R_d of 730 ml/g (sorption), 5700 (desorption)) was not eluted in 165 d at a flow rate of ≤ 1.020 ml/d. Since the ^{141}Ce had decayed significantly in that period of time and the column could not be continued much longer, the flow rate was increased to ≤ 0.6 ml/h until a total of 250 ml had been collected from the column. No ^{141}Ce was detected, indicating that the R_d value is >880 ml/g; however counting the whole column loaded with ^{141}Ce , both before and after elution, indicated that ~6% of the ^{141}Ce had been removed from the column. The YM-38#2 column was run for 112 d at a flow rate of 0.911 ml/d with no ^{141}Ce detected in the eluate; it was stopped due to insufficient activity remaining on the column. The "lower limit" column R_d was >430 ml/g. Batch values were 830 ml/g for sorption and 3800 ml/g for desorption.

Another column, JA-18#2 was recently loaded with ^{141}Ce as well as ^{152}Eu . No ^{141}Ce has been detected in 14 weeks, although the elution of a small amount of ^{152}Eu (~50 dpm/ml) has begun.

A tuff column, YM-54#4, loaded with spikes of tritium, ^{131}I and ^{237}U gave an R_d value of 0.72 ml/g for uranium, compared with an average batch R_d value of 1.5 ml/g. The uranium peak was quite asymmetric and the activity eluted per ml is slowly decreasing. Again, the marked asymmetry could be an effect of the complicated "sorption" illustrated by the large difference between batch sorption (1.5 ml/g) and desorption (11 ml/g) ratios.

With technetium, breakthrough curves were obtained simultaneously with tritium and ^{131}I on argillite CN-2#2 (atmospheric conditions) and argillite CN-3 (controlled-atmosphere conditions, ≤ 0.2 ppm oxygen and ≤ 20 ppm carbon dioxide). The ^{131}I and HTO gave identical breakthrough curves, indicating no retardation

of iodide on argillite, as was previously indicated by batch measurements.⁵ The column R_d values for ^{95m}Tc , 0.40 mL/g on CN-2 and 0.31 mL/g on CN-3, were considerably less than those obtained by batch techniques, 30.5 mL/g for CN-2, in air (Ref. 2) and 175 mL/g for CN-3, in ≤ 0.2 ppm oxygen, ≤ 20 ppm carbon dioxide (Ref. 5). However, the columns were run at a fast flow rate (~ 2 mL/h), reducing the time of contact between technetium and the rock by 80 to 700 times that of the batch measurements. This could also explain the apparent lack of effect of the ≤ 0.2 ppm oxygen atmosphere; the fast flow rate would limit the time available for reduction of pertechnetate. Since the sorption of technetium on argillite has been shown to be strongly time dependent, particularly under ≤ 0.2 ppm oxygen conditions⁵, the difference between batch and column R_d values is probably reasonable. This could be most easily checked by short-contact-time batch measurements.

If a general conclusion can be stated from these observations, particularly from the data of ^{85}Sr , ^{137}Cs , and ^{133}Ba on granite, argillite, and tuff, it is probably that--except in the simplest of cases, where sorption coefficients are relatively low, and ion-exchange equilibria not only exist but are the dominant mechanism for removal of radioisotopes from solution--the simple relation between the distribution coefficient R_d or K_d and the relative velocity of radionuclides with respect to groundwater velocity may be insufficient to permit accurate modeling of the retardation of radionuclides. This indicates the need to isolate and study the (probably many) mechanisms causing retardation which could lead to an understanding of the relationship between the behavior in a dynamic laboratory experiment (and, ultimately, behavior in the field) and the many available batch R_d data.

REFERENCES

1. E. N. Vine, R. D. Aguilar, B. P. Bayhurst, W. R. Daniels, S. J. DeVilliers, B. R. Erdal, F. O. Lawrence, S. Maestas, P. Q. Oliver, J. L. Thompson, and K. Wolfsberg, "Sorption-Desorption Studies on Tuff. II. A Continuation of Studies with Samples from Jackass Flats, Nevada and Initial Studies with Samples from Yucca Mountain, Nevada," Los Alamos Scientific Laboratory report LA-8110-MS (1980).
2. B. R. Erdal, R. D. Aguilar, B. P. Bayhurst, P. Q. Oliver, and K. Wolfsberg, "Sorption-Desorption Studies on Argillite," Los Alamos Scientific Laboratory report LA-7455-MS (1978).

3. B. R. Erdal, R. D. Aguilar, B. P. Bayhurst, W. R. Daniels, C. J. Duffy, F. O. Lawrence, S. Maestas, and K. Wolfsberg, "Sorption-Desorption Studies on Granite," Los Alamos Scientific Laboratory report LA-7456-MS (1978).
4. B. R. Erdal, Ed., "Laboratory Studies of Radionuclide Distribution Between Selected Groundwaters and Geologic Media, Annual Report, October 1, 1978 - September 30, 1979," Los Alamos Scientific Laboratory report LA-8038-PR (1980).
5. B. R. Erdal, Ed., "Laboratory Studies of Radionuclide Distributions Between Selected Groundwaters and Geologic Media," Los Alamos Scientific Laboratory report LA-8210-PR (1980).

APPENDIX C
Mine Design

Table C1
Repository Geometry and Initial Conditions

Repository depth (to top of heat-producing zone): 800 m
Thickness of heat-producing zone for generalized repository: 10 m
Repository area: 2000 acres
Geothermal heat flux: $1.6 \mu\text{cal}/\text{cm}^2\text{s}$
Static water level (depth): 470 m
Air surface temperature: 20°C
Initial temperature at disposal horizon: 55°C
(Note: Recent field results indicate a different geothermal condition giving a disposal horizon temperature near 35°C)

Table C2
Canister Dimensions and Initial Power Output

Spent-Fuel Canister Description

Total length: 4.67 m
Outside Dia: 0.355 m
Inside Dia: 0.30 m
Heated Length: 3.66 m
Air-Filled
Canister material: carbon steel

HLW Canister Description

Total Length: 3.05 m
Outside Dia: 0.32 m
Inside Dia: 0.30 m
Heated Length: 3.0 m
Canister Material: stainless 304

Power at Time of Emplacement (Waste Assumed 10 yr old)

HLW: 3.5 kW/can and 2.16 kW/can
Spent Fuel: 0.55 kW/can

Table C3
Normalized Decay - Heat Generation*

<u>Year After Emplacement**</u>	<u>HLW</u>	<u>Spent Fuel</u>
0	1.0	1.0
1	0.95	0.956
2	0.907	0.919
3	0.871	0.889
4	0.851	0.861
5	0.810	0.838
6	0.783	0.819
7	0.769	0.799
8	0.734	0.782
9	0.714	0.763
10	0.692	0.750
15	0.600	0.681
20	0.529	0.622
30	0.402	0.525
40	0.313	0.449
50	0.246	0.387
70	0.157	0.301
100	0.0864	0.238
190	0.0296	0.137
290	0.0215	0.108
390	0.0163	0.0919
490	0.0145	0.0806
590	0.0127	0.0711
690	0.0113	0.0633
790	0.0100	0.0569
890	0.00897	0.0514
990	0.00810	0.0466
1990	0.00404	0.0247
5990	0.00230	0.0148
9990	0.00175	0.0114

*See Y/OWI/TM-34, "Nuclear Waste Projections and Source Term Data for FY 1977". The HLW decay rates correspond to waste arising from fuel which is a 3:1 mix of fresh UO₂ and MOX fuels.

**Assumes waste is 10 years old at emplacement.

Table C4

Assumed Stratigraphy and Material Thermal Properties for Far-Field Modeling--Tuff Mine Design Activity

Depth	m(ft)	Porosity	Bulk Density (Mg/m ³)	Grain Density (Mg/m ³)	ρC (cal/cm ³ °C)		K (W/mK)		T _{boil} (°C) (hydrostatic)	
					< T _{boil}	> T _{boil}	< T _{boil}	> T _{boil}		
0- 53	(0- 173)	0.11	2.38	2.56 (m)	0.66	0.46	2.6	2.3	100	Tiva Canyon Member
53- 63	(173- 208)	0.28	2.07	2.53 (m)	0.82	0.36	1.9	--	100	
63- 84	(208- 276)	0.50	1.53	2.46 (m)	0.84	0.25	0.9	0.7	100	
84-139	(276- 457)	0.12	2.37	2.56 (a)	0.67	0.45	2.6	2.3	100	
139-192	(457- 631)	0.50	1.78	2.56 (a)	0.50	0.26	0.85	0.7	100	Tonopah Springs Member
192-286	(631- 939)	0.12	2.37	2.57 (m)	0.67	0.45	2.6	2.3	100	
286-328	(939-1076)	0.50	1.78	2.56 (a)	0.50	0.26	0.85	0.7	100	
328-388	(1076-1273)	0.11	2.38	2.56 (m)	0.67	0.46	2.6	2.3	100	
388-401	(1273-1317)	0.13	2.26	2.43 (m)	0.68	0.43	1.2	1.0	100	
401-416	(1317-1364)	0.28	2.05	2.45 (a)	0.86	0.35	1.10	0.7	100	
416-545	(1364-1789)	0.31	1.97	2.40 (m)	0.89	0.33	1.05 (calc) 1.10 (meas)	0.67 (calc) 0.71 (meas)	100	Tuffaceous Beds of Calico Hills
545-560	(1789-1836)	0.25	2.12	2.50 (a)	0.85	0.37	1.1	0.8	175	
560-578	(1836-1897)	0.29	2.15	2.61 (a)	0.92	0.37	1.55	1.0	187	
578-594	(1897-1950)	0.25	2.21	2.61 (m)	0.88	0.39	1.65	1.1	189	Provo Pass Member
594-614	(1950-2014)	0.18	2.34	2.62 (m)	0.80	0.43	1.80 (meas) 1.80 (calc)	1.39 (calc) 1.33 (meas)	195	
614-643	(2014-2110)	0.32	2.13	2.55 (m)	0.98	0.36	1.90	1.2	203	
643-697	(2110-2288)	0.29	2.10	2.55 (a)	0.90	0.36	2.0	1.3	214	
697-711	(2288-2333)	0.29	2.17	2.65 (a)	0.93	0.38	2.1	1.4	221	
711- --	(2333- --)	0.23	2.28	2.66 (m)	0.87	0.41	2.4 (meas) 2.35 (calc)	1.65 (meas) 1.7 (calc)	223	Bullfrog Member

(a) = assumed
(m) = measured

Paintbrush Tuff

Crater Flat Tuff

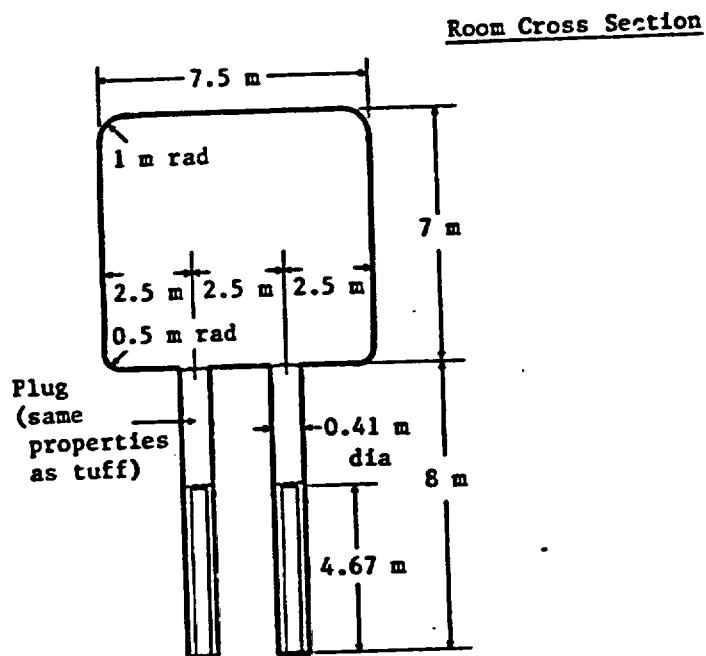
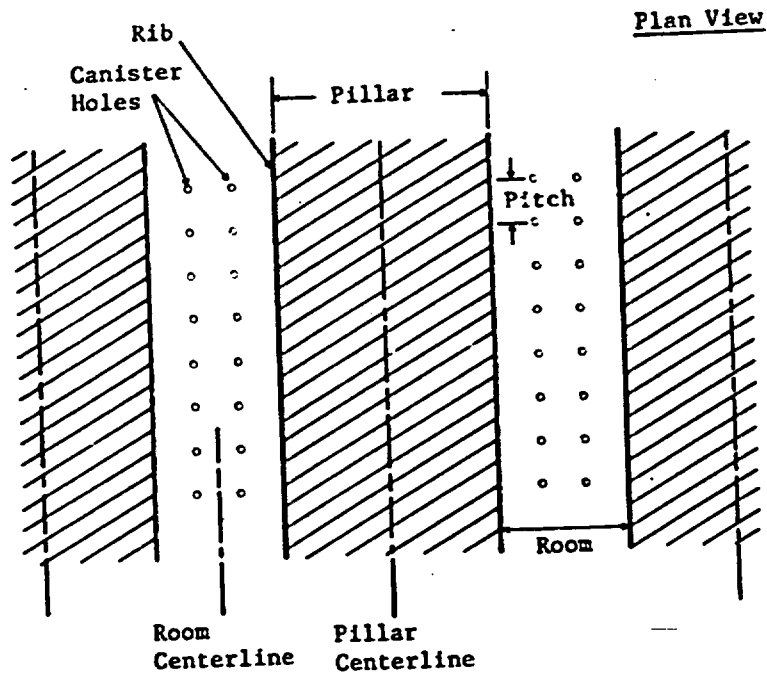


Figure C-1. Initial Room Design for Spent-Fuel Repository in Welded Tuff

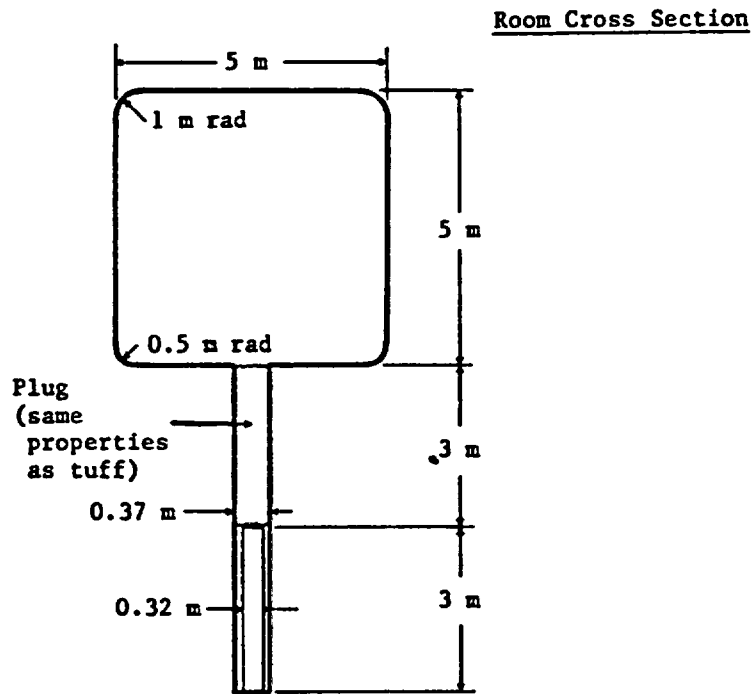
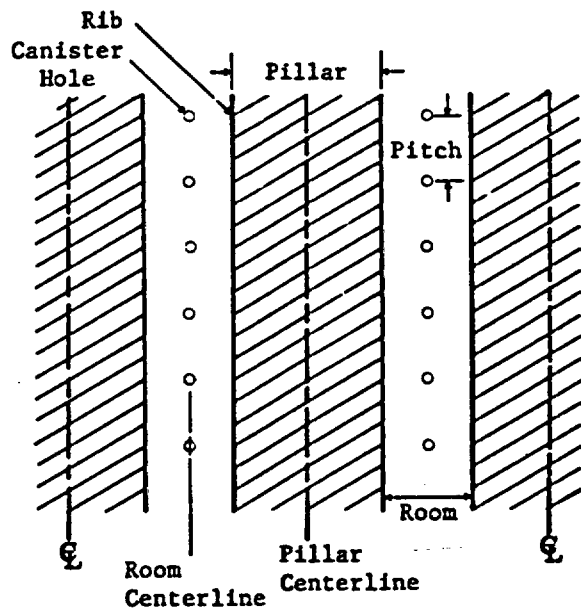


Figure C-2. Initial Room Design for HLW Repository in Welded Tuff